APPLICATION OF INTERACTIVE GRAPHICS TECHNIQUES TO MAGNET DESIGN

M J Newman
Rutherford Laboratory, Chilton, Didcot, Oxon, OX11 0QX

1. INTRODUCTION

The purpose of this paper is to show how the techniques of interactive graphics can be used as an effective tool to enable a designer to make the best use of the power of modern computers. The design process is analysed to see which functions are suitable for computers and which need experienced human intervention.

The capabilities of interactive graphics techniques are reviewed, and areas of the design process where they can be of assistance are identified. Existing programs for magnet design which use these techniques are reviewed, and finally, a general purpose computer-aided design system which is being implemented at the Rutherford Laboratory is described.

2. ANALYSIS OF THE DESIGN PROCESS

The problem of designing a magnet is a particular case of the general problem of minimising a non-linear function of many variables, subject to non-linear constraints. Algorithms for solving such general problems are not known even for local minima, let alone global minima. Unfortunately, the magnet design problem is even more difficult than this. Figure 1 shows a block diagram of a typical optimisation algorithm to find a local minimum with say linear constraints and where first derivations of the function are available.

When we attempt to interpret this diagram in terms of magnet design we see immediately why the problem is difficult. It is usually not too difficult to specify the constraints and the function to be minimised. For example the function might be the inhomogeneity of the field strength over a given volume of space. Typical constraints would be the minimum central field strength, and the minimum aperture needed to gain access to the uniform field region. However, the number and form of the independent variables cannot be specified so easily, and in general may be said to be unlimited. The experience of the designer is immediately invoked to limit the number of variables and impose further constraints which he hopes will result in a solution not too far from the true minimum. Of course, if he decides not to use iron for concentrating the flux, and if he limits the complexity of the conductor configuration, he will be able to solve the problem automatically on a computer using known algorithms - always providing that he can provide an initial guess that will lead to a sensible local minimum.

However, for most designs the problem will be approximately as shown in Figure 2. Having decided on the constraints and the function he wishes to minimise, the designer makes a guess at a configuration of iron and conductors and at values for their properties (ie. permeability curve and current density) which his experience indicates will meet the constraints and produce a reasonable design. This is the step which we are furthest from being able to do on a computer.

The next step is to set up a discrete model. As is usual with a continuum problem such as this, a model must be constructed which approximates the real problem by a finite number of discrete elements. As the number of elements is increased and their size decreased, the results of the analysis should converge to a true solution of the continuum problem. Figure 5 shows an example of such a mesh. The total number of elements will be limited in practice by the computing power available. It is therefore important to suit the size of elements to the local needs of the geometry. The decision on how to distribute the elements has normally been taken by the designer, although some progress is being made towards allowing the program to optimise this choice.[1]

The next step of analysing the model is the only step which can be done without human intervention.

For a given guess at the geometry and current densities, it will be necessary to try several models of increasing refinement to get a reliable measure of the error introduced by the model. The decision as to what criteria to apply to the results of the analysis in deciding whether the model is sufficiently refined is certainly also a long way from being suitable for an automatic algorithm.

Similarly, the designer is almost always involved in deciding whether a particular guess has satisfied his constraints. It is usually much easier for him to make this decision than it is for him to specify his constraints to a computer in a general form. Usually his constraints will not be met until he has refined his guess at the solution several times. Indeed, sometimes this loop is never left because of time limitation, and the resulting design is a compromise. When the constraints are satisfied, he may refine his guess in order to try to reduce the value of the function he is trying to minimise.

It is clear from this description of the design process, that most of the decisions are taken by a human. We hope to show that the techniques of interactive graphics are a valuable tool in making these decision as easy and as fault-free as possible.

3. REVIEW OF INTERACTIVE GRAPHICS TECHNIQUES

An interactive graphics system consists of the hardware and software necessary to allow a fluent dialogue between man and computer with input and output in some graphical form. Systems with a wide range of sophistication and cost are employed in many applications. The usual medium for high speed graphical output is some form of cathode-ray tube (CRT). One convenient way of classifying these is into storage tube devices and refresh devices. Refresh devices can be either raster scan or directed beam. Each type of device has advantages and disadvantages which make them best suited to certain applications.

In a refresh CRT (of which the domestic television set is an example) an image is sustained by repeatedly reproducing the necessary electron beam at a rate which is fast compared with the natural persistence of the phosphor on the screen. A small computer or part of a large computer is devoted to this task of refreshing. With a raster scan device the information is stored in the computer in a line by line digital form. This data is scanned and reproduced on a TV type monitor. With a directed beam device, the electron beam can be directed to any part of the screen. Different parts of the screen can be illuminated in any order.

In a storage tube, each image is produced once and is continuously refreshed by the hardware of the device. The picture can be added to indefinitely and will remain in view. When a different picture is needed, the whole screen is erased with a bright flash, and a new picture can be stored. Storage devices all use directed beam techniques.

Various hardware options are available to perform graphics functions more quickly than with software. The following list gives an indication of what is available:

1. Character Generation.
2. Vector Generation.
3. Curve Generation.
4. Blinking or Flashing.
5. Dotted or Dashed Vectors.
6. Range of Character Sizes and Fonts.
7. Translation.
8. Scaling.
9. Rotation.
10. 3D Transformations
11. Windowing and Clipping.
12. Multiple Intensity Levels.

The advantages of directed beam refresh devices are that the picture can be partially or completely changed between refresh cycles thus simulating dynamically changing data, and hardware transformations can be implemented comparatively easily. All refresh devices can support a range of intensity levels. The disadvantages are that they are comparatively expensive (£10K - £40K), and the amount of information which can be displayed is limited by the onset of an irritating flicker when the time taken to reconstruct the picture becomes greater than the persistence time of the phosphor. They also require either an extra independent small computer, or some fraction of the store and processing power of a large computer. They are most suitable for applications involving a limited amount of information which is changing rapidly (eg. monitoring air traffic).

The advantages of raster scan refresh devices is that the information content can be much greater, and the monitors can be good quality TV tubes which are comparatively cheap. Several monitors can be attached to

one controller. Domestic colour TV sets can also be adapted. The cost is in the region of £10K. They are most suitable where good quality pictures containing much detail including grey scales are needed and when the data changes rapidly. They become economical when several monitors are required all showing the same picture. The disadvantage is that hardware transformations are more difficult because of the way in which the information is stored.

The advantages of storage tubes are that they are cheap (£2½K - £5½K), that they never flicker, and that an unlimited amount of information may be displayed. The disadvantage is that even if only a small part of a picture is to be changed, the whole screen must be erased (½ sec) and the whole picture redrawn. The time taken to redraw will depend on the amount of information and the line speed. Most cannot support a range of intensity levels. They are most suitable for applications where a large amount of data is to be displayed and erasure is only necessary at comparatively infrequent intervals.

One device is available which attempts to obtain the best of both worlds. This stores the picture on a small storage tube with the facility for selective erasure, and repeatedly scans this tube to reproduce the picture on a TV tube. Selective erasure is obtained by switching the device into erase mode and 'drawing' the vector or character. These devices are not common in the United Kingdom, and no first-hand experience of their use is available.

For graphical input, a range of devices is available:

1. Keyboard.
2. Function switches.
3. Cursor control device.
4. Light Pen.

For some purposes, such as providing numerical values, the keyboard is probably the best device. The function switches are really a special purpose extension of the keyboard. Typically a bank of 16 push buttons is provided with a choice of metallic overlays which identify the meaning allocated to each switch for a particular application program.

However, for many purposes it is more convenient to be able to interact directly with the picture. The most universal way of doing this is to provide a small cross on the screen called a cursor, which can be moved around the screen in a continuous manner by some mechanical device under manual control of the user. Even storage tubes can have a cursor which operates in a dynamic refresh mode. The user will move the cursor until it coincides with the part of the screen he wishes to indicate and then operate some switch which will cause the two co-ordinates of the cursor position to be sent to the program. Many devices are available to control the cursor position. The device which is currently gaining most popularity is called a Mouse. This is a hand-held object which runs on wheels over any horizontal surface. Two orthogonal wheels keep track of the movements. A few finger-operated button switches may be included, thus adding limited function switch capabilities. Other devices are a tablet with stylus, a tracker ball, a joystick, or a pair of orthogonal wheels mounted on the graphics terminal.

The light pen, which is only available on refresh devices, operates by detecting light on the screen when held next to a part of the picture. It can inform a program immediately which picture component is being indicated. Some recent refresh devices allow the light pen to return the co-ordinates of the screen position within a limited accuracy. The light pen can also be used as a cursor control device.

The advantages of cursor techniques are that they can be used on both storage and refresh devices, and that they can indicate positions on the screen which are not illuminated. The disadvantage is that in order to find which part of a picture is being indicated, a software search of the picture co-ordinates must be performed. This may be a slow process for a large amount of data.

The advantages of the light pen are that it can indicate picture parts without a search and that it is a more natural way for a user to operate. The disadvantages are that it cannot be used with storage tubes, and that it cannot indicate positions on the tube which are not illuminated. Some users of light pens find the arm position tiring over a long period and object to the arm obscuring part of the screen.

Connections, between graphics terminals and the computer containing the application program, can range from intercontinental satellite and telephone lines to short fast dedicated lines. If a refresh tube is to be connected over a distance (by telephone line for example) a local small computer will be needed to refresh it. This should be taken into account in cost comparisons.

Computers to which such devices are attached range from a small minicomputer acting as a message switcher in a network, through dedicated medium-sized computers, to large multiprogramming computers.

Since software is becoming an increasingly expensive component of any system, portability between different computers and different graphics devices is becoming of paramount importance. Standardisation amongst graphics packages is a long way from that obtained by Fortran for example. To some extent this represents an inherent difference in capabilities between different types of device.

The choice of a configuration will depend on what equipment is already available, whether the equipment chosen must also suit other applications apart from magnet design, and what the demands on the facilities are likely to be. At the Rutherford Laboratory we have chosen storage tubes with limited cursor control attached to a medium-size real-time computer (GEC 4080) with a fast link to a number crunching host computer. The magnet design application can be programmed in such a way that the disadvantages of a storage tube are not serious compared with the advantage of being able to afford several terminals in simultaneous use to service a large user population. Experiments are also in progress with a refresh device to which hardware for three-dimensional rotation, scaling, and translation, developed at the Laboratory[2], has been added. The value of dynamic rotation to portray three-dimensional depth is being estimated.

4. AREAS WHERE THESE TECHNIQUES CAN BE APPLIED

The techniques of interactive graphics have five main uses in the design process.

1. Making subtle errors in the data clearly obvious.
2. Allowing these errors to be corrected immediately.
3. Displaying the mesh model for evaluation.
4. Allowing this model to be edited easily.
5. Displaying the results of the analysis in graph or contour map form for rapid evaluation.

Four areas of application will be examined in detail.

4.1 Data Specification. The main functions of interactive graphics in data preparation are assistance in detection of errors and allowing immediate correction of errors. There are two types of error. The first can be detected by the program because of internal inconsistency. (For example, if two adjacent nodes in a polyhedron are given identical co-ordinates.) The interactive facility allows the user to be informed at the time he inputs the faulty data, and he can correct it immediately while his attention is still focussed on the problem.

The second type of error is more serious because no program can detect it. A typical example is a mis-typed figure which results in data which is completely consistent but totally false. If Figure 3 is compared with Figure 4, the benefits of graphics should be obvious. A good interactive graphics program will display each item of data graphically as it is entered. It will also take every opportunity, subsequently, of displaying all aspects of the data to the user in the hope that subtle errors will be detected as soon as possible. In the batch mode, much computing time and designer time is wasted on such faulty data. Indeed many subtle errors are never detected with disasterous consequences for the accuracy of the results.

Several methods have been used to facilitate the definition of three-dimensional objects. Sutherland's original Sketchpad[3] system was extended to three dimensions by Johnson.[4] This allows the user to define dimensions on the screen with a light pen. Sutherland[5] has also developed a technique for simultaneously digitising orthogonal views of a three-dimensional object. The accuracy of such methods is generally not sufficient for defining details of the geometry of magnets. Numerical data is best input on a keyboard. Notley[6] devised a

language for describing the creation of 3D objects. This would need developing to make it competitive with alternatives. Braid[7] uses a finite set of unit primitives which can be moved, rotated and scaled to synthesise a general solid. His work is aimed at producing tapes for numerically controlled machines. Newman et al[8,9,10,11] in the original implementation of the GFUN program used a set of shape codes whose dimensions were defined using a parameter format. Newman's MOD3D package (see Section 6) also uses a set of primitives to synthesise a general solid. His POLLY language forms an efficient way of specifying the dimensions in a natural way which is easy to use.

4.2 Generation of the Mesh Model.

4.2.1 Two Dimensions. Much work has been done on algorithms for automatically sub-dividing generally shaped two-dimensional regions into suitably graded finite element meshes. Pathalogical geometries can usually be found for which any algorithm will either fail, or produce unsuitably distorted meshes. With a range of algorithms available, it is generally possible to select one which will solve the problem. Alternatively details of meshes can be refined by hand using light pen or cursor techniques. Reid's algorithm[12] for triangulating multiple regions with included voids consists of superimposing a single equilateral triangle over the whole domain, and sub-dividing until local boundary constraints are met. The user can specify local grading of the mesh size. Beretta et al[13] use a different approach. A general polygon is automatically divided into a combination of triangles or quadrilaterals by joining nodes. Algorithms are available for further sub-division allowing for all the special cases which may arise. Andrews et al[14] use a version of the Winslow[15] technique. They superimpose a regular triangular mesh over a general polygram (optional arcs for sides) and move nodes near the boundary to lie on the boundary. Finally, internal nodes are relaxed to remove local distortions by moving each in turn to the average of its neighbour's co-ordinates. This algorithm at present only handles single regions and cannot grade the mesh size within a region. Newman[16] produced an interactive graphics version of the TRIM[17] mesh generator. This is aimed at producing a mesh over a rectangular domain including all conductors and air spaces for a finite difference program. Mesh size can be graded within the limitation that the mesh must be topologically uniform. Jones[18], Zienkiwicz et al[19], Gordon et al[20], and Newman et al[8,9,10,11] all use variations of a common algorithm. A general polygonal region is mapped on to a unit regular polygon of the same order by a polynomial mapping. Butlin's method[21] is similar and has been extensively developed for interactive use. Libraries of meshed sub-structures can be created for subsequent use. These methods are simple and inexpensive to implement and work well provided the polygon is convex and not too far distorted from the regular polygon. Frederick et al[22] have yet another algorithm which synthesises a mesh based on a crude set of nodes digitised by the user. Martin et al[23] use a combination of automatic fitting of a regular mesh to the boundary and use of a light pen to touch up unsuitable areas.

4.2.2 Three Dimensional. No algorithm is known which will automatically generate a suitably graded mesh for a generally shaped three-dimensional domain. If the problem is 2½D (ie. problem of finite length with uniform cross-section) the two-dimensional algorithms can be used for generating a mesh over the cross-section and some simple algorithm used to sub-divide the length.

For truly three-dimensional problems, most success has been obtained by extending the two-dimensional method of polynomial mapping to handle general polyhedra. Newman et al[8,9,10,11] have used this technique in the GFUN magnet design program. Hexahedra are mapped on to a unit cube, for example. This can be sub-divided by a specified number of planes in each of the three basis directions. Each sub-cuboid can be further sub-divided into a specified number of tetrahedra. Kamel et al[24], and Cook[25] each adopt a similar approach. Grading of the mesh size is not automatic. The full power of interactive graphics techniques is needed to allow the user to display sub-sections of his mesh so that he can visualise the process, and decide how to distribute his available elements for maximum efficiency and accuracy. The mesh shown in Figure 5 was obtained from the GFUN program using this technique.

4.3 Refining the Mesh Model. If his analysis shows model dependence, the designer will want to examine his mesh and refine it. He will use his

judgement to decide which parts of the model need a finer mesh, and which parts are possibly unnecessarily refined. This process is highly interactive, and clever use of graphics techniques is needed to highlight the problem area amongst a wealth of data.

4.4 Evaluating the Results. Sometimes the efficiency of a design can be computed as a single number, or a small table of numbers. More usually, the designer will require to know the variation of some property (field uniformity for example) over a one, two or three dimensional domain. He will want this information displayed as a graph or contour map. His choice of domain may depend on the results themselves, and so he needs to be able to interact quickly with the results to re-display them in the best way. This is another ideal application of interactive graphics. Figure 6 was created by the GFUN program. It shows the position and value of the peak field experienced by some superconductors.

5. REVIEW OF MAGNET DESIGN PROGRAMS USING INTERACTIVE GRAPHICS

The first reported use of interactive graphics for magnet design was a conversion of the TRIM[17] batch program. This is a two-dimensional program using finite difference methods and including variable permeability iron regions. The regions in real space are mapped on to a regular triangular mesh in logical space by allocating each real node a pair of logical co-ordinates. The numerical process invoked simulates the effect of pinning an infinitely elastic sheet containing the regular mesh to the real boundaries at the specified positions. The resulting shape of the mesh is identical to the minimum energy configuration of the elastic sheet.

Colonias[26] has adapted TRIM to use a refresh graphics device with light pen on a CDC 6600 computer. Logical co-ordinates are picked out using the light pen and the corresponding real co-ordinates are input on the keyboard. The resulting mesh is displayed and can be edited with the light pen. Contour maps of flux distributions resulting from the finite difference analysis are also displayed. Newman[16] has also written the MNEMONIC program which is a similar adaptation of TRIM. This is implemented on a Computek 400/15 storage tube attached to an IBM 360/195 computer. No cursor facility is available, so all input is via the keyboard. Lari[27] implemented a system using a Tektronix T4012 Storage Tube with cursor on an IBM computer. The cursor is used to specify the logical co-ordinates and to edit the mesh. The results are displayed as tables, graphs, or contour maps. Lari[28] also adapted the MAGNET[29] program for the same hardware. This program allows a limited variety of infinitely permeable iron boundaries.

The next major program to be produced was GFUN[8,9,10,11] which was the first magnet design program written to make use of interactive graphics. The formulation involves an integral equation which has the advantage of needing a mesh only in the non-linear iron regions. It was also easily extended to three dimensions. All input is by keyboard using a convenient parameter format. The hardware is identical to that described for MNEMONIC. The geometry and the mesh are displayed and can be edited. Data defining particular designs can be stored as a named file on a private data-set. Simple problems can be analysed on-line and also some automatic optimisation can be invoked. A harmonic analysis of the resulting field can be displayed. Results can be displayed as tables, graphs, or contour maps. GFUN has been implemented on many systems in many countries. Work is currently in hand (see Section 6) to improve the interactive graphics facilities and to split the tasks between a minicomputer and the main computer.

Martin[30] has written the MAGINT program for conductors only, which is aimed at plasma containment problems for fusion research. Data input is by keyboard, and graphics output is on a Cossor CSD 1000 refresh tube. Display of results includes surface plots with removal of hidden lines.

6. RUTHERFORD LABORATORY COMPUTER-AIDED DESIGN SYSTEM

Apart from a few special programs, the operation of the central computer at the Rutherford Laboratory, an IBM 360/195, is aimed at satisfying a large demand for batch processing. The GFUN interactive graphics magnet design program (one of the special programs) occupies 210 Kbytes of memory for several hours each day, but only uses the central processor for a few per cent of that time. We are in the process of transferring the interactive graphics part of the program, which does not need such a powerful computer, into a medium size computer, a GEC 4080. The hardware

and software of this computer is aimed at the interactive environment. When functions are requested which do need the power of the main frame, a batch job will be launched via a high speed link, and the output from this job retrieved along the same route. This method of operation will improve both the batch efficiency in the main frame and the interactive service. Several simultaneous users will be allowed without the schedule being restricted to two hours for a single user as at present. Since it was necessary to redesign the program for a new environment, we are taking the opportunity of splitting the program into several well defined modules. Each of these will take the form of a Fortran package which could be used for many applications apart from magnet design. With a view to such future developments, a data-base has been designed so that a stress analysis program, for example, could use files containing data for a magnet design and calculate the forces in such a structure. Figure 7 shows the structure of the GFUNMINI system. Five main processes are incorporated:

1. GEOM Geometry Definition
2. MATP Material Properties Definition
3. FEMG Finite Element Mesh Generation
4. ANAL Analysis
5. RESU Result Interpretation.

These processes communicate via files on the database. The file management process FILM handles all GFUNMINI files which are accessed through the data-base manager DBM process. The DCOD process does syntax decoding and error diagnostics for messages received from the keyboard. The DOCU process provides the user with instant up-to-date documentation, also from the data-base. The JOBS process handles communication with the main frame.

6.1 Geometry Definition (GEOM). The purpose of this package is to allow the designer to specify the geometry of iron and conductor regions to the computer with the minimum amount of information. The package also provides graphics illustration of the data as it is being specified, so that errors can be detected and corrected immediately. The keyboard is the main input device since specific numerical values for dimensions need to be supplied.

To facilitate data entry, only a limited number of simple shapes can be defined, and complex general shapes must be synthesised from these. Only closed surfaces which are convex and homeomorphic to a sphere (ie. genus zero) may be used. However, surfaces may intersect, and a region may be defined to be a logical combination of the union or intersection of two or more surfaces or their negations. The three-dimensional shapes are based on the following set of two-dimensional shapes:

1. Triangle
2. Quadrilateral
3. Parallelogram
4. Polygram
5. Circle
6. Sector

A polygram is a polygon, each side of which may optionally be an arc of a circle. Three families of three-dimensional shapes are built from these

1. Cone
2. Prism
3. Surface of Revolution

A cone is defined to be the closed surface formed by a line with one end at a fixed point (vertex) and the other tracing out a closed two-dimensional curve (directrix). The directrix may be any of the six two-dimensional shapes.

A prism is defined to be the closed surface formed by joining corresponding nodes of two similar two-dimensional shapes taken from the same set. The end faces are planar. Each other face must be either planar, or part of the surface of a cylinder or cone. For similarity, both end shapes must have the same number of nodes, and corresponding sides must have the same curvature. Each end face of the prism may be optionally inclined to the axis of the prism which itself may be in any direction. The end faces may be defined as congruent.

A surface of revolution consists of the closed surface defined by rotating

one of the two-dimensional shapes about a given axis by a given angle.

The following set of three-dimensional primitives are available at present. The user specifies a four letter name, and the system understands the symmetry inherent in each figure.

FAMILY	2D SHAPE	CONGRUENCE	NAME
CONE	TRIANGLE	-	TETRahedron
CONE	QUADRILATERAL	-	PYRAmid
CONE	CIRCLE	-	CONE
PRISM	TRIANGLE	YES	TPRIsm
PRISM	TRIANGLE	NO	WEDGe
PRISM	QUADRILATERAL	YES	QPRIsm
PRISM	QUADRILATERAL	NO	HEXAhedron
PRISM	PARALLELOGRAM	YES	BRICk
PRISM	CIRCLE	YES	CYLInder
PRISM	POLYGRAM	YES	PPRIsm
REVOL.	CIRCLE	-	SPHEre
REVOL.	CIRCLE	-	TORUs

These primitives are illustrated in Figure 8. The designer first conceptually divides his general three-dimensional shape into regions which can be formed from these primitives. Each surface is defined using the POLLY language which is decoded by the package and stored as a set of three-dimensional co-ordinates. The co-ordinates of a node can be specified in four ways.

1. Three numeric values separated by one or more spaces.

2. If only one or two of the co-ordinates differ from the last node defined, one or two alphanumeric fields in free format.

3. An incremental version of 2.

4. By the cursor, if it coincides with any previously defined node.

The incremental alphabetic codes are U or D for up or down, L or R for left or right, and O or I for out or in, each with respect to the screen basis. For codes to define absolute co-ordinates as opposed to incremental, T is added to these codes. If the direction of the edge being defined is not along the screen basis directions, several codes can be combined on a single line, and a vector sum will be taken. The numeric value follows immediately after the code letter in free format.

For example, to define an orthogonal block 40 x 20 x 5 units, the commands would be:

SHAP = BRIC (defines 3D primitive)

Ø , Ø , Ø (defines co-ordinates of corner)

R4Ø (defines the first edge)

U5 (defines next edge and complete end face, since opposite edges of a brick are parallel)

02Ø (defines third basis vector, and the complete brick)

The object is developed on the graphics tube as each item of data is specified. Any error can be immediately erased by typing the privileged code E.

Various display options will be available. The user will be able to scale, move or rotate his objects, and view them with one of the following set of projections:

1. Cabinet projection (default)

2. View from infinity

3. Perspective view

4. Hidden line perspective

5. Stereo wire frame perspective pair.

An example of the hidden line perspective view is shown in Figure 4. If the object has planes of symmetry, these can be specified to reduce the amount of data even further. The data can be edited and stored on the data-base.

6.2 Finite Element Mesh Generation This will be a suite of packages, each of which can take a geometry file and sub-divide it as automatically as possible into small elements (tetrahedra, or triangular or quadrilateral prisms). The first to be implemented uses the same technique as the present GFUN program. A hexahedron, for example, is mapped by a polynomial mapping on to a unit cube. The user may specify a number of planes in each of the basis directions to sub-divide this cube. Each smaller cuboid can be further sub-divided into a specified number of elements in a regular way. The mapping is inverted to find the co-ordinates of the elements in the original hexahedron. (See Figure 5.) This method is cheap to compute and effective, provided the general polyhedron is not too far distorted from the equivalent regular polyhedron. Other algorithms will be added in a modular fashion. Mesh files are also stored on the data-base.

The analysis process (ANAL) will collect data from a specified set of geometry and mesh files and material property files, and submit a batch job to the main frame. When the result file is available on the data-base, the RESU process will be used to display the results in a similar fashion to that employed in the present GFUN program (eg. Figure 6).

Each process is coded in standard ANSII Fortran to ensure a high degree of portability between machines. The data-base manager uses the standard data management software available on all similar computers, the unit of data being a sequential file. The graphics package is GINO-F.[31] This is also almost all in Fortran and provides a high degree of device independence. It is also available at many centres.

Such a system could form a basis for a network of interactive graphics computing facilities. A small remote station could consist of a cheap storage tube (eg. Tektronix T4010) connected by telephone line to a remote graphics computer (eg. GEC 4080) containing the CAD system software. Users whose demands were greater could have a local graphics computer serving several terminals.

7. CONCLUSIONS

Magnet design has progressed a long way since 1960 when the beam transport magnets for the Nimrod Accelerator at the Rutherford Laboratory were designed. Computers were much less powerful, and experience in even two-dimensional magnetostatics programs was limited in the United Kingdom. The design process consisted of building small-scale model magnets (6 months from start of paper design to delivery of model) and constructing special apparatus to measure the very accurate fields involved. Refinement of the model in the best case consisted of using non-magnetic jacks to support varying thicknesses of steel shim on the pole-pieces, and experimentally determining the optimum shim size. In the worst case, part or all of the model had to be machined.

Not only can the whole design be done in a fraction of the time now, but the resulting design is often closer to the ideal requirement because experimenting on the computer is a comparatively rapid process. When a large project is to be designed and built, it is important to keep the design time within reasonable limits without launching into production with an inferior design. It is this problem to which the techniques of interactive graphics are so well suited. The designer is able to make full use of the computer while being able to concentrate on the aspects of the design for which he is best suited.

There is still room for refinement of techniques in several areas. General three-dimensional mesh generators with automatic grading of the mesh size will be a major step forward. Several techniques for displaying three-dimensional objects on a two-dimensional screen need to be experimented with. The possibilities of networks need to be exploited.

Magnet design is a large potential growth area for interactive graphics. As hardware costs come down; as machine and device-independent code becomes a reality; and as networking makes powerful facilities available remotely, it will be surprising if such techniques do not become

common-place for magnet design within 5 years.

8. REFERENCES

1. Leyvraz, R. Iterative Generation of Optimal Triangular Grids for the Solution of 2-Dimensional Field Problems. Proc. COMPUMAG Conf. on the Computation of Magnetic Fields, Oxford, April 1976.

2. Holmes, M and Thorne, A R. The Design of a Graphics Processor. RL-75-190, 1975.

3. Sutherland, I E. Sketchpad, a Man-Machine Communication System. Proc. Spring Joint Computer Conf., Michigan, May 1963.

4. Johnson, T E. Sketchpad III; A Computer Program for Drawing in Three Dimensions. Proc. Spring Joint Computer Conf., Michigan 1963.

5. Sutherland, I E. Three-Dimensional Data Input by Tablet. Proc. IEEE 62, No.4, April 1974, p.453.

6. Notley, M G. A Graphical Picture Drawing Language. Comput. Bull. 14, No.3, March 1970, p.68.

7. Braid, I C. The Sythesis of Solids Bounded by Many Faces. Commun. Ass. Comput. Mach. 18, No.4, April 1975.

8. Newman, M J, Trowbridge, C W, and Turner, L R. GFUN: An Interactive Program as an Aid to Magnet Design. Proc. 4th Int. Conf. on Magnet Technology, Brookhaven, 1972.

9. Newman, M J, Simkin, J, Trowbridge, C W and Turner, L R. GFUN User's Guide - A User Guide to an Interactive Graphics Program for the Computer-Aided Design of Magnets. RHEL/R244, 1972.

10. Collie, C J, Diserens, N J, Newman, M J and Trowbridge, C W. Progress in the Development of an Interactive Computer Program for Magnetic Field Design and Analysis in Two and Three Dimensions. RL-73-077. Also in Proc.Conf. on Analysis of Magnetic Fields,Nevada, 1973.

11. Armstrong, A G A M, Collie, C J, Diserens, N J, Newman, M J. Simkin, J, and Trowbridge, C W. New Developments in the Magnet Design Computer Program GFUN. RL-75-066. Also in Proc. 5th Int. Conf. on Magnet Technology, Rome, 1975.

12. Reid, J K. Mesh Generation. Proc. Finite Element Symposium, Atlas Computer Laboratory, Chilton, March 1974.

13. Beretta, L, d'Amico, G and Tiramani, A R. TMG - A Program for the Automatic Discretisation of a Plane Region. G2/28-6, ENEL, Milan. 1974.

14. Andrews, D H and Marshall, J F. GFUN Mesh Generator: Status on 27 June 1975. RL-74-108 (revised) 1975.

15. Winslow, A M. Numerical Solution of the Quasilinear Poisson Equation in a Non-Uniform Triangular Mesh. Jnl. of Computational Phys. 1, No.2, 1966.

16. Newman, M J. MNEMONIC: An Interactive Graphics Program to Generate a Triangular Mesh for TRIM. RL-73-126, RHEL/R238, 1972.

17. Winslow, A M. Numerical Calculation of Static Magnetic Fields in an Irregular Triangle Mesh. UCRL.7784.

18. Jones, R E. A Self Organising Mesh Generation Program. J.Press. Vessel Tech. August 1974.

19. Zienkiewicz, O C and Phillips, D V. An Automatic Mesh Generation Scheme for Plane and Curved Surfaces by 'Isoparametric' Co-ordinates. In.t J. Num. Meth. Eng. 3, No.4, pp.519.

20. Gordon, W J and Hall, C A. Construction of Curvilinear Co-ordinate Systems and Applications to Mesh Generation. Int.J. Num. Meth. Eng. 7, pp. 461, 1973.

21. Butlin, G A. Interactive Graphics for Finite Elements. Proc. Finite Element Symposium, Atlas Computer Laboratory, Chilton, March 1974.

22. Frederick, C O, Wong, Y C and Edge, F W. Two-Dimensional Automatic Mesh Generation for Structural Analysis. Int.J. Num. Meth.Eng. 2, No.1. p. 133, 1970.

23. Martin, T J and Sykes, A. Applications of Interactive Computing in a Scientific Environment. Proc. Int. Conf. on On-line Interactive Computing, Brunel, 1972, Vol.2, p.747.

24. Kamel, H A and Shanta, P J. A Solids Mesh Generator and Result Display Package. J. Press. Vessel Technology, August 1974, p.207.

25. Cook, W A. Body Oriented (Natural) Co-ordinates for Generating Three-Dimensional Meshes. Int. J. Num. Meth. Eng. 8, p.27, 1974.

26. Colonias, J S. Calculation of Two-Dimensional Magnetic Fields by Digital Display Techniques. Proc. 2nd Int. Conf. Magnet Technology, Oxford, 1967.

27. Lari, R J. A Graphic, Time-Sharing Version of the Computer Program TRIM for Magnet Design. ANL/RJL-10, Feb. 1974.

28. Lari, R J. A Graphic, Time-Sharing Version of the Computer Program MAGNET for Magnet Design. RUL-R6209, ANL/RJL-11, Nov. 1974.

29. Lamb, W H. Instructions for using Program MAGNET. ANL/WHL-1, April 1964.

30. Martin, T J. The Interactive Design of Magnetic Fields for Controlled Thermonuclear Research. Proc. COMPUMAG Conf. on Computation of Magnetic Fields, Oxford, April 1976.

31. Gino-F, A Brief Introduction to the Facilities. Computer Aided Design Centre, Cambridge, 1973.

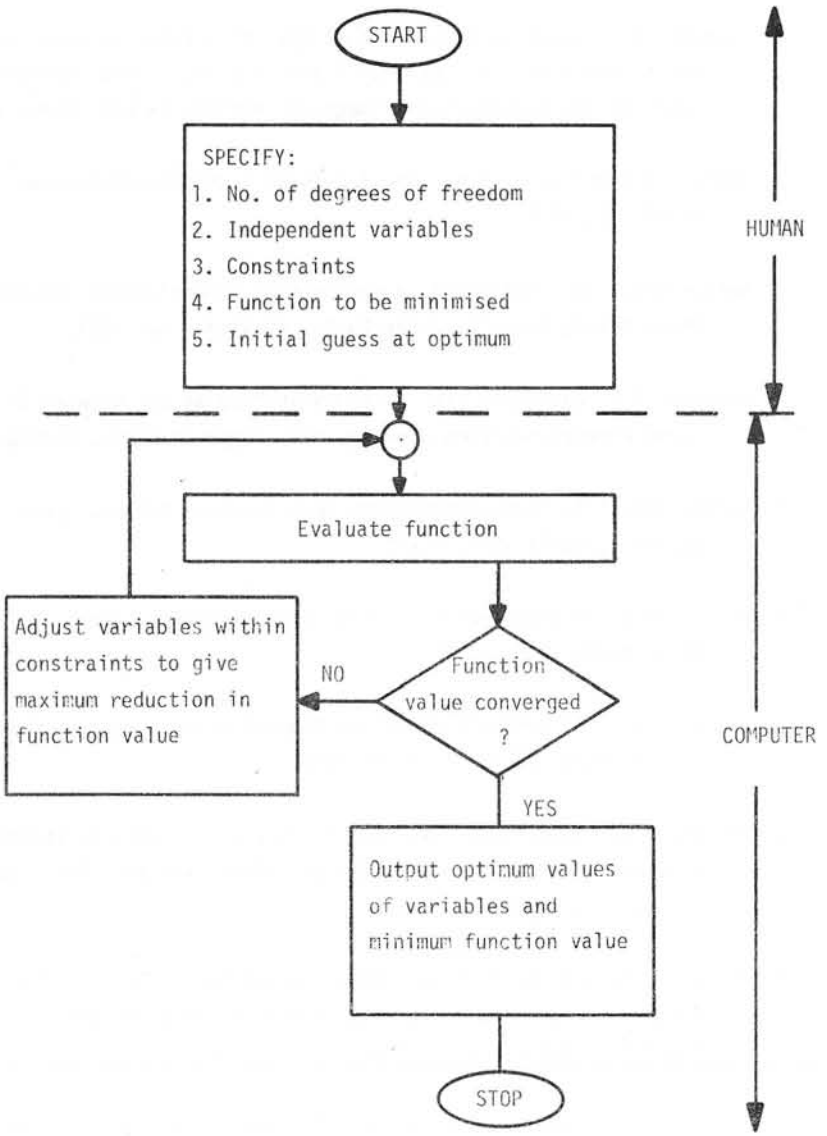

FIGURE 1 - BLOCK DIAGRAM OF OPTIMISATION ALGORITHM

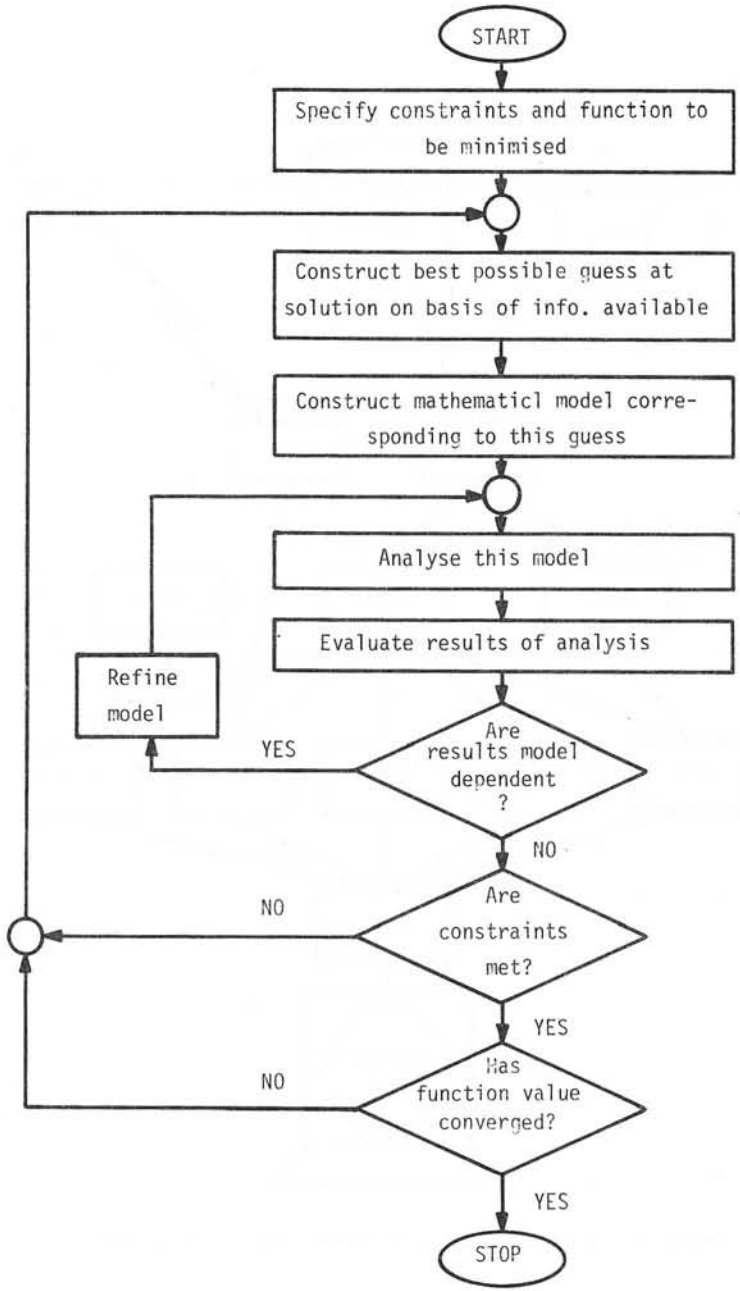

FIGURE 2 - BLOCK DIAGRAM OF DESIGN PROCEDURE

0.0	0.0	0.0	6.83	3.41	0.0	6.83	13.65	0.0
27.3	0.0	0.0	20.48	3.41	0.0	8.19	10.24	0.0
27.3	3.41	0.0	19.11	6.83	0.0	19.11	10.24	0.0
0.0	3.41	0.0	8.19	6.83	0.0	20.48	13.65	0.0
0.0	0.0	27.3	6.83	3.41	27.3	6.83	13.65	27.3
27.3	0.0	27.3	20.48	3.41	27.3	8.19	10.24	27.3
27.3	3.41	27.3	19.11	6.83	27.3	19.11	7.24	27.3
0.0	3.41	27.3	8.19	6.83	27.3	20.48	13.65	27.3
0.0	13.65	0.0	0.0	3.41	0.0	23.89	3.41	0.0
27.3	13.65	0.0	3.41	3.41	0.0	27.3	3.41	0.0
27.3	20.48	0.0	3.41	13.65	0.0	27.3	13.65	0.0
0.0	20.48	0.0	0.0	13.65	0.0	23.89	13.65	0.0
0.0	13.65	27.3	0.0	3.41	27.3	23.89	3.41	27.3
27.3	13.65	27.3	3.41	3.41	27.3	27.3	3.41	27.3
27.3	20.48	27.3	3.41	13.65	27.3	27.3	13.65	27.3
0.0	20.48	27.3	0.0	13.65	27.3	23.89	13.65	27.3

FIGURE 3 - TABLE OF CO-ORDINATES CONTAINING SINGLE DIGIT ERROR

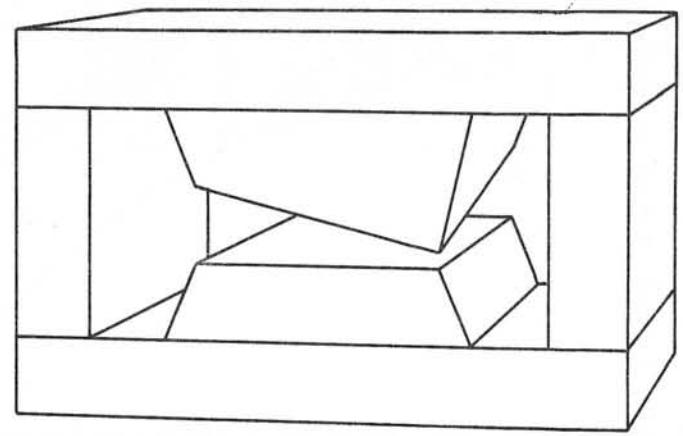

FIGURE 4 - COMPUTER DISPLAY SHOWING ERROR

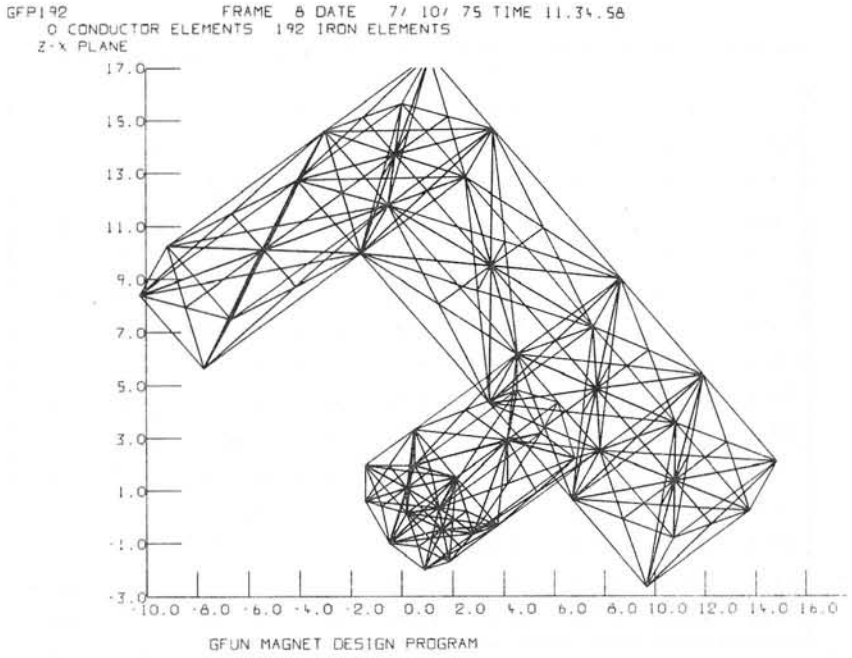

FIGURE 5 - EXAMPLE OF 3D MESH

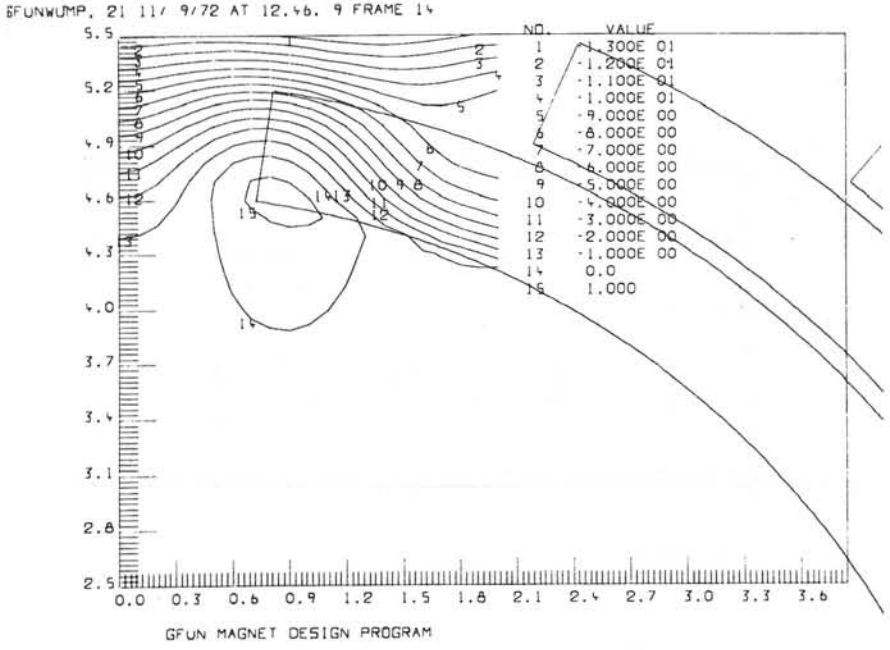

FIGURE 6 - EXAMPLE OF CONTOUR MAP

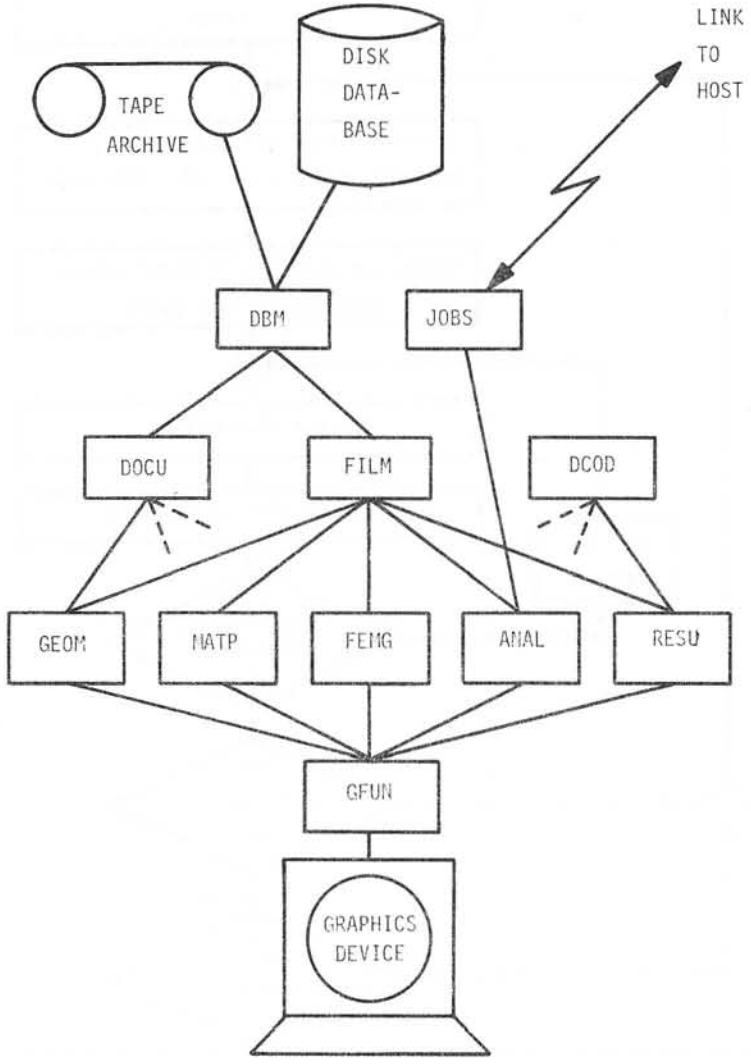

FIGURE 7 - BLOCK DIAGRAM OF GFUNMINI SYSTEM STRUCTURE

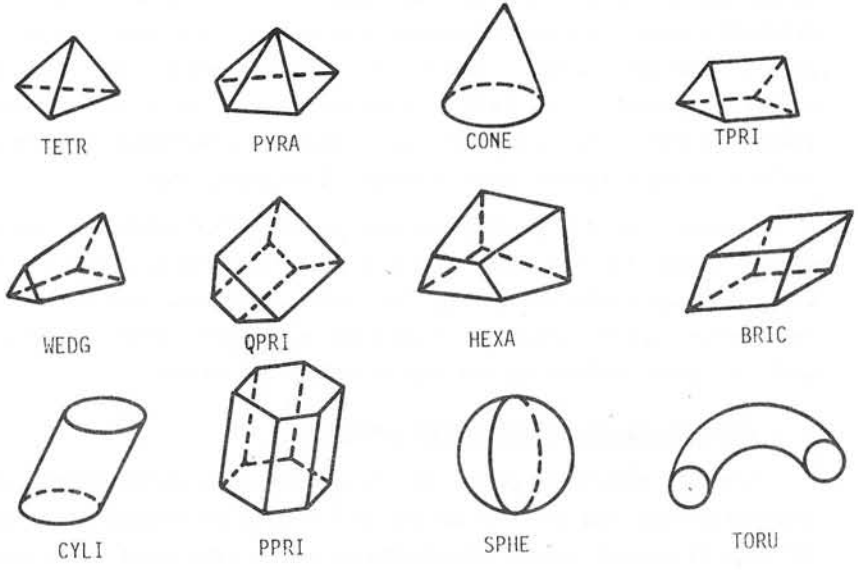

FIGURE 8 - SAMPLE OF 3D PRIMITIVES

Discussion following paper:

(Diserens, Rutherford) What is the future of colour displays in interactive graphics?

(Newman) The development of colour displays is of less immediate importance then monochrome techniques for displaying three dimensional objects. Dynamic rotation and hardware perspection, hidden lines, and intensity variation with depth should be exploited first. If colour can be added independently it would be useful for separating conductors from iron and for distinguishing iron regions of differing permeabilities.

(Jacobs,CERL) You mentioned the development of software to assist users to find mistakes in data input, etc; this must extend to all software development and program usage in the future as software costs increase comparatively fast yet hardware costs will decrease. Could we have your views please?

(Newman) Yes I agree. Fortran, in spite of its lack of flexibility is already accepted as the first language simply because of the guarantee of portability. Standards in graphics packages are already showing some signs of appearing and this again is encouraged by the demand for portable software. There will always be applications for which these standards are in agreement but the vast majority of users will be happy to conform if this saves on software development time. High level interaction packages such as those being developed at the Rutherford Laboratory are a natural extension.

(Luciano, ENEL CRA) I have seen in your review an example of discretization of a plane region ("the front of a church") with holes subdivided into subregions for its discretization. In an improved and more efficient version of that program (paper is available) the mesh may be obtained treating the region with its holes like a whole region, without the need to tear it into subregions.

This means also that data input is much reduced.

THE INTERACTIVE DESIGN OF MAGNETIC FIELDS FOR CONTROLLED THERMONUCLEAR RESEARCH

T.J. Martin
Culham Laboratory, Abingdon, Oxon, OX14 3DB, UK
(Euratom/UKAEA Fusion Association)

1. INTRODUCTION

The controlled release of energy from nuclear fusion depends on the ability to heat and contain an ionised gas (plasma) of deuterium and tritium for sufficient lengths of time, which may be of the order of seconds. Since the particles are charged, a natural choice for the containment system is one based on magnetic fields. Many such experimental systems have been proposed and built to contribute to the understanding of the problems involved in plasma physics.

In the first instance, the magnetic field topology must satisfy certain constraints and much optimisation must take place before an experiment is eventually built. The cost of these devices demands that extensive calculations and evaluations are made at the design stage thus providing the motivation for the development of the computer program MAGINT described in this paper.

It will be appreciated that many physicists and engineers engaged in the design of magnetic containment systems are not interested in programming for its own sake and are understandably reticent about using computer programs which require complex procedures for setting up data and producing results. A good user image is essential therefore, if manpower (and computing power) is to be utilised in the most efficient and productive manner. To this end, the interactive, magnetic field design program MAGINT offers comprehensive facilities for the optimisation and evaluation of possible conductor configurations, the results where possible being presented in readily assimilated graphical form.

The vacuum magnetic field is regarded as a superposition of one or more elementary, pre-defined analytic fields (e.g. uniform fields) together with any combination of components produced by the following sets of conductor types:

i. Circular filamentary loops
ii. Rectangular filamentary loops
iii. Linear filaments
iv. Finite, rectangular cross-section solenoids with constant current density distribution

and v. General curvilinear filaments represented by sets of spatial coordinates joined by straight segments.

A whole range of operations are provided to manipulate and calculate these fields within a versatile and easy-to-use framework.

The program is written almost wholly in standard FORTRAN and runs on the Culham ICL 4-70 computer operating under the MULTIJOB regime which provides a fully interactive working environment. Data input to the program is primarily through a conventional teletype and on-line graphical output (generated by the GHOST[1] package) is directed to a COSSOR CSD1000 refresh display. The total store size required by MAGINT is 120 Kbytes and typical runs consume about a minute of processor time.

Section 2 of this paper introduces the philosophy adopted during the initial design and development stage of the program while section 3 describes the facilities in detail. The numerical methods used for field calculations and for following fieldlines are briefly mentioned and in section 5 some examples in the uses of MAGINT are given.

2. PROGRAM DESIGN AND STRUCTURED DEVELOPMENT

For this program we prefer the interactive mode of operation, rather than batch mode, for not only is the user's train of thought uninterrupted, but he will possess specialised knowledge and/or experience which completes the 'iteration loop' in a manual optimisation[2]. Additional benefits are that errors in data input and incorrect usage of the program are picked up immediately, resulting in faster turnround and minimisation of computer time. Disadvantages with the interactive mode are normally restrictions on the size of the program and the complexity of the problem to be analysed, the first being obviated by suitable segmentation of the program. Again by careful programming and selection of optimal numerical methods, it is our experience that useful calculations can be performed on-line for this type of problem. This question is raised again at the end of this section.

During the initial development stage of the program, the following precepts were kept firmly in mind :

i. The program must be easy to use by both inexperienced and expert computer users.

ii. The data input should be kept to an absolute minimum.

iii. The facilities should reflect current requirements and be easily extensible to accommodate growing needs.

iv. Good protection must be provided against misuse of the program.

v. Printed output should be minimal unless specifically requested - immediate graphical output being a more efficient vehicle for the transmission of information.

The strategy adopted for data input consistent with the first requirement is that of a command structure. Every program action is invoked by a four-letter mnemonic keyword and an associated parameter. Any additional information required by the program is requested by issuing a prompt at the terminal. After the action has been carried out, the program returns to the command mode in readiness for the next task. As an example, the following command generates sixteen circular loops equispaced around a given torus (hereinafter, all user-typed information will be underlined):-

```
CMND? TOR 16
RMAJ,RMIN,CURRENT?
? 1.0 0.15 1.27E6
16 TYPE 1 TOROIDAL COILS ADDED
CMND?
```

For the user who is familiar with the program, a facility is provided to switch off the prompts so that faster interaction is made possible. At present about sixty commands are available and are described in more detail in section 3. This form of data input has two main advantages; firstly it is easy to learn and use, and secondly it serves to document particular runs of the program.

The minimisation of information typed by the user is achieved in several ways. All program parameters such as contouring matrix size, accuracy criteria etc. are given sensible default values, commands being provided to change them if necessary. In the same vein, to avoid identifying the type of conductor each time some geometric manipulation is performed, the program assumes a "Currently Active Conductor" type with provision for selecting the alternatives. To avoid repeated input of the same configuration each time the program is executed, sequences are included for storing the geometric details in a magnetic disc file. Finally, specialised commands have been written to take into account any particular configuration symmetry.

The third precept implies a modular program structure so that new facilities can be simply 'plugged in' - an additional advantage being that selected pieces of code may be easily incorporated into other programs.

The final two points are largely self-explanatory; a comprehensive set of diagnostic and error messages being provided to guide the unwary user.

Fig. 1 shows a schematic diagram illustrating the program in its operating environment, the arrows indicating all possible directions of information flow between MAGINT and its hardware peripherals and file storage.

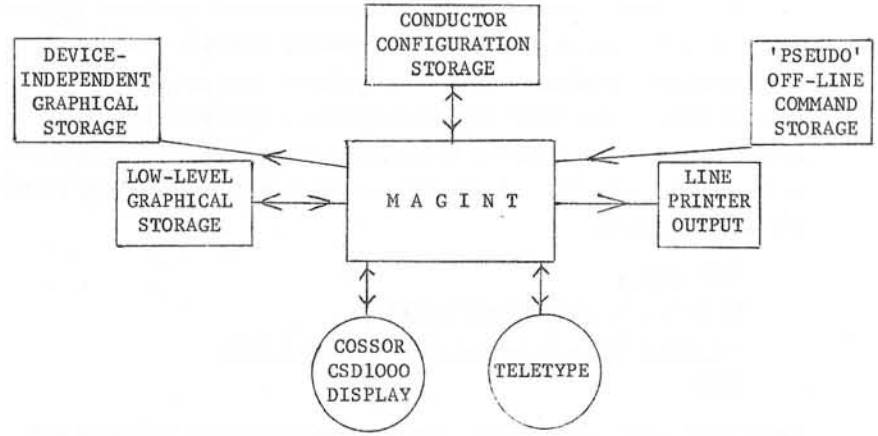

Fig. 1 : Information routes between MAGINT and peripherals

There are of course some aspects of containment system design which require complicated and prolonged calculations such as magnetic surface generation, charged particle and guiding centre trajectory plots. However, MAGINT can be used to set up and verify the configuration before embarking on long (and expensive) batch program runs. A subset of the MAGINT commands that handle conductor manipulation have been incorporated

into a separate input package shared by all the Culham magnetic field programs, thereby creating a completely compatible and uniform user image - a very desirable feature.

3. PROGRAM FACILITIES

All but one of the commands can be classified into five logical subsets, each of which are described in detail below. The exception is the 'USER' command. Provision has been made for executing program actions tailored to suit individual user's requirements. Generally these operations are only of interest to particular people and therefore do not warrant a place in the overall command structure - nevertheless they play an important rôle in ensuring that the designer can perform precisely the operation he has in mind. This facility is introduced by the simple expediency of supplying a FORTRAN subroutine with a pre-defined framework.

3.1 Conductor Manipulation Commands

All of these commands act on the pre-selected conductor type and form a powerful basis with which to speedily assemble the desired configuration. Conductors can be introduced into the system by several means. The 'ADD' command requires a complete geometric specification - for example, if a single solenoid is required centred at the origin with its axis at 45° to the x and y axes, the following would be used:-

```
CMND? ADD 1
XS,YS,ZS,AL,AM,AN,RI,RO,W,CUR?
? 0.0 0.0 0.0 1.0 1.0 0.0 0.5 0.7 0.1 2.75E5
CMND?
```

Right hand screw conventions are used throughout in defining the direction of positive current. Taking symmetries into account, coaxial and toroidal coils can be conveniently distributed by the 'COAX' and 'TOR' commands. For stellarator experiments, 'THLX' is available for generating the toroidal helical windings. It is also possible to interact with the refresh display to draw arbitrarily shaped planar conductors using a tracker cross and ball.

Having established the basic conductor set, commands are provided to perform mirror reflections in any of the three principal planes and to spatially translate and rotate all or specified conductors together with the option of retaining the originals.

A group of commands to alter specific geometric properties of the conductors is also available, thereby saving a user the task of retyping the complete specification. Centres of coils and their orientation together with currents and individual points on curvilinear conductors may be quickly changed.

Finally, the ability to delete all or selected conductors is introduced through the 'DEL' command, the conductors being uniquely identified by a number assigned at generation time.

The use of these commands is demonstrated in section 5 and it can be seen that a particular construction may be performed in many different ways, the user choosing the one which is most convenient.

3.2 Parameter Setting Commands

On entry to the program, certain common variables used throughout the various sections are given sensibly selected values in order to avoid repeated specification. For example, circular filamentary loops are assumed to be the currently active conductor type, others being invoked by use of the commands 'RECT', 'LINE', 'SLND' or 'CURV'. The user can also set up his own limits for graphs (the default being automatic limits); he can specify the relative accuracy at which the solenoid routines operate or select the type of three-dimensional projection for viewing the conductor configuration. Suppression of data prompts (for experienced users) and altering the matrix size containing the magnetic field components are effected through the 'MSG', 'MU' and 'MV' commands.

Commonly used, predefined analytic magnetic fields are selected by 'ANAL' e.g. an I/R toroidal field being established by the sequence

```
CMND? ANAL 4
TOROIDAL CURRENT?
? 2.96E6
CMND?
```

giving the field

$$B\varphi = \frac{2.96 \times 10^6 \, \mu_o}{2\pi R} .$$

3.3 Graphics Commands

Picture information can be handled at two levels; in low-level hardware form using the special instructions related to the COSSOR display or at high, device independent level enabling selected pictures to be processed onto any locally available plotter. 'PSTR' controls whether picture information is retained in a file on disc or only shown once and subsequently lost. In this way picture files can be built up that only contain frames of interest. Commands are available for reshowing, combining and overwriting stored pictures and converting all or selected frames into the device-independent format.

Before any field calculation takes place, it is reassuring for the user to 'VIEW' the conductor configuration in some three-dimensional projection to establish its correctness. (see figs. 2, 3, 4, 5, 6, 7 and 8)

After the magnetic field has been evaluated over some plane, selected quantities can either be contoured (see fig. 10) or three-dimensional, isometric developments of the surfaces can be plotted by the command 'PLTM' (see fig. 11). The matrices of field components are not destroyed, enabling the maximum amount of information to be derived from the relatively costly field evaluations. In addition, the 'BDRN' command plots scaled arrows representing the projected direction and magnitude of the field at each of the matrix grid points giving an overall picture of the field without resorting to expensive fieldline calculations.

3.4 Field Evaluation Commands

This important class of commands uses the Culham magnetic field subroutine library to perform the various operations. 'FLDP' and 'FLDL' respectively calculate the cartesian components of the field and its strength at specified points and along an arbitrary line in space, the latter producing a graph of the four quantities together with an optional table printout. 'FLDC' allows the field to be found around a given plotting circle, the results being presented graphically in either a global or natural local coordinate system (see fig. 9). Again, detailed printout may be obtained if required. The user can also specify an arbitrary, rectangular plane over which the field components are evaluated by the 'FLDM' command, graphical interpretation of the results being performed by 'PLTM' as described in 3.3.

Detailed information about the fieldline structure is obtained from 'FLIN'. The ordinary differential equations of the fieldline

$$\frac{d\underset{\sim}{r}}{ds} = \frac{\underset{\sim}{B}}{|B|}$$

are integrated from a given starting point in both directions until certain stopping criteria operate, the points so obtained being projected onto a given plane and displayed. These pictures can be superimposed on $|\underset{\sim}{B}|$ plots to give a comprehensive idea of the field characteristics (see fig. 10).

Fieldlines for the axisymmetric experiments such as the superconducting Levitron are cheaply generated by the 'RAFI' facility where contours of the quantity $R.A\varphi$ (where $A\varphi$ is the azimuthal component of the vector potential) can be plotted.

3.5 Housekeeping Commands

All or part of the conductor configuration geometry can be directed to the teletype or display by using 'LIST' while the contents of the field component matrices and associated quantities can be sent to an output file which is processed on a line-printer at job termination.

Conductors can be stored and retrieved from a disc file using the 'FILE' and 'READ' options. This facility not only reduces the data input when analysing the same configuration over several runs of the program but also offers additional security against possible system/program failures.

The normal input channel to MAGINT is a teletype, but it is possible, through the 'OBEY' command, to redirect this channel to read commands from a disc file. If any errors are encountered, the program immediately returns to interactive mode for corrective action. In its simplest application, the user might require the same sequence of commands for several different runs of the program.

Finally, provisions are made for adding titles to graphs, obtaining summaries of the assembled configuration and parameter

values and for correctly terminating the program.

4. NUMERICAL METHODS

Closed, algebraic forms derived from the Biot-Savart law for the field due to linear and circular filamentary conductors (the latter involving elliptic integrals of the first and second kind) are well known and are not reproduced here. The rectangular loops and general curvilinear conductors both use the linear segment approximation. Fields due to finite, rectangular cross-section solenoids are calculated from a method by Snow[3]. Essentially, an infinite series representation of the field is generated for a solid, semi-infinite cylinder, four of which are superimposed to form the solenoid, the current directions being arranged in such a manner as to cancel except in the region of interest.

The method used for integrating the fieldline equations is an eighth order hybrid multistep/Runge-Kutta process described by Butcher[4]. To advance the integration from one point to the next, derivatives and function values are used from the previous three steps together with intermediate values calculated within the new step. Large steps can be taken with this method whilst maintaining a high degree of accuracy - in fact the step can prove too coarse for some plotting purposes. This is overcome by fitting a seventh order Hermite polynomial to the last four function values and associated derivatives enabling accurate interpolation within the current integration interval.

5. EXAMPLES OF USE

To illustrate the use of MAGINT, we reproduce below the commands which could be used to construct and view the superconducting Levitron configuration shown in fig. 2.

PROGRAM RESPONSES	COMMENTARY
CMND? COAX 3	Input 3 circular loops coaxial with the z-axis
AXIS 1,2 OR 3?	
? 3	
HT,RAD,CUR?	
? 0.0 0.3 0.5E5	Superconducting ring
? 0.23 0.158 -0.4E5	Inner vertical field coil
? 0.237 0.6 -0.125E5	Outer vertical field coil
3 TYPE 1 COAXIAL COILS ADDED	Confirmatory message
CMND? TRAN -2	Generates remaining B_v coils in upper plane by the save and translate method
COND NO,DX,DY,DZ?	
? 2 0.0 0.0 0.048	Create 2nd inner B_v coil
COND NO,DX,DY,DZ?	
? 3 0.0 0.0 -0.044	Create 2nd outer B_v coil
CMND? RFLT 3	Reflect the four coils in the x-y plane (N.B. Coils in the reflection plane are not duplicated)
4 TYPE 1 CONDUCTORS REFLECTED	
CMND? RECT 1	Select rectangular, filamentary loops
CMND? TOR 12	Generate 12 toroidal B_φ coils
RMAJ,A,B,C?	
? 0.5325 1.2 0.935 0.83333E5	
12 TYPE 2 TOROIDAL COILS ADDED	Confirmatory message
CMND? PROJ 2	Select conical projection
CMND? VIEW 6	Look at complete configuration (fig.2)
XC,YC,ZC,XE,YE,ZE,RI?	
? 0.0 0.0 0.0 90.0 100.0 100.0 1.5	Specify centre of interest, position of eye and the radius of the sphere of interest
CMND?	

A further example demonstrating the power of MAGINT is in the design of a poloidal field coil assembly for the proposed Joint European Torus experiment (JET). We sought to quantify the magnitude of the perturbations in the field caused by the physical connections to the windings and to find the optimum positions such that the perturbations were minimized. Each connection was represented by a five point general conductor and the final distribution is shown in fig. 8 and the corresponding field perturbations around a plotting circle in fig. 9. This calculation would have been prohibitively tedious to perform without the sophisticated conductor manipulations provided by the program.

6. CONCLUSIONS

The computer program described in this paper was developed in collaboration with those people most closely associated with the design of magnetic containment systems and forms the foundation on which future computational aids will be built.

It was pointed out in the introduction that the program is extensible and new facilities are being added all the time as the need arises. Currently, sections to calculate forces on conductors are being implemented and in the future it is hoped to include the effects of magnetic materials.

7. ACKNOWLEDGEMENTS

The author would like to thank his colleagues at Culham Laboratory, particularly C.M. Wilson and C.J.H. Watson, for their helpful comments and criticisms which have greatly contributed to the shaping of the program as it now exists.

8. REFERENCES

[1] Prior, W.A.J., "The GHOST graphical output system user manual" Culham Report CLM-PDN 8/71, Issue 2, 1973.

[2] Martin, T.J. Sykes, A. 'Applications of interactive computing in a scientific environment', ONLINE72, Brunel University, Uxbridge, England, 4 - 7 Sept. 1972.

[3] Snow, Chester 'Magnetic fields of cylindrical and annular coils', U.S. Dept. of Commerce, N.B.S. App. Maths. Series 38, Dec. 1953.

[4] Butcher, J.C. 'A multistep generalisation of Runge-Kutta methods with 4 or 5 stages', J.A.C.M. Vol. 14, no. 1, Jan. 1967, pp. 34 - 99.

Discussions following paper:

(Wind, CERN) Does your program take into account the current flowing in the plasma?

(Martin) Not explicitly- however the modular structure of the program makes it very easy to add such a facility. The plasma could of course be modelled by existing filamentary conductors.

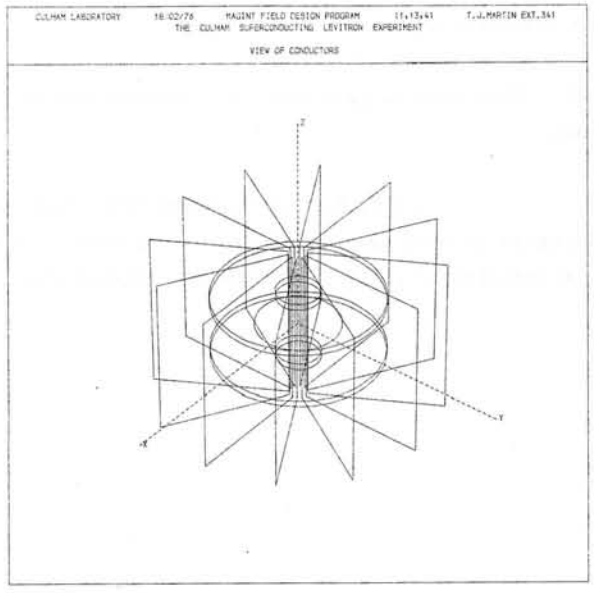

Fig.2 The Culham Superconducting Levitron assembly.

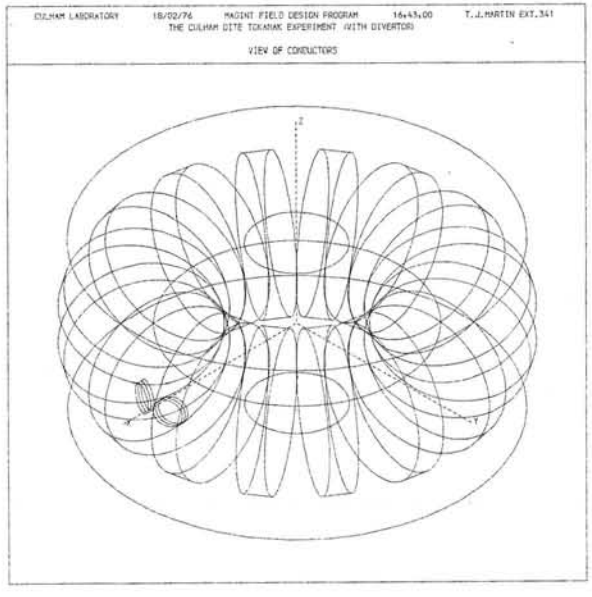

Fig.3 The Culham Dite tokamak experiment with divertor.

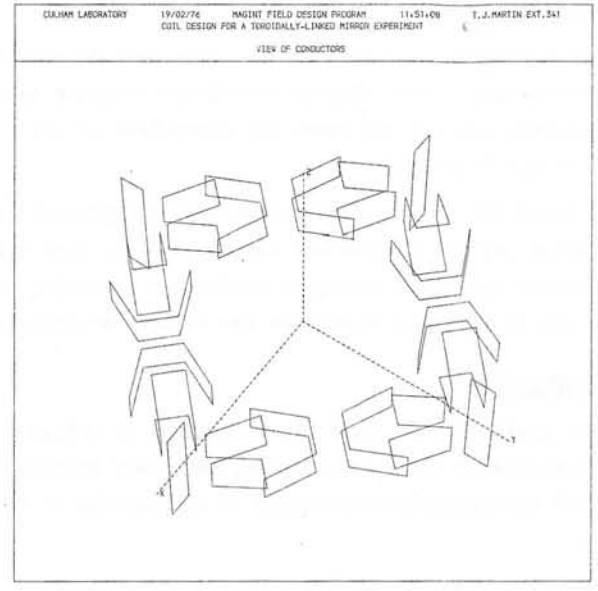

Fig.4 A proposed, toroidally-linked mirror experiment using Yin-Yang coils.

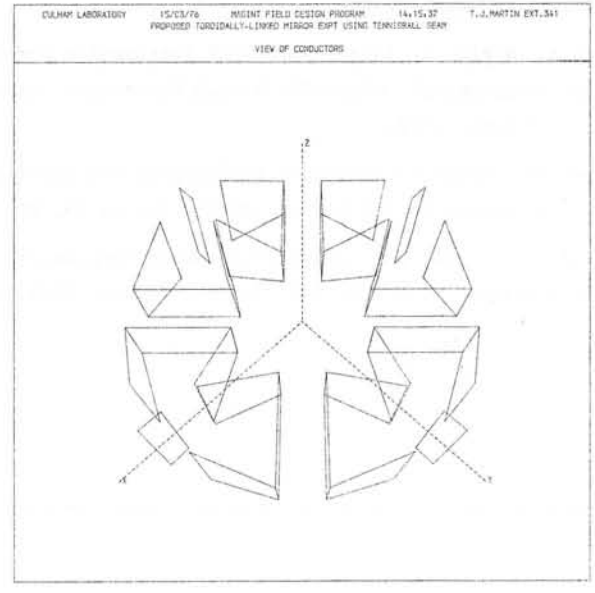

Fig.5 A proposed, toroidally-linked mirror experiment using tennis ball seam conductors.

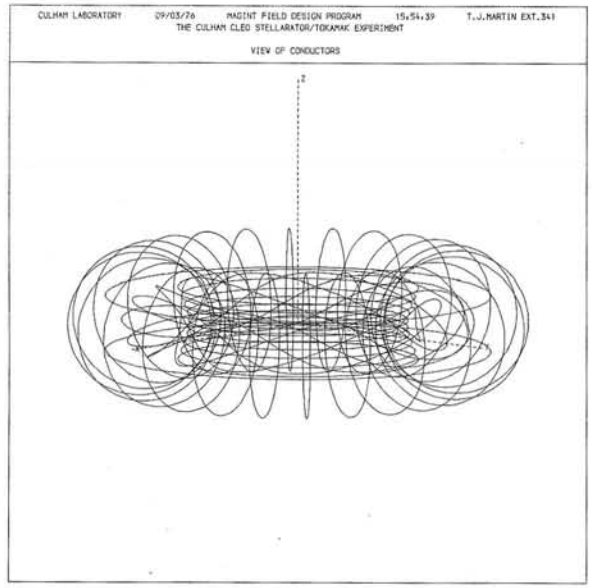

Fig.6 The Culham Cleo Stellarator/Tokamak experiment (general view).

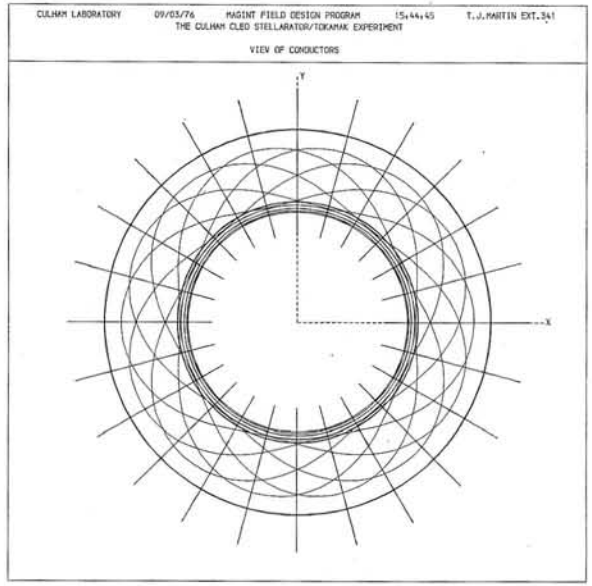

Fig.7 The Culham Cleo Stellarator/Tokamak experiment (plan view).

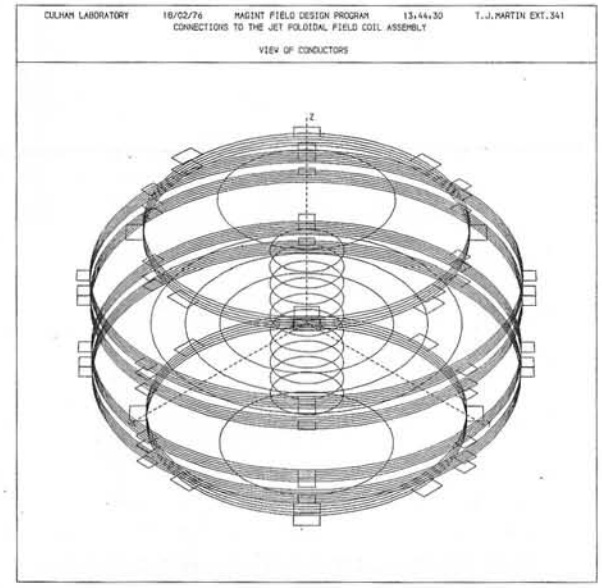

Fig.8 Connections to the poloidal field coils of the proposed JET experiment.

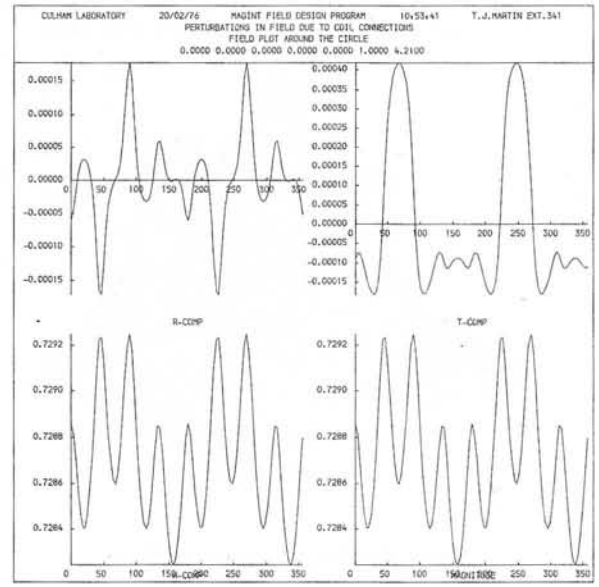

Fig.9 Perturbations in field caused by coil connections (see above).

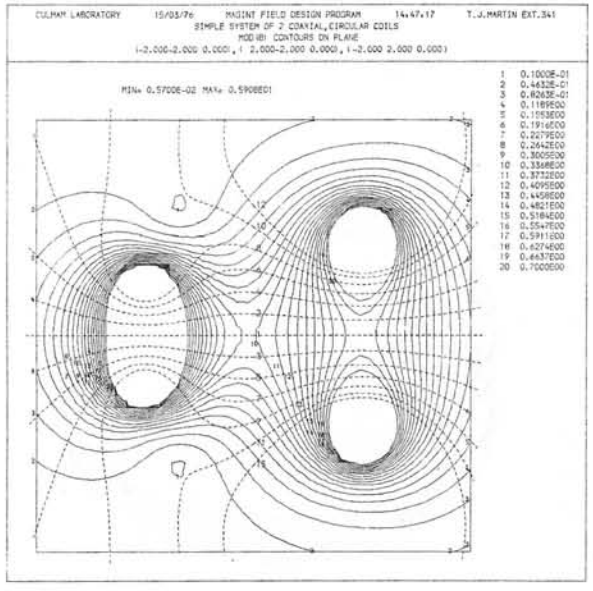

Fig.10 Field lines and $|\underset{\sim}{B}|$ contours for a simple 2 coil system.

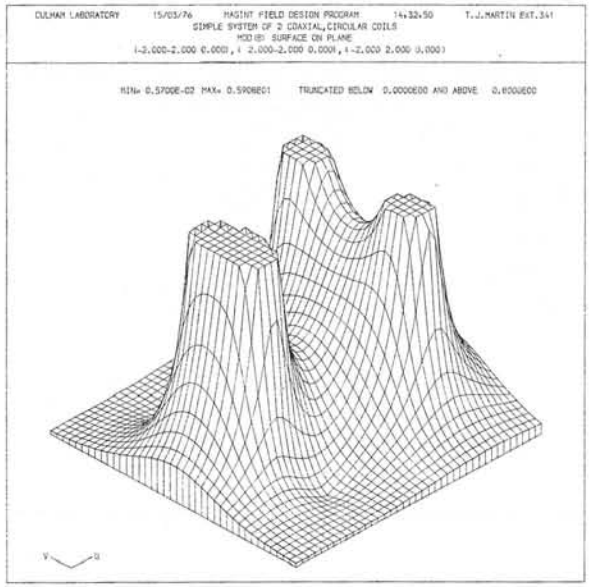

Fig.11 $|\underset{\sim}{B}|$ surface for a simple 2 coil system.

DESIGN METHODS FOR TOKAMAK OHMIC HEATING WINDINGS

A. J. Federowicz, Lois C. Lintner & J. H. McWhirter

Westinghouse Research Laboratories
Pittsburgh, PA 15235
U.S.A.

SUMMARY

The Tokamak Fusion Test Reactor (TFTR) is a device proposed to be completed by 1981 at the Princeton University Plasma Physics Laboratory [1,2]. The device (Figure 1) is planned to achieve a "breakeven" fusion reaction with the assistance of high energy beams of neutral deuterium particles injected into a plasma containing tritium.

The plasma of a Tokamak device is also heated by an electrical current which is electro-magnetically induced by a changing flux generated by an ohmic heating (OH) winding.

The initiation of the plasma is controlled by a hexapole null. A winding to generate this null could be separate but it has been proposed that both the ohmic heating and the formation of a hexapole null be accomplished by means of the same winding. At this reported stage of development the winding to accomplish the hexapole has been considered as a perturbation on the ohmic heating winding and this perturbation is designed in a separate process. However, it is anticipated that, eventually, both design processes should be combined into one. The techniques which have been used in the conceptual design of the OH winding and the hexapole null are the subject of this paper.

The main intent in this paper is to describe mathematical and computational design processes rather than Tokamak technology or design results. The basis of the design method has been the formulation of the design problem in terms of linear expressions and the optimal solution of the design problem by means of linear programming computer codes.

Other approaches to similar design problems are reported in references 3-5.

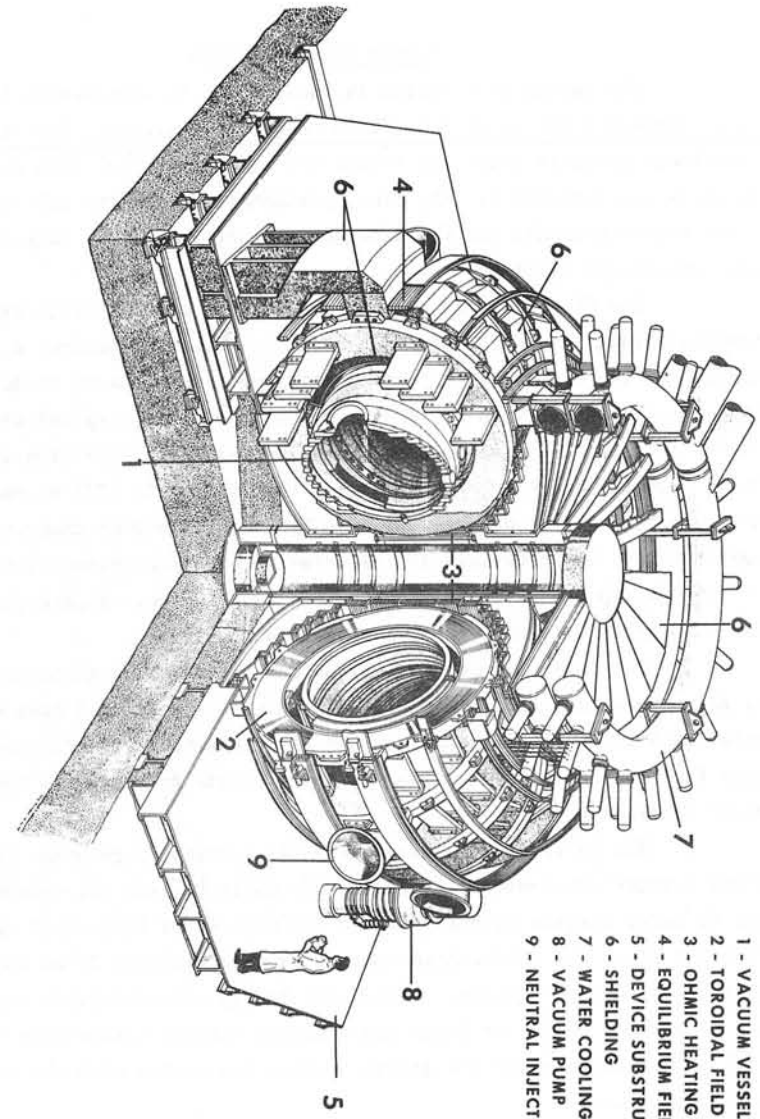

Fig. 1 Tokamak Fusion Test Reactor

DESIGN CONSIDERATIONS

The design description is facilitated by considering the device in a right-hand (R, θ, Z) cylindrical coordinate system. The fields have rotational symmetry about the Z axis and are symmetrical with respect to positive and negative Z. The field parameters which vary only with R and Z are termed poloidal and the winding currents which have only a θ component are called toroidal.

The OH field winding provides a large magnetic flux linking the toroidal plasma current. A rapid change in this flux induces a toroidal current in the plasma. Considering this function alone it is desirable that the flux density in the plasma be very small as compared to other fields. It is also desirable that the mechanical intersection of the OH field with the currents that produce a toroidal field (TF) be small. Although the subject device will have TF coils at higher than room temperatures, later devices are expected to have superconducting TF coils. It will be important to limit the pulsed flux in these superconducting coils in order to preserve their superconductivity.

The initiation of plasma ionization will tend to occur at points of zero magnetic field intensities. A multipole null will have a definite point null (in the R-Z plane) and the field strength will increase rapidly away from this null point. The region of plasma formation is thus accurately controlled.

The OH winding is one of several sources of poloidal fields. Other sources are equilibrium field (EF) coils [2] and the plasma. The OH and EF coils compete with each other and with other functional devices for the same space. A rational resolution of this conflict is an important part of the design problem. Mechanical design considerations favor the use of a fewer number of turns and a higher current (preserving the product). This accentuates the design problem associated with the resolution of integer turns.

LINEAR PROGRAMMING

Linear programming computer codes will solve problems of the type

$$\text{Minimize} \quad \sum_{j=1}^{n} a_{oj} x_j$$

Subject to constraints

$x_j \geq 0.0$ and

$$\sum_{j=1}^{n} a_{ij} x_j \begin{matrix} \leq \\ = \\ \geq \end{matrix} b_i \qquad i = 1,M$$

where the a_{ij} and b_i are known numerical constants, and the x_j are the unknown optimal values of the variables. The symbol $\begin{matrix} \leq \\ = \\ \geq \end{matrix}$ indicates a choice for each expression i of the relationships $\leq$, =, or $\geq$.

The codes which solve such problems are mathematically well founded and are essentially guaranteed to produce an optimum solution if a feasible solution exists or to indicate without excessive computation that there is no feasible solution if such is the case.

The output information from a problem solution contains additional numbers which provide insight into the problem economics. For example, there are sensitivity constants which disclose the way in which the minimized function is affected by changes in the constants.

MATHEMATICAL PROGRAMMING - AN ENGINEERING TOOL

Mathematical programming, which to these authors includes geometric programming and linear programming, has been found to be a very powerful design tool. In contrast to other design methods we see the following advantages:

1. The engineering design problem can usually be literally and precisely stated so as to lead to a unique optimum solution.

2. The technique requires the designer to focus on, and think clearly about, the tradeoffs among the cost and various performance characteristics. This also permits a systematic and logical compromise among these considerations.

3. If a solution exists, the code is essentially guaranteed to find it. If several solutions exist the best of these will be found. If no solution is possible the code will determine this without excessive searching. A problem with no feasible solution can be viewed as having a solution of infinite cost.

4. A solution yields by-products in the form of partial derivatives of cost with respect to the many constraint parameters. Through these sensitivity parameters it may be found, for example, that a small change of one unit of performance parameter A is worth the same amount of money as 10 units of performance parameter B. If the present value of parameter B is marginal and the value of A more than is needed, we can trade evenly a large improvement in B for a small worsening in A.

DESIGN RESULTS

The fields resulting from the design processes are shown in the form of lines of flux in Figures 2 and 3. The final design result would be to superimpose the ampere turn distributions of these two windings to produce the design of an OH winding yielding a hexapole null.

ACKNOWLEDGMENTS

The authors wish to acknowledge the contributions to this work of the staff of the Princeton University Plasma Physics Laboratory. This work was performed for the Plasma Physics Laboratory under ERDA Contract E(11-1), subcontract 192.

REFERENCES

1. TFTR Papers, Transactions American Nuclear Society, 1975, Vol. 21.
2. D. K. Davies, A. J. Federowicz, and J. H. McWhirter, Design of Poloidal Field Windings for TFTR, Symposium on Engineering Problems of Fusion Research, San Diego, California, November, 1975.
3. D.I. Brown and U. R. Christensen, The Magnetic Design of the PDX Poloidal Coil System, Ibid.
4. M. Pelovitz, A computer Code for Generating a Magnetic Field Free Region in an Ohmic Heating Coil System, Ibid.

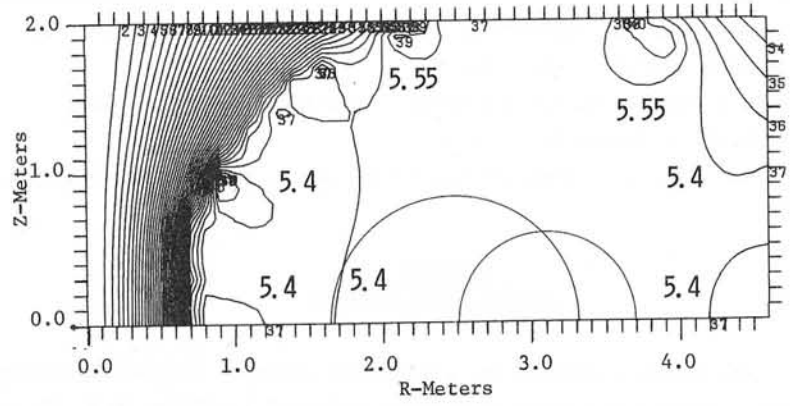

Fig. 2 Lines of Flux From Ohmic Heating Winding

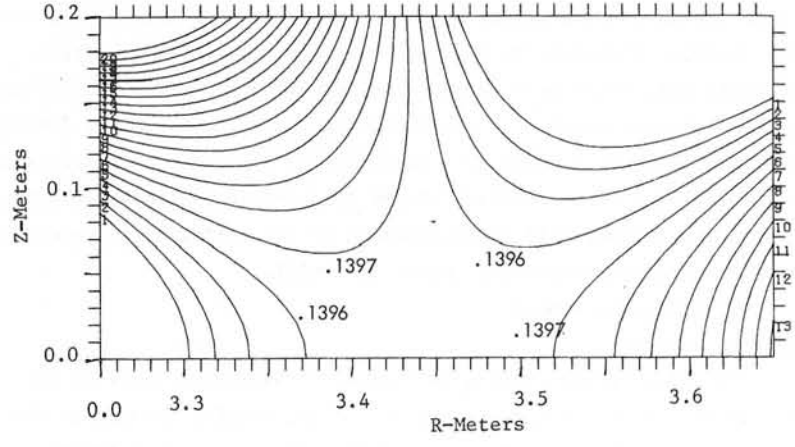

Fig. 3 Lines of Flux From Hexapole Null Winding

5. Y.-K.M. Peng, F. B. Marcus, R. A. Dory, and J. A. Moore, Optimal Poloidal Field Coil Design for Tokamak Experimental Power Reactor (EPR), Ibid.
6. J. H. McWhirter, Optimum Design by Geometric Programming, IEEE Power Engineering Society, July, 1971.
7. William R. Smythe, Static and Dynamic Electricity, pp. 290, 291, Third Edition, McGraw-Hill, 1968.
8. Princeton University Plasma Physics Laboratory, Private Communication, 1974.

APPENDIX A
DESIGN OF OH WINDING

Model

The design variables are filamentary currents of unknown magnitude, x(j). These are assumed at a large number of locations, e.g. 98, in the upper half plane; the linear programming (LP) solution typically contains a smaller set of non-zero values and thus selects these winding locations from the larger set. A symmetrical set of solution values is assumed in the lower half plane. Each turn should carry the same current and thus feasible x(j) must be integral multiples of the same current. This discrete constraint is somewhat difficult to meet without degrading the performance with respect to other constraints. The technique developed for dealing with discrete (integer) variables is described in Appendix B and would be useful here. Because linear programming variables can only take on positive values, x(j) is represented as the difference between its positive and negative components, xp(j) and xm(j).

$$x(j) = xp(j) - xm(j)$$

Minimization of Cost

The cost of the winding is assumed to be proportional to its volume. If we assume a constant winding current density throughout the winding, the volume is also proportional to ohmic loss. As a consequence of this same assumption, the number of turns at any location is proportional to the absolute value of x(j) which is given by

$$|x(j)| = xp(j) + xm(j)$$

The length of a turn at location j is proportional to the radial position R(j). Therefore the total volume is proportional to

$$\sum_j R(j)(xp(j) + xm(j))$$

which is to be minimized.

Magnetic Flux Constraint

The magnetic flux linking the plasma is a linear combination of the x(j) and must be at least equal to a specified value $\bar{\phi}$. That is,

$$\sum_j \phi_{oj} x(j) \geq \bar{\phi}.$$

ϕ_{oj} is the flux linking the plasma due to a unit positive value of x(j) [7] and involves the computation of elliptic integrals [8].

Field Strength Constraints

At points i within the plasma cross-section (or wherever we may wish to place them), we require that the absolute values of both B_Z and B_R be less than a given maximum value. This is imposed by the constraints derived as follows. The Z component of $\underline{B}$ at location i is defined by the equality

$$\sum_j B_{Zij} x(j) - B_{Zi} = 0$$

This is subject to a constraint that

$$-\bar{B} \leq B_{Zi} \leq \bar{B}$$

where B_{Zij} is a constant involving an elliptic integral.

B_{Zi} is a variable, the Z component of $\underline{B}$ at field point i.

$\bar{B}$ is the maximum magnitude of B_{Zi}.

The difficulty with these constraints is that B_{Zi} should be free to take on positive and negative values. We introduce the auxiliary variable

$$B^*_{Zi} = B_{Zi} + \bar{B}$$

and our constraints become

$$\sum_j B_{Zij}x(j) - B^*_{Zi} = -\bar{B} \quad \text{and}$$

$$B^*_{Zi} \leq 2\bar{B} \qquad i = 1,NI.$$

In a similar manner we can arrive at the constraints

$$\sum_j B_{Rij}x(j) - B^*_{Ri} = -\bar{B} \quad \text{and}$$

$$B^*_{Ri} \leq 2\bar{B} \qquad i = 1,NI.$$

It may be desirable and necessary to constrain components of $\underline{B}$ at points within the toroidal field coils. The constrained components of $\underline{B}$ may be in the direction either perpendicular or parallel to the toroidal field current or both.

At field points k we require that the component of $\underline{B}$ in the direction of a unit vector $\underline{V}_k$ with R and Z components (a_k, b_k) be limited to $\bar{B}_V$. If the component of $\underline{B}$ in the direction of $\underline{V}_k$ is B_{Vk}, this is defined as

$$a_k \sum_j B_{Rkj}x(j) + b_k \sum_j B_{Zkj}x(j) - B_{Vk} = 0$$

and the constraint is

$$-\bar{B}_V \leq B_{Vk} \leq \bar{B}_V$$

By defining the variable

$$B^*_{Vk} = B_{Vk} + \bar{B}_V$$

we arrive at the constraints

$$\Sigma(a_k B_{Rkj} + b_k B_{Zkj})x(j) - B^*_{Vk} = -\bar{B}_V \text{ and } B^*_{Vk} \leq 2\bar{B}_V$$

We have a set of constraints specifying that the maximum value $|x(j)|$ may have is $\bar{x}(j)$. That is

$$x(j) = xp(j) + xm(j) \leq \bar{x}(j)$$

In working toward an engineering solution we find useful a set of constraints

$$x(j) = x'(j).$$

That is, x(j) must be equal to a given value x'(j).

APPENDIX B
DESIGN OF HEXAPOLE NULL

Model

The model for the hexapole null winding is much the same as that for the OH winding.

The field from the OH winding is known and this known field plus the field from the winding to be designed are to form a hexapole null. In the discussion to follow, the effect of the OH winding is neglected for the sake of simplicity and clarity.

The minimization of cost is identical to that of the OH winding.

Null

The Z component of $\underline{B}$ must be within given tolerances from zero at the null point. The field at the null is defined by

$$\sum_j B_{Zoj}x(j) - B_{Zo} = 0$$

and the constraint is

$$-\bar{B}_{Zo} \leq B_{Zo} \leq \bar{B}_{Zo}.$$

In order to eliminate variables which take on negative values we define

$$B^*_{Zo} = B_{Zo} + \bar{B}_{Zo}$$

and our constraints become

$$\sum_j B_{Zoj}x(j) + B^*_{Zo} = -\bar{B}_{Zo}$$

$$B^*_{Zo} \leq 2\bar{B}_{Zo}$$

Hexapole Lobes

The contours of $|\underline{B}|$ for an ideal hexapole are circles concentric about the null point. We define the hexapole in terms of a small circle with radius α having the null point as its center and radius vectors i from the null point making an angle θ_i with the R axis. We also consider that $|\underline{B}|$ will ideally go as the inverse square of the distance from the null point.

The hexapole is to be controlled at values for θ_i, of 0, 30, 60, 90, 120, 150, 180 degrees and on the small circle with radius α; symmetry about the R axis will take care of the field in the lower half plane. At $\theta_i = 30°$ and 150°, $\underline{B}$ should ideally be radially outward from the null and at $\theta_i = 90°$, $\underline{B}$ should be radially inward. At $\theta_i = 0°$ and 120° $\underline{B}$ should be perpendicular to the radius vectors in a counter-clockwise sense and at $\theta_i = 60°$ and 180°, $\underline{B}$ should be perpendicular to the radius vectors in a clockwise sense.

The definition of the radial and tangential components of $\underline{B}$ which are to be constrained are

$$\sum_j (B_{Rij} \cos\theta_i + B_{Zij} \sin\theta_i)x(j) - B_i = 0 \quad i = 2 \text{ and } 6$$

$$\sum_j (B_{Rij} \cos\theta_i + B_{Zij} \sin\theta_i)x(j) + B_i = 0 \quad i = 4$$

$$\sum_j (B_{Rij} \sin\theta_i - B_{Zij} \cos\theta_i)x(j) - B_i = 0 \quad i = 1 \text{ and } 5$$

$$\sum_j (B_{Rij} \sin\theta_i - B_{Zij} \cos\theta_i)x(j) + B_i = 0 \quad i = 3 \text{ and } 7$$

Our requirement is that the B_i should have positive values at least equal to some minimim field strength $\bar{B}\alpha^2$ and less than some value $(1+K)\bar{B}\alpha^2$. This is expressed as

$$\bar{B}\alpha^2 \leq B_i \leq (1+K)\bar{B}\alpha^2.$$

This bounding of a variable is often handled by a specialized feature of a linear programming code. If this is not available it is handled as a double set of ordinary constraints. If K is made zero, the hexapole will be quite regular. Non-zero values of K permit a distortion of the hexapole.

The hexapole winding should not provide flux linking the plasma. This requires a constraint.

$$\sum_j \phi_{oj} x(j) = 0$$

Integer Turns

The constraint of integer turns is restrictive in the case of a null. Rounding of a non-integer solution is not sufficient. An integer programming code was investigated but appeared to be awkward, costly, and a more powerful tool than was required. The following technique was developed. The candidate current locations were divided into groups k and the following constraints are imposed.

$$\sum_j x(j) - S_k = 0$$

$$\bar{S}_{k1} \leq S_k \leq \bar{S}_{k2}$$

The values $\bar{S}_{k1}$ and $\bar{S}_{k2}$ correspond to integer turns. If one of the constraints is active, the sum of the turns is an integer. If the upper and lower bounds are the same, the sum must be an integer. If the bounds correspond to one turn, the sum must be one turn. By successive solutions, each increasing the number of groups, it is possible to reach an integer turn solution with very tight tolerances on the design performance.

If the location of a turn can be judged to lie within bounds in R and Z, the four corners of the bounding square can be proposed as locations. The solution will be fractional turns at two or more of these four locations.

An average of the coordinates of these points weighted with their partial turn solution value provides an estimate of the location of one turn.

Discussions following paper:

(Moses, University of Wisconsin) I would like to comment that a very similar problem was solved for the shield in the FERMILAB pulsed energy storage device. This was published at the Applied Superconductivity Conference, Oakbrook, Illinois (1974) by Moses and Ballou.

(McWhirter, Pittsburgh) I believe that the problem solution which Mr Moses has mentioned is obtained by a method other than linear programming, of course we did not intend to infer that we were the first to solve this type of problem. Our contribution is thought to be the use of linear programming with the advantage mentioned in the paper.

MAGNETIC FIELD COMPUTATION AND STRESS ANALYSIS IN TOROIDAL CIRCULAR AND DEE SHAPED COILS FOR TOKAMAK FUSION EXPERIMENTS

N J Diserens
Rutherford Laboratory, Chilton, Didcot, Oxon, OX11 0QX

ABSTRACT
Data preparation for stress analysis of windings for Tokamak fusion reactors can be a very time-consuming process. A program 'TOK' is described in which simple data input can be used to compute fields and forces in toroidal systems of circular and Dee shaped coils. In addition a complete data deck can be output for use as input to a special version of the 'FINESSE' stress analysis program.

1. INTRODUCTION

The future generation of fusion experiments will require very large TOKAMAK devices. These machines will contain toroidal field windings which will produce a very high magnetic field. In addition there will be poloidal windings which are used to shape and excite the plasma.

Because of the high magnetic fields and high currents involved in the superconducting toroidal windings, the forces on these coils will be very large, and careful design is required to minimise the shear stresses.

A dee shaped toroidal coil will avoid large in-plane shear stresses but it will still be necessary to know what the maximum stresses are likely to be.

Poloidal coil fields will exert a twisting force on the toroidal coils and so the designer must know what stresses are produced by these.

This paper describes a suite of computer programs which have been written at the Rutherford Laboratory to handle this work. Results are given for one possible experiment and details of future developments are also outlined.

2. THE TOK PROGRAM

2.1 General Description. The computer program TOK[1] will accept a simple data input, consisting of a command followed by a string of sub-parameters, similar to that used in the on-line magnetostatic program GFUN.[2,3] Figure 2.1 shows a sample data deck. Starting with the basic parameters of a toroidal coil system, such as the number of coils, cross section of coils, major radius of torus and outer radius of torus, the command DOPT will produce an optimisation of the shape of the dee to give zero in-plane shear along a specified filament of the coil. This optimisation process has been described by Collie.[3]

Alternatively, the full geometry of the coil could be read in.

Poloidal coils of rectangular cross section can be described and also the plasma is treated as a coil which has a curvilinear polygon for its cross section and also has varying radial current.

Commands DISP and PRINT produce a graphical display of the coils (Figures 2.2 and 2.3) and also a print out of the coil parameters (Figure 2.4).

Command GETB will enable magnetic fields to be plotted along any given line.

The GETF command will produce a mesh of points at which fields and body forces are computed over the toroidal coil. Failure conditions can be reproduced by 'switching off' any of the desired coils.

The CODA command will enable a complete data deck to be assembled for input to the Swansea University stress analysis program FINESSE.[4,5] At the same time a cladding of a suitable supporting material can be added to the inside, outside or ends of coils.

2.2 Field Computations. Three types of conductor element are used in the TOK program, these are:

1. Circular coils

```
TITL TBX OPTIMISATION AND FIELDS AND FORCES
GEOM COILS=20,NIT=6,ROPT=0.11,ZOPT=0.,J=1340,NARC=7,RADI=157.2,CORE=157.2,
RADB=1008.4,LENG=44,UNITS=MIXED,SHAP=RECT,THICK=66
OPTI
PRINT
GEOM GROU=PLASMA,R1=352.5,R2=410,R3=506,R4=563.5,H1=0,H2=158,
H3=158,H4=0,C1=.005,C2=.0167,C3=.005,J=0,J1=.1392,J2=0,REFL=YES
GEOM GROU=COAX,J=-2000,H1=650,H2=670,R1=657.2,R2=677.2,REFL=YES
GEOM GROU=COAX,J=-2000,R1=1007.2,R2=1027.2,H1=320,H2=340,REFL=YES
GEOM GROU=COAX,J=-2000,R1=150,R2=151.83,H1=0,H2=423,REFL=YES
PRINT
DISP XMAX=1600,XMIN=-1600,YMAX=1600,YMIN=-1600,PLAN=XY,COOR=GLOB,GROU=BOTH
DISP ZMIN=-1600,ZMAX=1600,PLAN=XZ,COOR=GLOB,GROU=BOTH
DISP COOR=BOTH,YMIN=-1600,YMAX=1600
GETF IPRN=0,NR=2,NZ=2,GROU=TORR,C1=1,C2=20,COOR=POLA,OUTP=YES
CODA E1=0.2E+08,C1=0.33,NTMAX=3,NZMAX=9,NZMIN=1,NTMIN=1
END
```

FIGURE 2.1 - SAMPLE INPUT DATA DECK FOR TOK PROGRAM

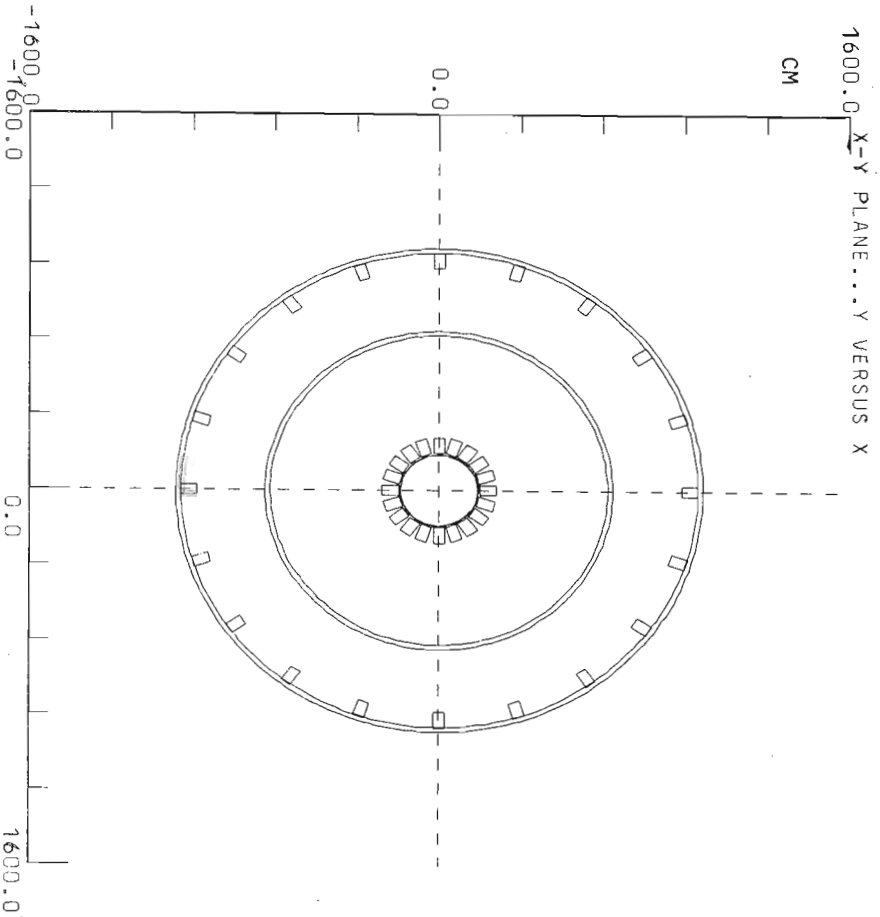

FIGURE 2.2 - SECTION THROUGH Z= 0 PLANE OF TBX TOKAMAK

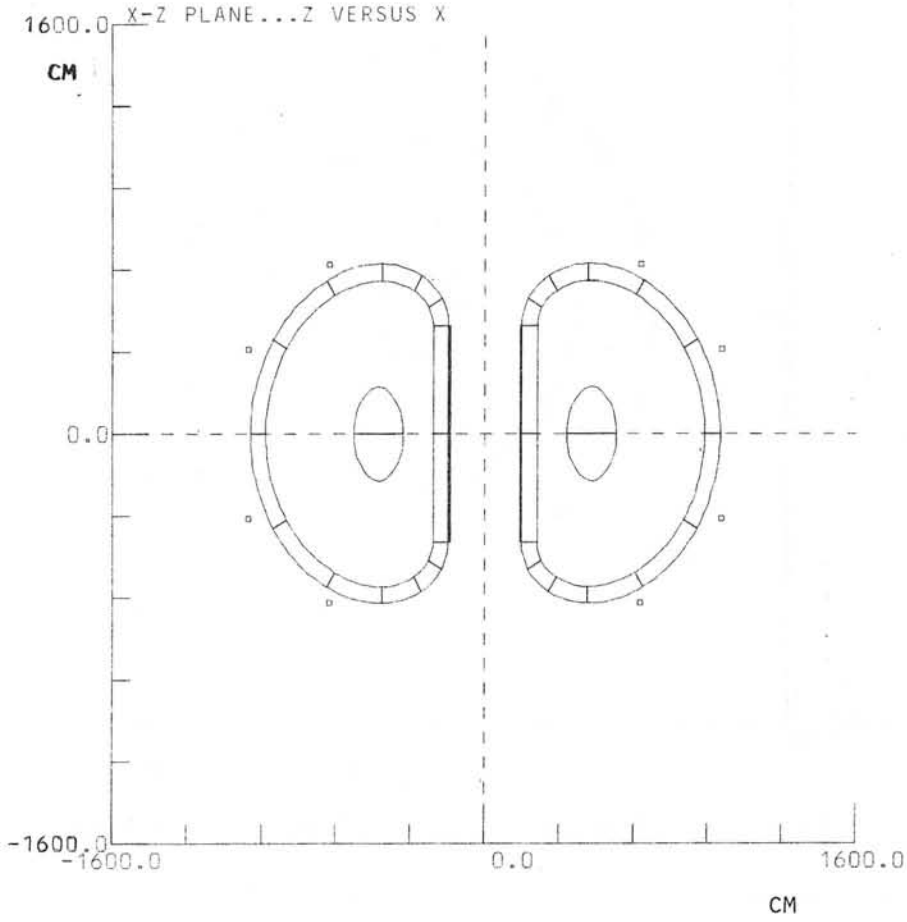

FIGURE 2.3 - SECTION THROUGH θ = 0 PLANE OF TBX TOKAMAK

```
UNITS
SPACE DIMENSIONS IN CENTIMETRES
          CURRENTS IN AMPERES
          FIELDS IN KILOGAUSS
          FORCES IN LBS
          STRESSES IN PSI


TORROIDAL SYSTEM OF DEE SHAPED COILS
CORE RADIUS=    157.200 NUMBER OF COILS=    20
COIL THICKNESS=     66.000 NUMBER OF ARCS=     7

R OF CUR   ANGLE       XCEN       YCEN
    0.0     -90.000    423.069      0.0
  205.476   -60.000    423.069    205.476
  246.626   -30.000    402.494    241.113
  336.052     0.0      325.048    285.826
  473.658    30.000    187.442    285.826
  628.502    60.000     53.344    208.404
  735.189    90.000      0.0      116.010

COIL LENGTH=     44.000 CURRENT DENSITY=  1340.000


COAXIAL SYSTEM OF COILS
   IR         OR         H1         H2       C-DEN    REFLECT
  657.200    677.200    650.000    670.000 -2000.000     YES
 1007.200   1027.200    320.000    340.000 -2000.000     YES
  150.000    151.830      0.0      423.000 -2000.000     YES
PLASMA
     H          R          C
    0.0      352.500     0.005
  158.000    410.000     0.017
  158.000    506.000     0.005
    0.0      563.500     0.0
REFLECT= 1
CURRENT DENSITY COEFFICIENTS
     0.0              0.1392E+00       0.0
```

FIGURE 2.4 - PRINT OUT OF COIL PARAMETERS FOR TOK PROGRAM

2. Arc elements of rectangular cross section.

3. Straight elements of rectangular cross section.

Fields due to circular coils are computed by regarding the coil as an array of thin current carrying cylinders, the numerical integration is done radially. This enables coils of varying cross sectional thicknesses to be handled, and with radially varying current density. The method has been previously described.[6]

Arc elements are computed by regarding the element as an array of infinitesimal wedges, the numerical integration being done in the azimuthal direction. It is possible to handle elements with varying thicknesses in the radial direction or in the transverse (Z) direction, and this will be shortly included in the program. This method has been described by Mansfield.[7]

Straight elements are calculated analytically by a subroutine written by Ch. Iselin.[8] At present the elements must have rectangular cross section but it is intended to include trapezoidal elements shortly.

3. FINESSE

The Swansea Stress Analysis program FINESSE has been modified at the Rutherford Laboratory to handle coil body force data. A special version of the output routines enables the stresses to be output as radial or tangential components. Graphical output is available for the three components of tensile stress and three components of shear stress, plotted along a coil filament.

Anisotropic elastic properties can be input to FINESSE, such that one set of properties hold in a given direction and a second set hold in any plane transverse to this direction. The program is being modified to allow the properties to rotate around with the coil elements so as to maintain their correct orientation. A short treatise by Collie[9] has shown that two values of elasticity E, two of Poisson's ratio V and one value of shear modulus G should be adequate to describe the elastic behaviour of a layered superconducting coil.

Before entering the data into FINESSE, after output from the TOK program, it is possible to add additional elements or to change the data as required.

4. RESULTS

Preliminary results[11] have been described by the author.

Further work is in progress. A proposal for a European superconducting TOKAMAK known as 'Tritium Burning Experiment' (TBX) is at present being investigated. This has a torus comprising 20 Dee shaped coils, each having an axial length of 0.44 metres and a radial thickness of 0.66 metres.

The shape has been optimised to give pure tension on a filament one third of the radial thickness in distance from the inside of the coil, and on the mid plane. This is the line of mean body force in the coil. Figures 4.1 to 4.3 show the tangential stresses due to the toroidal field, in the mid plane of the TBX Dee coils, for the inner radius, the central filament, and the outer radius, respectively. The stresses are plotted along a filament, in the direction of the current, over 180 degrees of the coil. The coils are assumed to be clamped such that the outer surface of the straight section, facing the centre of the torus, cannot move radially, but can expand along its length. In order to resist the poloidal field forces, it will, of course, be necessary to support the sides of the coil, but these supports are not allowed for at this stage.

Figure 4.4 shows the shear stress in the plane of the coil, along a filament which is radially in the centre of the winding and half way between the mid plane and the end of the coil. It can be seen that the values are quite low, only a few hundreds of pounds per square inch. (Compare this with the typical results for a Dee coil which is not optimised for shape (Figure 4.5) which has a maximum shear stress of about 7000 PSI in the plane of the coil.)

it can be seen from Figure 4.6 that the shear stress in a plane transverse to the direction of current is not insignificant. This is due to the finite axial length of the coil and the field 'leakage' in between the individual windings.

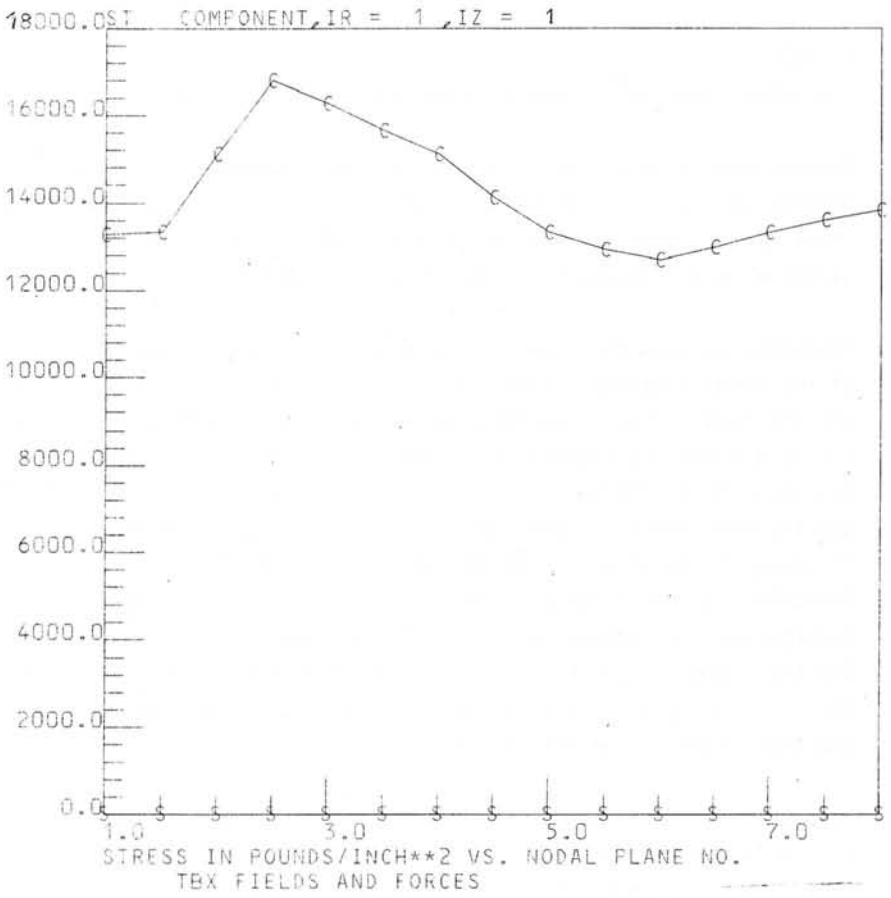

FIGURE 4.1 - HOOP STRESS ALONG INNER SURFACE OF MID PLANE OF TBX TOKAMAK

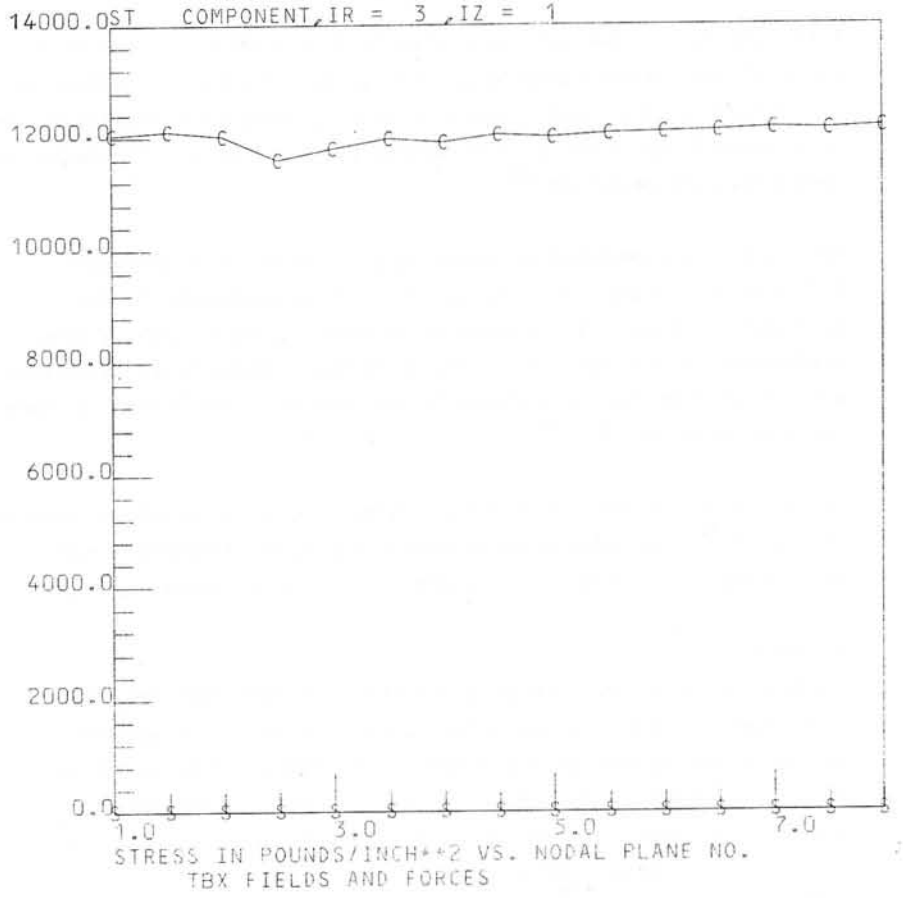

FIGURE 4.2 - HOOP STRESS ALONG CENTRAL FILAMENT OF MID PLANE OF TBX TOKAMAK

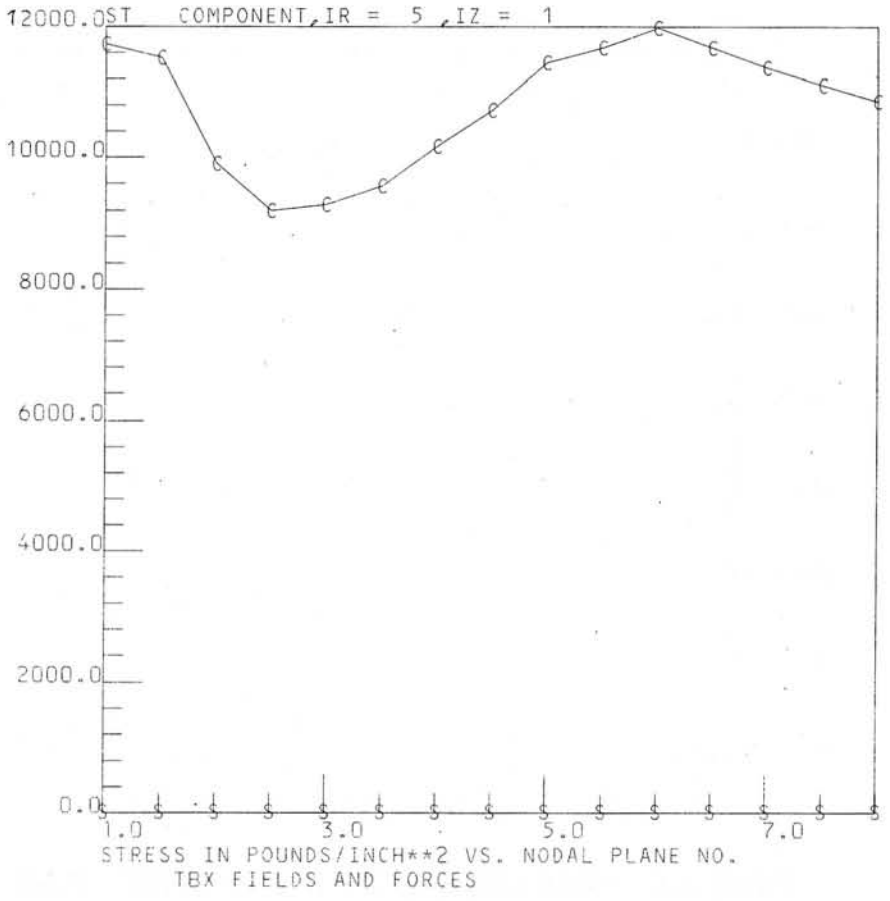

FIGURE 4.3 - HOOP STRESS ALONG OUTER SURFACE OF MID PLANE OF TBX TOKAMAK

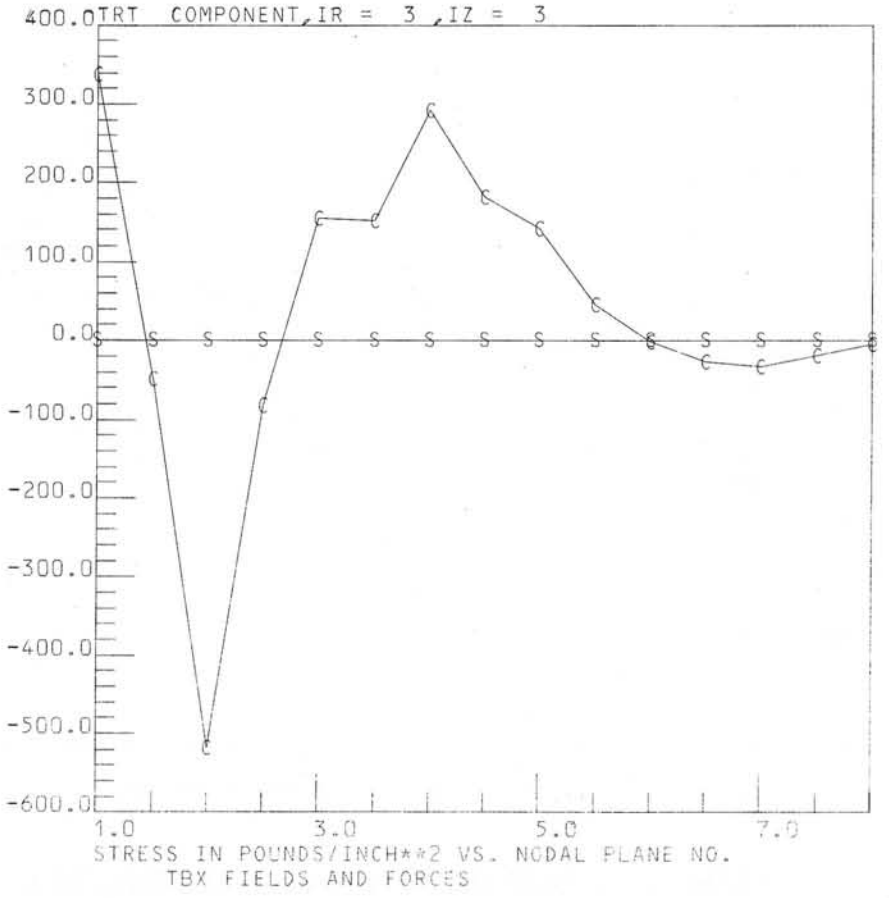

FIGURE 4.4 - SHEAR STRESS IN PLANE OF DEE COIL AT Z = 11.0 cm. ALONG A CENTRAL FILAMENT

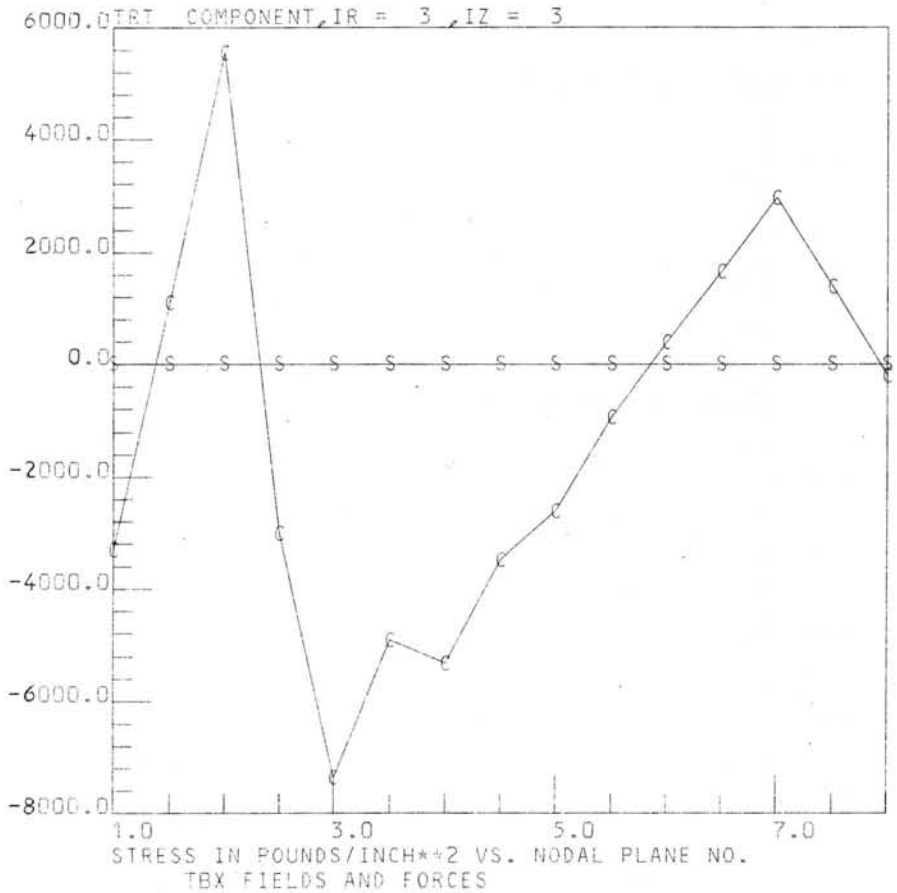

FIGURE 4.5 - SHEAR STRESS IN PLANE OF DEE COIL FOR A NON-OPTIMISED SHAPE

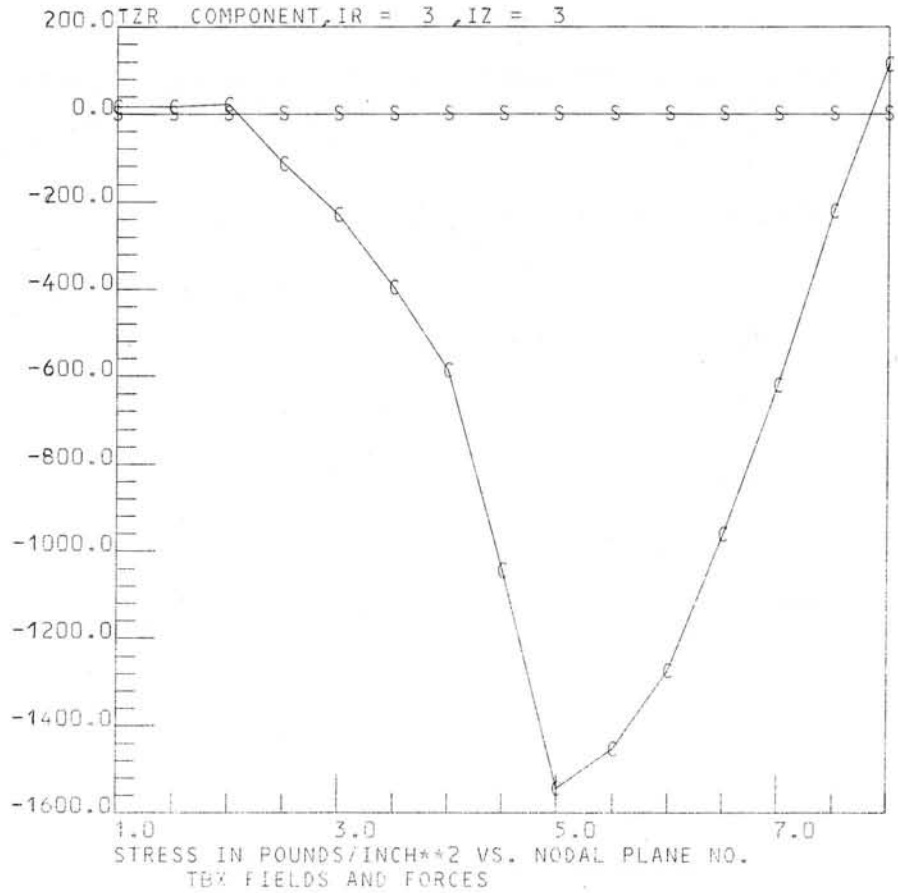

FIGURE 4.6 - SHEAR STRESS AT Z = 11.0 cm IN LOCAL PLANE DUE TO TOROIDAL FIELD

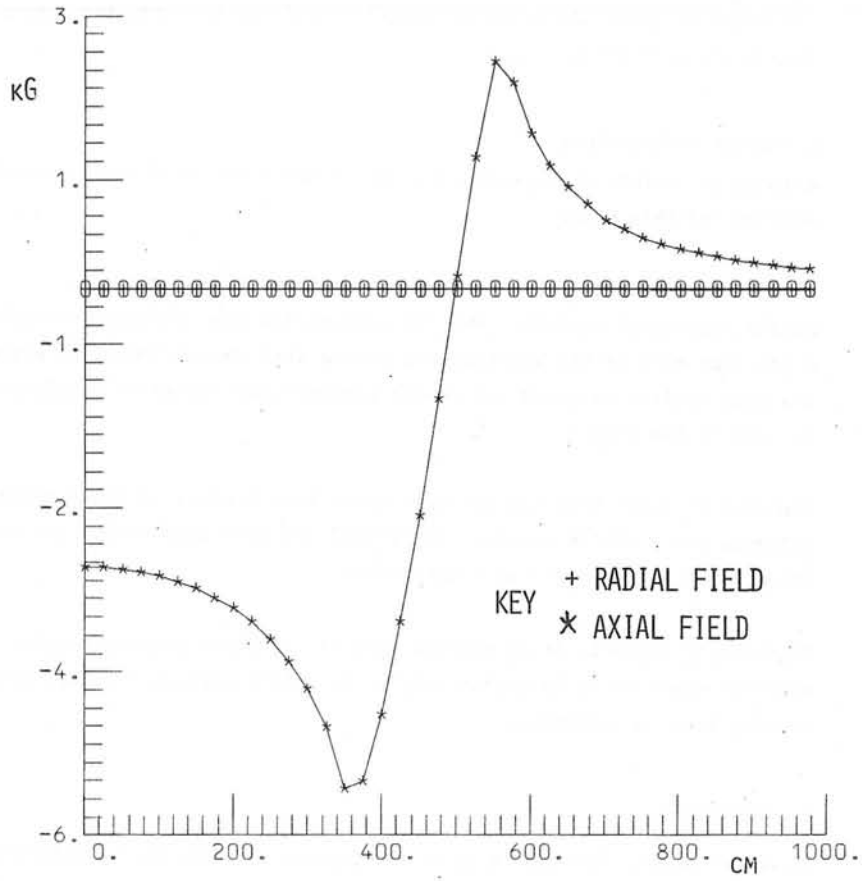

FIGURE 4.7 - MAGNETIC FIELD AT Z = 0. DUE TO POLOIDAL COILS AND PLASMA IN TBX TOKAMAK

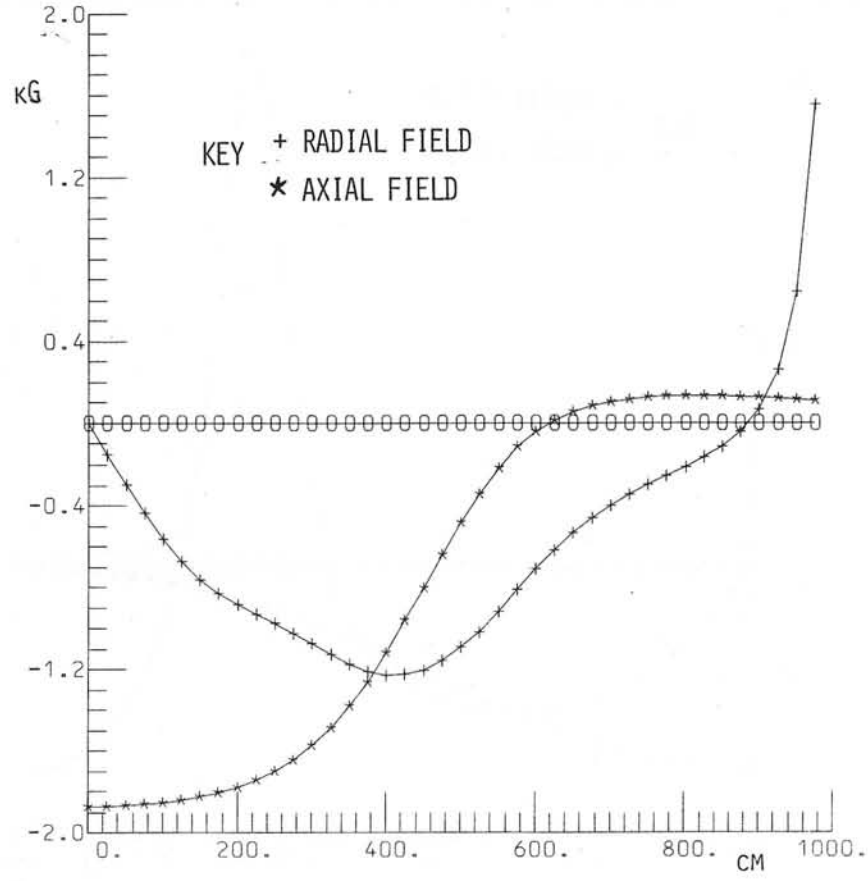

FIGURE 4.8 - MAGNETIC FIELD AT Z = 3M. DUE TO POLOIDAL COILS AND PLASMA IN TBX TOKAMAK

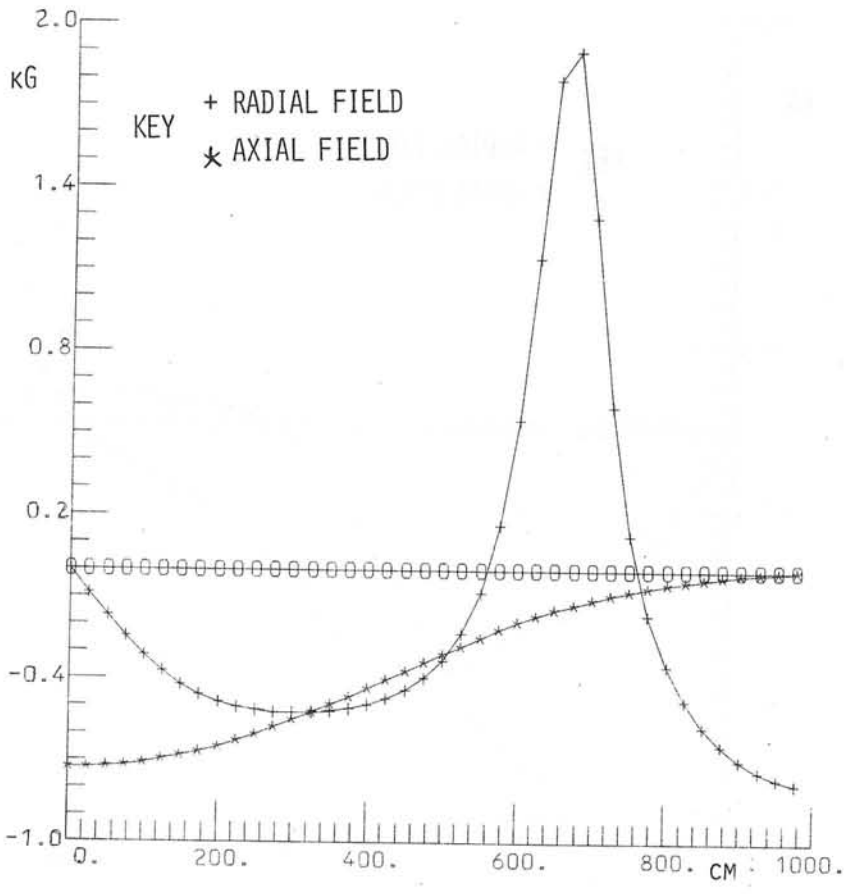

FIGURE 4.9 - MAGNETIC FIELD AT Z = 6M. DUE TO POLOIDAL COILS AND PLASMA IN TBK TOKAMAK

Graphical plotting of fields is available. Figures 4.7 to 4.9 show the three components of field due to the poloidal coils in Figure 2.2 along radial lines at Z = 0, Z = 3.0 M and Z = 6.0 M.

The poloidal coils shown are a typical example rather than the actual design which might be used.

5. FUTURE DEVELOPMENTS

A number of points of development have already been mentioned in previous sections of this paper.

In addition it is intended to develop a version of the program to handle iron cored systems. The TOK program has been designed in such a way that many of the routines are shared with the on-line GFUN program, and thus facilities which are in one program need little or no adaptation for use in the other.

Cooldown stresses have not yet been taken into account in these computations, but a facility exists in FINESSE and will need to be used in a complete evaluation of a working system.

Plotting of magnetic field vectors upon the geometry display diagram is a facility which would be useful and, as it exists already in GFUN, would be very easy to implement.

6. REFERENCES

1. N J Diserens. TOK User's Guide. A Computer Program for Calculating Magnetic Fields and Forces in Toroidal Coil Systems. RL-75-111 (1975).

2. N J Diserens, M J Newman, J Simkin, C W Trowbridge. GFUN User's Guide (2-Dimensional Version). RHEL/R.244 (Release 2) (1975).

3. J Simkin, C W Trowbridge. GFUN3D User's Guide. RL-76-029 (1976)

4. FINESSE Abstract. CNME/AS/18. National Research and Development Corporation.

5. FINESSE - Rutherford Laboratory Version User's Guide. RL-75-144(1975)

6. C J Collie, N J Diserens, M J newman, C W Trowbridge. Progress in the Development of an Interactive Computer Program for Magnetic Field Design and Analysis in Two and Three Dimensions. RL-73-077 (1973).

7. P Mansfield. Magnetic Fields of Curved Conductors. RL-75-184(1975).

8. Ch Iselin. Private communication.

9. C J Collie. The Optimisation of Dee Shaped Coils. Rutherford Laboratory CAG/75-7 (1975).

Discussions following paper:

(Turner, Argonne Nat. Lab) Jim, you mentioned that when you used the wrong shape for the dee coil, the shear stress changed from a few hundred psi to a few thousand psi. How much did that shape differ from the correct shape?

(Diserens) The coil was quite a long way out of shape. The straight section was lengthened from 4M to 6M which increased the height of the coil by about 30%.

(Leloup, Euratom-CEA) You mentioned that your calculation is not completely general because you can only represent plasma current distributions varying with R. You can make it general provided that you do not need to compute the magnetic field inside the plasma: in such a case, any plasma current distribution can be represented by surface currents determined using the "virtual casing artifice".

R Levyraz

Iterative Generation of Optimal Triangular Grids for the Solution of 2-Dimensional Field Problems
1. Principle and Applications

Engineers who apply the Finite Element Method need computer programs which solve with a minimum of input data problems with very complex and widely different geometries whereby the calculating effort must remain reasonable. A fundamental problem is the subdivision of the region into elements, i.e. the grid generation. The algorithm given here generates 2-dimensional optimal grids for many classes of applications and leads to quantitative information about the discretisation error. The optimisation principle is to minimise the total discretisation error, which means to get best information about the whole considered system. Triangular elements of first order are chosen, because they can easily be treated and allow a good representation of the geometry.

For the construction of such an optimal element subdivision the potential distribution must be known at least approximately, but a potential distribution can only be calculated within a grid. From this it is clear that more than one grid must be used and therefore the grid generation is an iterative process. Since the calculation effort increases with the number of gridpoints, the transient grids should be as coarse as possible. By this consideration the principle of the flow diagram in fig. 1 is obvious.

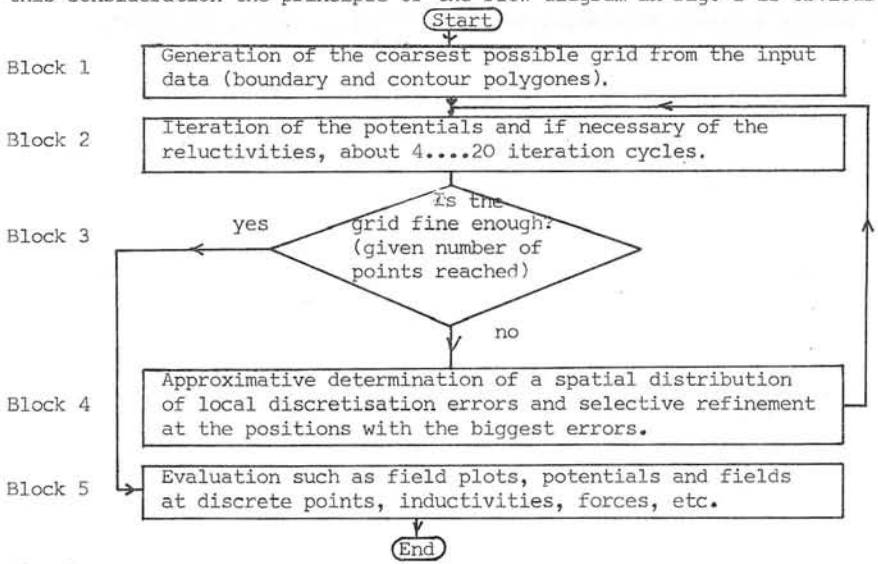

Fig. 1

The above process is very advantagecus if few or nothing is known about the potential distribution and the optimal grid and the behaviour of the total system is the principal objective. Nevertheless the algorithm may easily be adapted to other situations, particularly to the following ones:

- The optimal grid density distribution is approximately known: refinement to a given density in block 1.
- There is a special interest in the potential of a partial region: A modified block 1 is used which eliminates from a former grid the elements outside the new boundary and defines the potentials taken from the former calculation as fixed on the new boundary.
- As above, but with a simultaneous change of the geometry: A new grid is built up from the beginning and at block 1 boundary values from the former potential distribution are interpolated.
- A generated grid turns out to be too coarse: Entry at block 4 with the former final grid.
- A present grid is used to calculate a new potential distribution, for instance to determine a nonlinear characteristic: Only blocks 2, 3 and 5 are used.

2. Mathematical Optimisation Objetive and General Procedure

The definition of an optimal grid depends first of all on the field equation, but also on material properties, boundary conditions, coordinate system etc.. The selection presented here is given by the practice and the mathematical difficulties. The following field equations are considered:

$$\text{div}\ (\ \varepsilon\ (-\text{grad}\ V)) = Q, \quad \text{(capacitive electrostatic field)}$$
$$\text{curl}\ (\ \nu\ \text{curl}\ \vec{A}) = \vec{J}_0, \quad \text{(magnetostatic field)}$$
$$\text{curl}\ (\ \nu\ \text{curl}\ \vec{A}) = j\omega\sigma\vec{A} + \vec{J}_0 \quad \text{(harmonic eddy current field)}$$
$$\text{where } \vec{A} = (0, 0, A),\ \vec{J} = (0, 0, J)$$

The first equation includes the electrostatic conductance field and the thermostatic field. The problems are treated in 2 dimensions, i.e. cartesian x, y - or axisymmetric r, z-coordinates. The material properties ν, ε, etc. are considered as constant over partial regions or scalar functions of the square of the field strength. The first two equations are equivalent to the minimisation of the total energy W in the given region. For the eddy current equation the corresponding principle is not so simple.

In order to get a very general grid optimisation we must choose a discretisation error definition which represents the behavior of the total system and does not degenerate in any case. It is obvious to take the energy difference ΔW_N between the energy W_N calculated within a grid of N points and the real energy W of the system. This value is $\geq 0, \neq \infty$ and approaches 0 if the grid is made infinitely fine under very general conditions. We may therefore declare a grid to be optimal if for a given number N of grid points the energy difference ΔW_N is minimum.

Unfortunataly, a direct numerical optimisation with the well-known methods is practically excluded due to the great number ($\approx 2N$) of unknown coordinates and the almost infinite number of possible topologies. On the other side, the primary objective is the potential distribution, and practice has shown that with the successive application of very simple grid changes it is possible to reach ΔW_N by a factor of about 1.2. Furthermore it is not necessary to generate a grid of exactly N points. By these reason the successive grid refinement given in fig. 1 is justified. The intermediate grids should be optimal as soon as possible in order to reduce the calculation effort.

As elementary grid changes we choose a minimal set of simple operations, because changes in an irregular grid are not easy to program and because the effect of each operation on ΔW_N must be estimated.

The most simple but fully sufficient operation to increase the number of grid points is the segment halving (see fig. 2). Thereby the starting potential of the new point is interpolated according to the potential distribution in the adjacent elements. For the selection of the segments to be halved, there must be a halving index related to each segment which represents the discretisation error in the neighbourhood of a segment and/or the effect of the segment halving on this error. The segments with the greatest indices are halved, which leads as fast as possible to an optimal grid.

As mentioned above it is very important how the grid points are interconnected. The most simple topological change is the diagonal transposition (see fig. 3) which changes two triangles into two different ones. A simple example (fig. 6) shows that after a segment halving all useful transpositions becoming possible by this halving must be executed immediately. This complicates the program but avoids grid degenerations and restricts the possible transpositions to a neighbourhood of the new gridpoint.

To consider the effect of a segment halving it is assumed that in the grid before the execution of the halving the potentials are the exact solution of the corresponding system of equations. The situation after the halving is as follows:

- There is a new equation for the new point which is in general not fulfilled by the starting value of the new potential.
- The equations of the immediately neighboured points P_1, P_2, P_3, P_4 are in general changed and not further fulfilled.
- The sum of the equations of $P_1P_2P_3P_4$ before the halving is identical with the sum including the new point after the halving if the latter lies inside the calculated region or on a Neumann boundary.
- The total energy remains unchanged.

From this it may be concluded that:

- By the halving a part of the disctretisation error ΔW is changed to residual error which is eliminated by the following iterations.
- The residues in the new system of equations are bounded to a close neighbourhood of the new point and mostly add to zero.
- If the system is linear, the difference between the new and the old field may be seen as the field produced by the residues. It diminishes with the distance from the new point at least as much as a dipole field.

Therefore the total effect of the halving, which practically cannot be calculated exactly, may be approximated as the effect on the immediate neighbourhood of the halved segment. A further reason of the approximation is that the exact determination of all potentials before each refinement would take too much time. The estimation must be chosen such that in doubt halving indices get rather too big. Because of all these approximations it is not necessary to sort halving indices explicitly. A rough logarithmic classification and a scanning is completely sufficient.

To find a diagonal transposition criterion there are similar considerations. As a starting point we choose the energy in the concerned quadrangle to decide if the existing or the other diagonal is better, but also in this case it must be considered that the exact potential distribution is not known. Different from the effect of the halvings, most of the energy gain by the transpositions is realised immediately in the refinement stage.

Experience has shown that after a grid change all new segments should get new halving indices in order to guarantee a principally unlimited refinement. The other possibility, namely to allow only the segments present at the start of the refinement stage to be halved restricts very much the number of new points and therefore needs much more refinement stages.

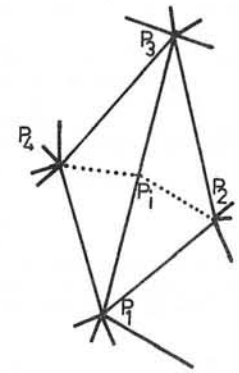

Segment halving
..... new segment
Fig. 2

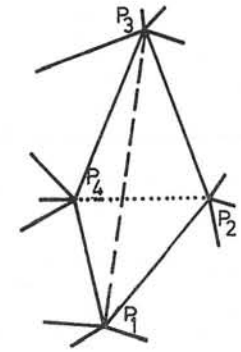

Diagonal transposition
---- eliminated segment
Fig. 3

3. Determination of the Halving Indices, Remainder Potential

Since the effect of a segment halving is mainly local it is obvious to try to define the halving index as the energy which can be gained by the change of the potential of the new point with all other potentials fixed. In the following it is shown that this definition may be used with some necessary modifications.

Firstly it is assumed that the potential A is real and the system of equations is linear. The energy gain by the introduction of the new point i then is

$$H_i = k_i / 2 \cdot (\Delta A_i)^2 \qquad (3.1)$$

where k_i is the diagonal element of the coefficient matrix and ΔA_i the potential difference between the starting value given by the discrete potential and the value which fulfills equation i. If the system is nonlinear, particularly if the reluctivity is field strength dependent, there must be taken the total differential for k_i which is the 2nd derivative of the energy with respect to A_i. If the potential is complex i.e. for eddy current problems, the problem cannot be taken as a minimisation of an energy, but an interpretation of the factors in (3.1) leads to reasonable grids. It is clear that

$$(\Delta A_i)^2 \rightarrow (\mathrm{Re}\,\Delta\underline{A}_i)^2 + (\mathrm{Im}\,\Delta\underline{A}_i)^2 \qquad (3.2)$$

For k_i there are the following two possibilities:

$$k_i \rightarrow |\mathrm{Re}\,\underline{k}_i| + |\mathrm{Im}\,\underline{k}_i| \qquad (3.3)$$

$$k_i \rightarrow |k_i| \qquad (3.4)$$

For grids with a fairly small discretisation error there is anyway

$$|\mathrm{Im}\ k_i| \ll |\mathrm{Re}\ k_i|$$

The maximum difference between (3.3) and (3.4) is a factor of $\sqrt{2}$ which is tolerable with respect to all other simplifications.

Unfortunately there are some types of situations in which (3.1) together with the above definitions fails; these are mainly the following cases:

- The energy gain is mainly or wholly realised only by the diagonal transpositions becoming possible by the halving.

- There is only a considerable energy gain if several neighboured new points are generated (see example fig. 4)

In the first case it would be possible to consider the effect as an additional energy in (3.1) but in the second case the effort would be too big. Since all these problems arise because $(\Delta A_i)^2$ is too small an approximation must be found which represents the behaviour of A in the neighbourhood of the new point and by this the local discretisation error.

The real potential A may be split into the discrete potential A_o and the remainder potential A':

$$A' = A - A_o , \quad \vec{B}' = \vec{B} - \vec{B}_o \tag{3.5}$$

For first order elements A_o is a linear or similar function. To get an approximation for the discretisation error it is in general sufficient to define A' as a quadratic function of the coordinates with the new point i as origin. (3.1) then leads to

$$H_i = k_i / 2 \cdot A'^2 (P_\lambda) \tag{3.6}$$

where P_λ is one of the end points of the halved segment. The assumption is that the potentials of all points are correct and only the potential between the points is subject to discretisation error. The use of A' mainly eliminates degenerations of the second type.

The remainder potential in its most general form is

$$A' = c_1 x^2 + c_2 xy + c_3 y^2 \tag{3.7}$$

$$\vec{B}' = (c_2 x + 2c_3 y, \; -2c_1 x - c_2 y) \tag{3.8}$$

Since (3.7) is only valuable in a small neighbourhood of its origin considerations about A' may be performed in cartesian coordinates even if the whole system is defined in cylindrical coordinates.

A' can be transformed to its main axes x', y':

$$A' = c_1' x'^2 + c_3' y'^2, \quad \vec{B}' = 2(c_3' y'_1, - c_1' x') \tag{3.9}$$

If the signs of c_1' and c_3' are different the equipotentials of A' are hyperbolae with asymptotes of value zero. The fact that in a region with existing discretisation error there may be segments of any length with zero halving indices makes a reasonable grid generation impossible. As an example all boundary segments with fixed constant potential belong to this class which represents the first type of degeneration. A simple modification from A' to A'' eliminates the degeneration but keeps the main information about the local discretisation error:

$$A'' = |c_1'| \, x'^2 + |c_3'| \, y'^2, \; \vec{B}'' = 2(|c'_3| y', \; - |c_1| x') \tag{3.10}$$

A'' is positive definite, leads to the same halving indices as A' for segments lying in the directions of the main axes and enlarges halving indices for all other segments if A' is hyperbolic. A'' only vanishes outside the origin if at least one main axis coefficient is zero. It is interesting that

$$B'^2 \equiv B''^2 \tag{3.11}$$

and therefore the fictitious field energy of A' remains unchanged by the modification to A''. It may be said that the modification leaves the same local discretisation error but increases the part which will probably be eliminated. Instead of (3.6), the modified definition

$$H_i = k_i / 2 . A''^2 (P_\lambda) \tag{3.12}$$

will be used.

The coefficients c_1, c_2, c_3 are interconnected by the differential equation. As shown in the following the relation

$$c_1' + c_3' = 0 \tag{3.13}$$

is systematically true for certain classes of problems. Then

$$A'' = |c_1'| \, (x'^2 + y'^2) . \tag{3.14}$$

This isotropic A'' leads under fairly general conditions to an isotropic grid, i.e. a grid consisting of approximately equilateral triangles.

In the most general case the equipotentials of A''^2 are ellipses with the axes in the main axis directions and an axis relation of

$$q_a = \sqrt{|c_3' / c_1'|} \tag{3.15}$$

The relation and the direction of the axes varies over the region; therefore an optimal grid has a location dependent anisotropy which is mainly influenced by the spatial distribution of c_1, c_2, c_3. The axis relation q_a can systematically get values of 10...30 in practical applications. Hence it is not possible to avoid the local vanishing of c_1' or c_3' by a limitation of q_a.

If the potential is complex it is most natural to modify real and imaginary part separately. By this the equipotentials of $(\mathrm{Re}\underline{A}''^2 + \mathrm{Im}\underline{A}''^2)$ ar no more ellipses but have in general a sligthly different shape. This more general shape can be replaced by an ellipse with good approximation which facilitates the programming of segment halving and transposition.

In the following the relation between c_1, c_2, c_3 is determined starting from

$$\mathrm{curl} \; (\nu \vec{B}) = J \qquad [\mathrm{div} \; (\varepsilon \cdot \vec{E})] = Q \tag{3.16}$$

When "curl" or a vector product is used as a scalar, the z component of x,y,z or the φ component of r, z, φ is meant.

If ν, ε is regionwise constant, with the aid of (3.5) and (3.8) we get

$$\mathrm{curl} \; \vec{B}' = -2(c_1 + c_3) = R \quad [\mathrm{div} \; \vec{E}' = 2(c_1 + c_3) = R] \tag{3.17}$$

$$R = -\mathrm{curl} \; \vec{B}_o + J/\nu \qquad [R = -\mathrm{div} \; \vec{E}_o + Q/\varepsilon] \tag{3.18}$$

Under the further assumptions

$$J = 0 \qquad [Q = 0] \tag{3.19}$$

and

$$\mathrm{curl} \; \vec{B}_o = 0 \qquad [\mathrm{div} \; \vec{E}_o = 0] \tag{3.20}$$

we get

$$\mathrm{curl} \; \vec{B}' = 0 \qquad [\mathrm{div} \; \vec{E}' = 0] \tag{3.21}$$

which means that (3.13) is valid and that the optimal grid is isotropic.

The condition (3.19) says that isotropy may only be awaited in current-free (charge-free) regions. Equ. (3.20) is always fulfilled for linear A_o in cartesian coordinates, but not in cylindrical coordinates:

$$\mathrm{curl} \; \vec{B}_o = A_o / r^2 , \qquad [\mathrm{div} \; \vec{E}_o = E_{or}/r] \tag{3.23}$$

which means an unfavorable anisotropy even in current-free regions and in general a significant increase in discretisation error. It can be avoided by using

$$\bar{\varrho}_o = \bar{\varrho}_1 + \bar{\varrho}_2 r^2 + \bar{\varrho}_3 z, \quad \vec{B}_o = (\bar{\varrho}_3/(2\pi r), \; - \bar{\varrho}_2/\pi) \tag{3.24}$$

$$[V_o = V_1 + V_2 \ln r + V_3 z, \quad \vec{E}_o = -\mathrm{grad} \; V_o] \tag{3.25}$$

Besides the much better discretisation error behaviour (3.24) and (3.25) have disadvantages, i.e. there is no continuity of potential on the element boundaries and the discrete field strengths become infinite on the rotation axis. When using $\bar{\Phi}$ the definition (3.7) is slightly different if (3.8) is kept:

$$\bar{\Phi}' = 2\pi\, r_o(c_1x^2 + c_2xy + c_3y^2) \quad ; \tag{3.7'}$$

for r_o we can put in most cases the radius of the new point. In case of the eddy current field most quantities are complex and equ (3.18) is replaced by

$$\underline{R} = -\mathrm{curl}\,\vec{\underline{B}}_o + (j\omega\sigma\underline{A} + \underline{J})/\nu. \tag{3.18'}$$

In case of a field strength dependent material value the relation between c_1, c_2, c_3 is more complicated. The procedure to get it is shown for the example

$$\mathrm{curl}(\nu\vec{B}) = J, \qquad \nu = \nu(\vec{B}^2) \tag{3.26}$$

in cartesian coordinates. In the following for each spatial dependent factor the value at the position of the new point is put. Equ. (3.26) can be transformed into

$$\nu\,\mathrm{curl}\,\vec{B} - [\vec{B}, \mathrm{grad}\,\nu] = J \tag{3.27}$$

and

$$\nu\,\mathrm{curl}\,\vec{B}' - [\vec{B}_o, \mathrm{grad}\,\nu] = J. \tag{3.28}$$

Replacing grad ν in (3.28) we get

$$\nu\,\mathrm{curl}\,\vec{B}' - \partial\nu/\partial B^2 \cdot [\vec{B}_o, \mathrm{grad}\,B^2] = J, \tag{3.30}$$

$$\nu\,\mathrm{curl}\,B' - 2\,\partial\nu/\partial B^2 \cdot [\vec{B}_o, \mathrm{grad}\,(\vec{B}_o, \vec{B}')] = J. \tag{3.31}$$

Putting (3.8) into (3.31) we get

$$\begin{aligned} &k_1c_1 + k_2c_2 + k_3c_3 = J \\ &k_1 = -2\nu - 4B_{oy}^2 \cdot \partial\nu/\partial B^2 \\ &k_2 = 4 \cdot B_{ox} \cdot B_{oy} \cdot \partial\nu/\partial B^2 \\ &k_3 = -2\nu - 4B_{ox} \cdot \partial\nu/\partial B^2 \end{aligned} \tag{3.32}$$

or transformed to main axes

$$\begin{aligned} &k_1'c_1' + k_3'c_3' = J \\ &k_1' = -2\nu - 4B_{oy'}^2 \cdot \partial\nu/\partial B^2 \\ &k_3' = -2\nu - 4B_{ox'}^2 \cdot \partial\nu/\partial B^2. \end{aligned} \tag{3.33}$$

Usually J is zero; then A' is hyperbolic. In general A'' is anisotropic, the main axis relation depends on $\vec{B}_o$. The anisotropy is maximum when $\vec{B}_o$ lies in a main axis direction; then the relation is

$$q_a = \sqrt{(\nu + 2B_o^2 \cdot \partial\nu/\partial B^2)/\nu} \tag{3.34}$$

with the minor axis (shorter segments) in the $\vec{B}_o$ direction. For common magnetisation curves values of $q_a = 4\ldots5$ can be reached. If $\vec{B}o$ lies in an asymptotic direction of A' there is a local isotropy.
Also for the factor k_i a modification should be made for the following reasons:

- k_i depends on the grid topology in the region of the point, but this topology is in general changed after the halving by diagonal transpositions.
- The triangles' shapes approach automatically an optimal shape as the grid is getting finer.
- If some triangles differ extremly from the optimal shape a determination of H using optimal triangles results in a better estimation of the discretisation error than a calculation with the real triangles as is shown in the example of fig. 4.
- The application of normalised triangle shapes leads to simpler formulae for k_i; in most cases even to an approximate indepency on the segment's angle. The influence of several factors on the mesh size of an optimal grid can better be seen.

In a iteratively generated grid the optimal triangles shape is not necessarily the same as in a static grid. If for instance a segment of a regular triangular grid is halved the grid looses its regularity. A reasonable definition for the dynamically optimal triangles shape is as follows: In a parallelogram composed by two optimal triangles both possible diagonals have the same halving index. From (3.12) it follows that all corners must have the same value of A''^2. For a fixed A''^2 the area of the parallelogram must be maximum.

If A'' is isotropic the optimal triangle is rectangular and equilateral. A rotation of the concerned segment with respect to the new point changes the value of k_i few or not at all if the material value ν etc. is constant.

If A'' is anisotropic the diagonals of the parallelogram are conjugate with respect to A''. If the segment to be halved lies in a main axis direction the triangles are equilateral but not rectangular. For constant material value the maximum change due to the different positions of the segment to be halved is 5/4 which may be neglected.

The factor k_i for optimal triangles can be partitioned with good approximation:

$$k_i \approx k_m \cdot k_r \cdot k_a + k_e, \tag{3.35}$$

where:

k_m = material property factor
For constant material value m (= $\nu, \varepsilon, \lambda, \sigma, \ldots$)

$$k_m = 2m \tag{3.36}$$

(if on both sides of the segment different values m_1, m_2, then $k_m = m_1 + m_2$). For field dependent material property $\nu(B^2)$,

$$k_m = 2(\nu + k_\nu \cdot 2B^2\, \partial\nu/\partial B^2), \tag{3.37}$$

where $0 \leq k_\nu \leq 1$, k_ν is dependent on the main axis relation and the relative directions of $\vec{B}_o$ and the main axes.

k_r = radius factor.

For cartesian coordinates;

$$k_r = 1. \tag{3.38}$$

For cylindrical coordinates r, z and for scalar potential V or vector potential A:

$$k_r \approx 2\pi r_s, \tag{3.39}$$

for the flux function $\bar{\Phi}$

$$k_r \approx 1/(2\pi r_s). \tag{3.40}$$

For segments on the rotation axis the mean radius of the adjacent triangle can be put for r_s, in all other cases the radius of the new point.

k_a = anisotropy factor

$$k_a \approx q_a + 1/q_a \qquad (3.41)$$

For isotropic A'', $q_a = 1$ and

$$k_a = 2 \qquad (3.42)$$

k_e = eddy current factor

For real potential

$$k_e = 0, \qquad (3.43)$$

for eddy current problems

$$k_e = \frac{s}{3}\omega(\sigma_1 + \sigma_2), \qquad (3.44)$$

where s is the area of the optimal triangle and σ_1, σ_2 the electrical conductivities in the adjacent triangles.

Some general conclusions about optimal grids can be drawn. The assumption is that the halving indices of all segments are equal.

In the most simple case where all k_i in the whole grid are identical all segment end points must have the same A'' value. For an isotropic A'' the length ℓ of a segment is by (3.14)

$$\ell \sim 1/\sqrt{|c_1'|} \qquad (3.45)$$

where $|c_1'|$ may be called "local potential curvature". In the anistropic case this "curvature" is dependent on the direction.

On the other side it is interesting to consider the influence of other effects on ℓ when the "curvature" is given. Equ. (3.13) leads to

$$\ell \sim k_i^{-\frac{1}{4}} \qquad (3.46)$$

The influence is only significant if the coefficients of equ. (3.35) vary very much. The material value can change ℓ by factors 5...10 in the case of ν or the thermal conductivity λ. The direct effect of cylindrical symmetry is only significant near the axis. The anisotropy does not matter very much; with a geometrical relation of 1:32 the segment become shorter by a factor of 2. The eddy current factor is significant only for very coarse grids.

The following example shows a degeneration of the second type and how it is removed by the modification of A' and k_i. It also makes clear that in some cases the halving indices of boundary and contour segments must be adapted.

The grid of fig. 4a in taken as a starting point, where all points have fixed potentials according to the assumptions

$$A' = x^2 - y^2, \quad A'' = x^2 + y^2, \quad \nu = 1; \qquad (3.47)$$

which leads to

$$A(P_1, P_2, P_5, P_6) = 1 - \varepsilon^2, \; A(P_3, P_6) = -1, \; W_6 \approx 4 \qquad (3.48)$$

An additional condition is that the segments P_1P_5 and P_2P_4 cannot be transposed because they are contour segments. Fig. 4b and 4c show optimal grids with one and two additional points.

The use of A'' and of k_i for optimal triangles leads to

$$k_{opt.} = 4, \; A'' \approx 1, \; H_7 = H_8 \approx 2 \qquad (3.49)$$

which is in the same order of magnitude as

$$W_8 \approx 2, \quad \Delta W_{6-8} \approx 2 \qquad (3.50)$$

If the halving indices are determined by an attempted introduction of one of the points we get

$$k_{Real} \approx 1/(2\varepsilon), \; \Delta A_7 \approx -4\varepsilon, \quad H_7 = H_8 \approx 4\varepsilon, \qquad (3.51)$$
$$W_7 \approx 4 - 4\varepsilon, \; \Delta W_{6-7} \approx 4\varepsilon$$

The halving indices are much too small because the estimation of the final potential of the new points in this way is much worse than by A''. On the other side the use of A'' and k_{Real} leads to

$$H_7 = H_8 \approx 1/\varepsilon \qquad (3.52)$$

which is much too big

The arrangement given in fig. 4a shows another difficulty. The segment P_2P_5 gets a slightly higher halving index than P_1P_5 and P_2P_4, but a halving of P_1P_5 would be very unfavourable because the small distance 2ε between some points would be reduced to ε due to the impossibility of transposition of P_1P_5 and P_2P_4. The difficulty is removed if P_1P_5 or P_2P_4 is halved first and P_2P_5 eliminated by transposition.

The general problem can be described as follows:

A new point besides a boundary (or contour) is generated which has a smaller value of A'' than the end points of a boundary segment with the origin of A'' on the segments center. This degeneration can be eliminated by an eventual enlargement of boundary segment halving indices such that these are greater than the indices of segments which can produce such near-boundary points.

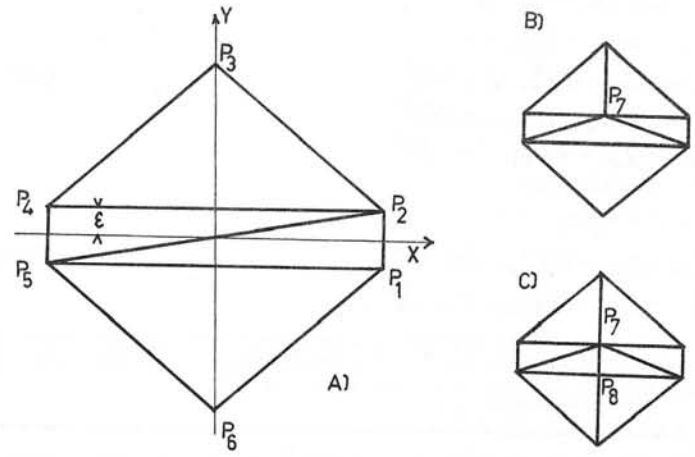

Fig. 4

4. Diagonal Transposition

Transposition Criterion

The transposition has to lead to the segment distribution with the least energy for a given grid point distribution. Here too it is not possible to determine the exact effect of a transposition. To get a reasonable approximation only the energy in the concerned quadrangle is considered and the potentials of the corners are taken as fixed.

The analysis is firstly made for an isotropic case, i.e. Laplace's equation in cartesian coordinates with constant reluctivity ν. At the points $P_1 \ldots P_4$ of fig. 3 the potential values $A_1 \ldots A_4$ are assumed, leading to a field strength $\vec{B}$ in the respective triangles. The potential A can be divided into

$$A = A_e + A_r \quad , \vec{B} = \vec{B}_e + \vec{B}_r \qquad \text{with}$$
$$A_e\,(P_1, P_2, P_3, P_4) = A_1,\ A_2 - k,\ A_3,\ A_4 - k, \qquad (4.1)$$
$$A_r\,(P_1, P_2, P_3, P_4) = 0,\ k,\ 0,\ k,$$
$$k = A_{D24} - A_{D13}$$

where A_{D24}, A_{D13} are the potential values in the intersection point for the respective diagonal. The quadrangles energy is

$$W_q = \nu/2 \cdot \int \vec{B}^2 da = \nu/2 \cdot \left[\int \vec{B}_e^2 da + 2 \int (\vec{B}_e, \vec{B}_r)\ da + \int \vec{B}_r^{\,2} da \right] \qquad (4.2)$$

The first integrand is the same for both diagonals; the second integral is zero for each diagonal. In case of nonzero k the evaluation of the third integral leads to the result that the diagonal with greater product of heights on it is better. An identical condition is that this diagonal is better for which the circumscribed circles of the triangles do not include the respective fourth point of the quadrangle. The diagonals are equivalent if all four points lie on a circle.

If k is equal to zero the energy criterion leads to the obviously wrong conclusion that both diagonals are of equal value irrespective of the shape of the quadrangle. The geometrical criteria are better because they do not degenerate in this way and are less subject to rounding errors.

It is remarkable that the above criteria are invariant with respect to rotation, even the energy criterion with the degeneration excluded. This fact further justifies the transition from A' to A''. Indeed a collaboration of an extremely position dependent halving index with a rotation-invariant transposition criterion seems not to be possible.

In an anisotropic optimal grid the above criteria are no more correct. Similar derivations starting with the energy of the quadrangle could be made, but the formulae replacing (4.2) are substantially more complicate and degenerate in more cases than (4.2). It is therefore better to introduce the modified potential A'' which also represents the anisotropy but contains security against degeneration. The geometrical criteria of the isotropic case can be brought into the following formulation which is also applicable to the anisotropic grids:

- The origin of A'' is put such that all corners of one partial triangle get the same values of A''.
- If the fourth point of the quadrangle has a greater/equal/ smaller value of A'', the existing diagonal is better/equal /worse.

For complex potential there are the following two possibilities: If A'' is adapted such that $|A''|$ is quadratic as mentioned in chapter 3, the above criterion may be used with $|A''|$. If this has not been done, the origins of real and imaginary part may be determined separately and the comparison is then applicated to $(\mathrm{Re}\ \underline{A''})^2 + (\mathrm{Im}\ \underline{A''})^2$.

An important property of the criterion is that in parallelograms the diagonal with the smaller halving index is considered to be better. Since all pairs of optimal triangles form parallelograms the transposition in general reduces the sum of the halving indices significantly.

There are some cases of the linear Poisson equation in cartesian coordinates in which also for an anisotropic A'' the A''-criterion may easily be compared with the energy criterion. The assumption is that the four grid point potentials coincide with A''. If A' is elliplic the energy criterion leads to an identical condition as the A''-criterion for equivalent diagonals, since A_r and B_r are zero. For hyperbolic A' and anisotropic A'' both criteria differ; for instance for a rhombus with diagonals in the main axes of A' the length relation for equivalent diagonals may differ by a factor $\sqrt{3}$ between both criteria.

Sequence of Transpositions and Transposition Tests

As mentioned in chapter 2 the grid is optimized by transpositions immediately after each halving. It is assumed that for given gridpoints there is only one energy minimum and that any sequence of transpositions in which every worse diagonal is transposed reaches that minimum. A simple algorithm which organises this sequence is the following:

1) Put all possibly worse diagonals into a queue
2) Test the last diagonal in the queue, reduce the number of diagonals by 1.
3) If the result of the transposition test is negative, test if the number of diagonals in the queue is 0. If true, the optimal grid is reached. If not, pass to point 2.
4) If the result of the transposition test is positive, perform the transposition. Put all segments into the queue which have possibly become worse diagonals by the preceding transposition. Pass to point 2.

Due to the optimality of the grid before the halving the initial content of the queue consists of a very restricted set of segments. These are the radial segments P_NP_1, P_NP_2, P_NP_3, P_NP_4 and the peripheral segments P_1P_2, P_2P_3, P_3P_4, P_4P_1 in fig. 5. For all other segments the adjacent triangles are the same as before the halving. A short analysis shows that all radial segments must be optimal; P_NP_2, P_NP_3, P_NP_4 for purely geometrical reasons and P_NP_1 due to the optimality of the grid before the halving (if P_2P_4 is better than P_1P_N, then it is also better than P_1P_3). Thus the queue contains only the four peripheral segments at the beginning.

If the transposition test on a segment, for instance on P_2P_3 is positive, the effect is:

- P_2P_3 is replaced by P_NP_5.
- There is a new radial segment P_NP_5.
- A peripheral segment is removed by two different ones.

Principally the radial segments P_NP_2, P_NP_3 and the peripheral segments P_2P_5, P_5P_3 may have become worse diagonals, but for the radial segments it may be shown that this assumption is contradictionary to the optimality of the grid before the halving. Thus it may be said that the transposition process after a halving is restricted to the connection of the new point N with additional neighbour points. For n transpositions the algorithm needs 2n + 4 transposition tests. In a statically optimal infinitely fine grid each point has got 6 neighbours; therefore we could expect a mean

value of 2 transpositions and 8 transposition tests per new point, which is in fairly good agreement with practice. In starting grids there may be much more transpositions per new point as can be seen in the example of fig. 6. For both examples isotropy was assumed.

If A'' is anisotropic a segment arrangement may be shifted out of optimality by iteration and subsequent recalculation of A''. Theoretically in this case there should be an additional transposition run for the whole grid with the new A'' before the first halving of the new refinement stage. In practice this is omitted because during the normal process unfavorable diagonals are transposed or halved.

Since for the optimisation of the starting grid A'' is in general not known, isotropy is assumed. If the grid generation is started at the coarsest possible grid, all N points lie on boundaries or contours. The maximum possible number of transpositions then is about $N^2/4$.

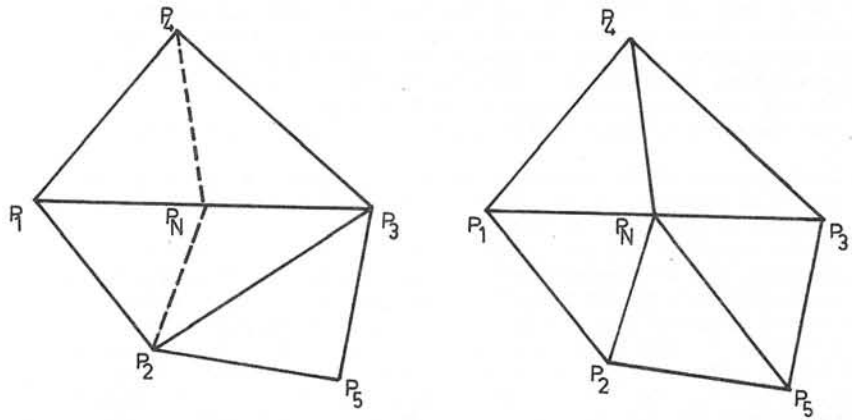

Fig. 5

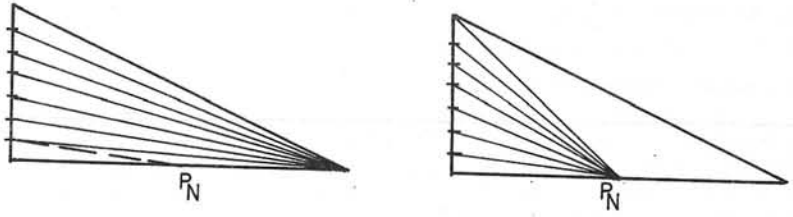

Fig. 6

5. Methods for the Numerical Determination of the Remainder Potential

The calculation must be simple and stable with respect to bad grids and residual errors, but represent significant changes within few elements. In practice the following method has proved to be good:

- The coefficients c_1, c_2, c_3 of the remainder potential are attributed to the triangles, mainly from reasons of programming technique.
- The numerical condition is formulated in terms of $\vec{B}$.A neighbourhood is selected, which contains the reference triangle and the adjacent triangles with the same material properties (ν , J) as the reference triangle. For each triangle i the discrete field strength $\vec{B}_{Di}$ is determined. The condition is that the energy of the difference field $\vec{B}_0 + \vec{B}' - \vec{B}_{Di}$ withhin the neighbourhood is minimum. The equation (3.17) or (3.32) is used, such that at least 3 triangles are needed.
- By positioning the origin of $\vec{B}'$ into or nearby the centre of gravity of the neighbourhood the minimisation can be partitioned into two separate calculations of $\vec{B}_0$ and $\vec{B}'$. After the calculation of $\vec{B}_0$ the field dependent quantities in (3.32) or if present in (3.17) can be numerically determined.
- The subsequent calculation of c_1,c_2 leads to two linear equations in case of (3.32); for (3.17) their coefficients matrix is even diagonal. c_3 then is determined by (3.17) or (3.32).

The discretisation to $\vec{B}_{Di}$ and the use of the relation between c_1, c_2, c_3 gives a great numerical stability. The algorithm yields reasonable values even if all grid points lie on boundaries. In some rare cases there can be degenerations, particularly if locally A'' vanishes in a main axis direction. To avoid this it is the best to enlarge the coefficients if necessary such that they reach at least a certain fraction of the coefficients in the adjacent triangles with the same material properties.

6. Effect of the Refinement on the Distribution of Halving Indices, Criterion to Stop the Refinement Step

The effects of the refinement process are best described with the frequency distribution of the halving indices n(H), the related distribution H.n(H) and its integral ΣH. In order to get reasonable plots of the distributions the H-axis must have a logarithmic scale.

Fig. 7 shows the selective refinement in a simple arrangement, namely the determination of the carter factor with the analytical value of W = 2.277437 in this case. The strong refinement near the singular point is obvious. Fig. 9 gives the distributions n(H) and H.n(H) for the different refinement steps at the beginning of each refinement . In the end phase the distributions approach standard forms with relatively small deviations, whereas at the beginning the deviation is much greater. The selective refinement compresses the distributions from the right to a certain broadness; later they are more or less shifted, which means a uniform refinement.

To halve all segments in a grid multiplies the number of grid points by 4. Under the assumption of an invariant A'' which is fulfilled for fine grids and arrangements with no singularities, we get the following equations:

$$n_{(new)}(H/16) \cdot d(H/16) = 4 \cdot n_{(old)}(H)dH, \qquad (6.1)$$

$$\Sigma H_{(new)} = \tfrac{1}{4} \Sigma H_{(old)} . \qquad (6.2)$$

This means, that for uniform refinement

$$\Delta W_N \approx \Sigma H \sim N^{-1} , \qquad (6.3)$$

which is a well-known relation for first order elements. The real error for the arrangement of fig. 7, which is shown in fig. 8 is in good agreement for the last refinement steps, if the refinement is done starting from the coarsest possible grid (curve A). The rule (6.3) may be used to estimate the discretisation error of the energy and other results, sometimes even to extrapolate more accurate values. At the beginning the decrease of the total error is much faster because the refinement process is selective. The agreement between ΔW_N and ΣH (curve D) is fairly good in spite of the many simplifications.

The deviation of the distributions in the end phase cannot be avoided since the refinement process is discontinuous. A single halving changes a segment with a halving index H into two segments with indices H/16 each; because of some additional effects the deviation is in general sligthly greater, but such a grid is by no means as bad as it seems. Under the very optimistic assumption that we may apply (6.1) in a continuous way to any position of the distribution we get

$$\Delta n(H/\alpha) \cdot d(H/\alpha) = -\sqrt{\alpha} \cdot \Delta n(H) \cdot dH . \qquad (6.4)$$

Theoretically, from a grid with the distribution n(H) a grid with uniform indices H_o could be built up, for which

$$N(H_o) = \Sigma\sqrt{H} \,/\, \sqrt{H_o} . \qquad (6.5)$$

If the number of gridpoints is the same as in the original grid, ΣH reduces by a quality factor

$$G = (\Sigma\sqrt{H})^2 / (N \cdot \Sigma H) . \qquad (6.6)$$

G is shown in fig. 8 for each grid; the first value is calculated before the iteration and the second after the recalculation of the halving indices. For the last grids values of 0.85 are reached, which means that by an optimal distortion of the grid the error could be reduced by about 15%. But even for the grids with higher number of points there is a considerable change by the iteration in the quality factor due to the singular point which causes a dispersion of the distributions. Fig. 10 shows this dispersion at a coarse and fine grid.

Curve B of fig. 8 shows energy error, quality factor and ΣH for a different way of refinement, namely a uniform refinement at the beginning which is obviously much worse than the selective refinement. By some selective refinement stages this bad quality may be removed if there are not too many points in the uniform grid. The proceeding B sometimes needs less calculation effort than A. The quality factor G for the first grid of B is very small; the least possible error for a grid with the same number of points is in good agreement with the real values of A. Point C also represents a uniform grid and shows that uniform refinement in general is worse than (6.3) if singularities are present.

Knowledge about the distributions may be used to stop the refinement step and to start the iteration. It is clear that the refinement step must be stopped if the halving indices are no more significant. On the other side refinement and iteration steps should not interchange too often because of the effort to determine the halving indices and the equations. In chapter 8 it is shown that the total effort for a grid with N points is about $N/(1-q_r)$, where q_r is the quotient of the point-numbers of two subsequent grids. It may be concluded that an enlargement of q_r beyond $\frac{1}{2}$ is not of great use, which means that a duplication of the point number at each refinement stage should be attempted if the distribution of the indices allows it. From (6.3) there is in this case also a halving of the energy error and of ΣH.

Obviously for very bad grids a duplication of the number of points is far from optimal. On the other side the refinement process in these cases gets very slow if each refinement stage is stopped when ΣH is halved. It is a fairly good compromise to stop the refinement if

$$\frac{N - N_o}{N_o} \cdot \frac{(\Sigma H)_o}{\Sigma H} \geq k , \qquad (6.7)$$

where the values at the beginning of the refinement step are signed by indices O. For uniform refinement, i.e. $(\Sigma H)_o / \Sigma H = N/N_o$, (6.7) leads to

$$(N - N_o)/N_o = \tfrac{1}{2} (\sqrt{1 + 4k} - 1), \qquad (6.8)$$

which leads to a duplication of the number of gridpoints if k = 2 and to the simple rule

$$\text{eliminated error} \approx \text{remaining error} \qquad (6.9)$$

In very bad grids, the number of points may be increased by only 10%, but in this case ΣH diminishes by a factor of 20 according to (6.7). Naturally it is not necessary to check with (6.7) after each halving; it is sufficient to apply the rule after each scanning cycle.

7. Effects of the Grid Refinement on the Iteration

The convergence of a normal iteration process is given in fig. 11, curves A and B. They represent a complete iteration process in the final grid of fig. 7; no overrelaxation was applied. At the beginning the residues have a rather random distribution and in general different signs, which makes the convergence fast. Later there is a transition to a situation with equal signs for all residuals and an error distribution which diminishes uniformly; the convergence is significantly slower.

A grid refinement step changes a part of the discretisation error into resudual error, i.e. new residues are introduced. As mentioned in chapter 3 the signs of these new residues are well intermixed. That is why the convergence after a refinement step is in general similar to the starting phase of a normal iteration, as may be seen from the part of curve C which concerns the final grid. For the coarser grids the slower convergence is not reached at all. Curve D shows the total energy error, whereby the generation and elimination of residual error is obvious. A part of the discretisation error is eliminated directly by the diagonal transpositions, particularly in the starting grids. It is interesting that sometimes an iterative grid generation needs not only fewer iterations of single potentials but also fewer iteration cycles to reach the same accuracy as in the present case. The reason is that convergence in coarser grids is in general faster. Experience shows that in few cases of slow convergence even the total effort of refinement and iteration may be smaller than that of a complete iteration in the final grid.

The consideration of the different energy errors allows to establish a reasonable criterion to stop the iteration. In order to ensure a good estimation of the halving indices for the following refinement step the residual error should be an order of magnitude less than the discretisation error. On the other side a very small residual error does not contribute much to the overall accuracy. As a rough approximation it is assumed that the total energy error is proportional to the square of the mean potential error (which is exact if the potential error diminishes uniformly). In order to get a relation of 1:5....10 between the residual and the discretisation error in the potential which allows a reasonable estimation there must be an energy relation of 1:25...100.

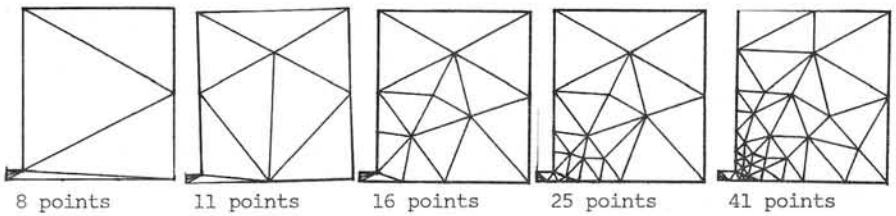

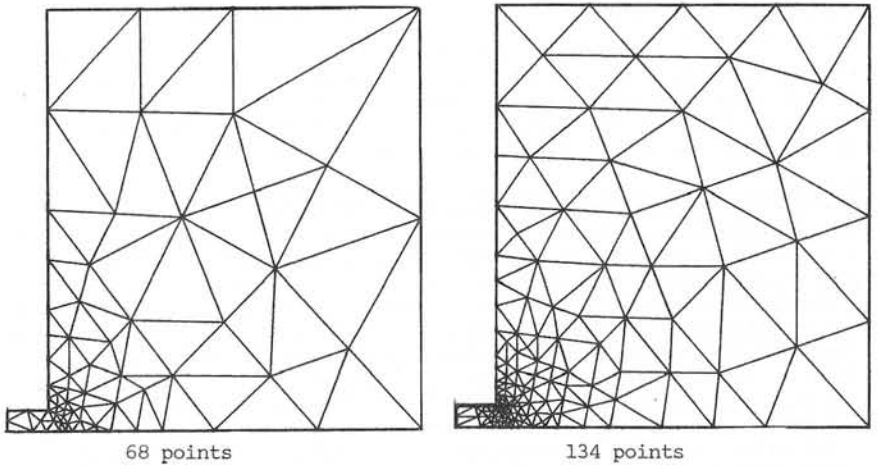

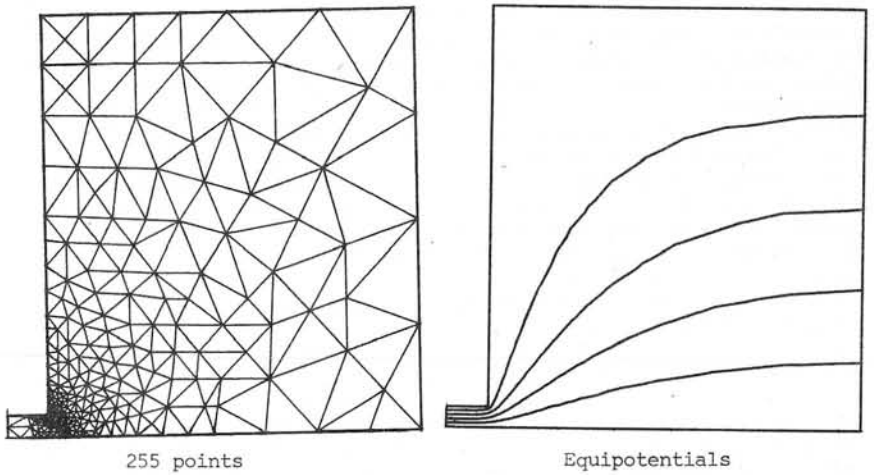

Fig. 7

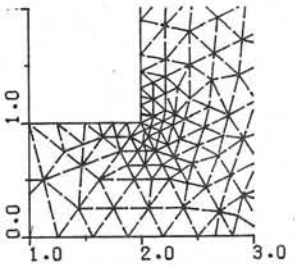

Detail of Final Grid

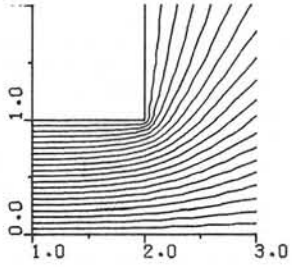

Detail of Equipotentials

Fig. 7 (continued)

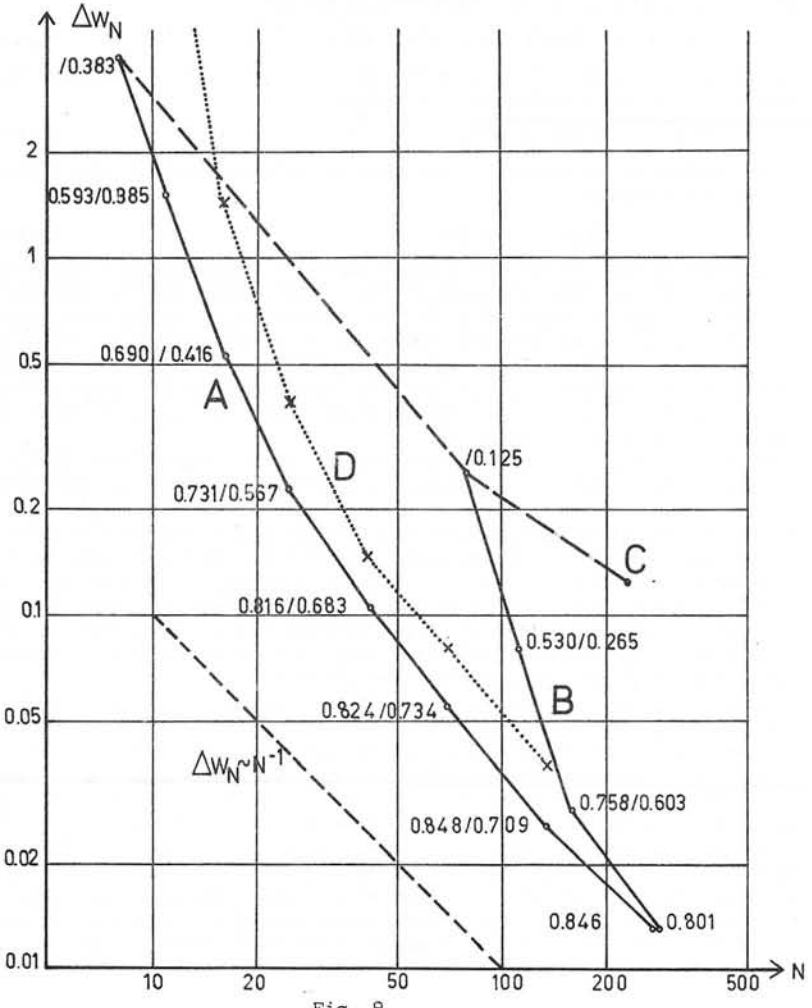

Fig. 8

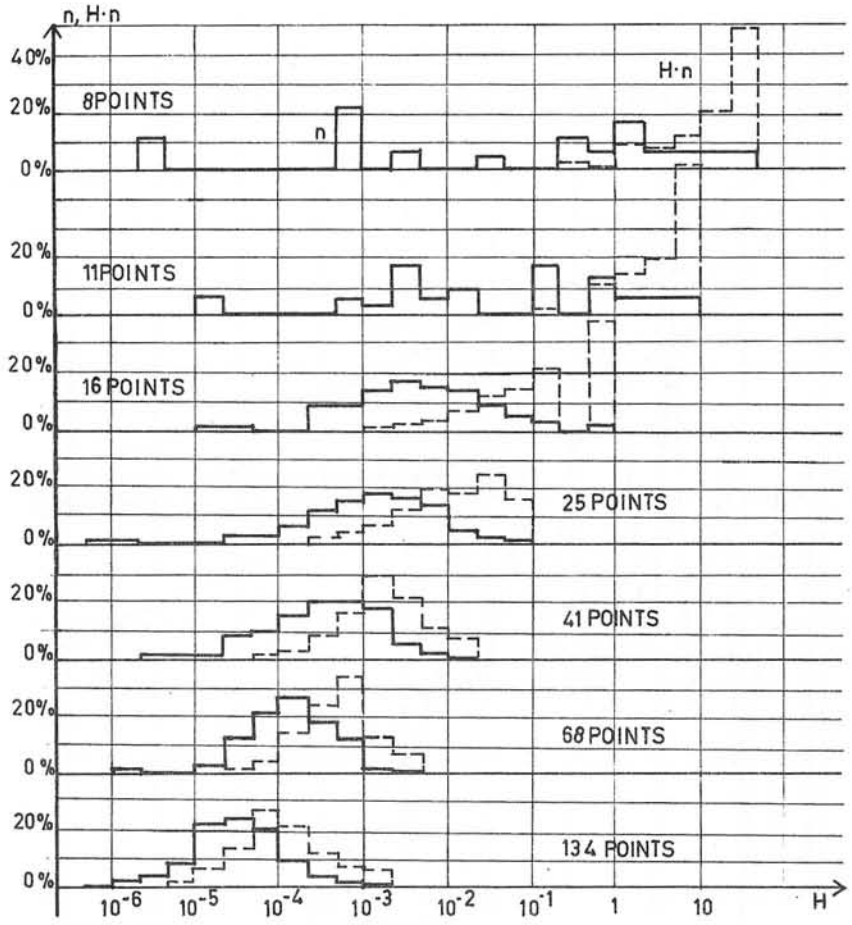

Fig. 9

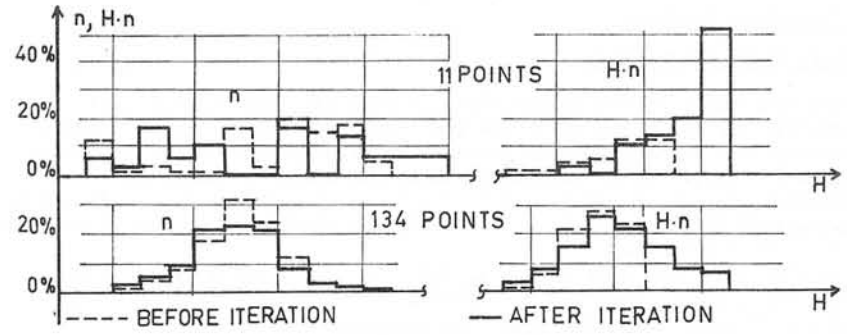

Fig. 10

The discretisation error contained in a grid is determined only at the subsequent refinement step, i.e. too late to be used to stop the iteration. It is much easier to use the relation (6.9) which equals the remaining discretisation error to the eliminated discretisation error. It must be noticed that (6.9) is only valid for uniform refinement, but in case of selective refinement all other estimations of the remaining discretisation error are also quite uncertain. In general a great part of the eliminated discretisation error is changed to residual error and usually the residual error remaining from the former iterations is much smaller. Thus it may be concluded that the iterations can be stopped when the probable remaining residual error is 1/25...1/100 of the eliminated or total residual error.

In the following it is assumed that the convergence speed is uniform, which means that the relation of two subsequent energy reductions is constant:

$$\Delta W_{i+1} / \Delta W_i = \lambda , \tag{7.1}$$

$$S_{NT} = \sum_{i=N+1}^{\infty} \Delta W_i , \tag{7.2}$$

where S_{NT} is the remaining error after N iterations . From (7.1)

$$S_{NT} / S_{OT} = \lambda^N . \tag{7.3}$$

The relation

$$S_{NT} / S_{OT} \approx q_I^2 \tag{7.4}$$

is reached when

$$N \approx 2 \ln q_I / \ln \lambda . \tag{7.5}$$

The following table shows the necessitated number of iterations for the realistic value $\ln q_I = -2$ ($q_I = 0.1353$) and for different convergence speeds:

N	4	6	10	15	20
λ	0,37	0,51	0,67	0,77	0,82

20 iterations correspond to a quite slow convergence, namely a diminuation of a potential error of about 10% by each iteration cycle.

There is a certain contradiction between the assumption of a constant convergence speed and the fact that the convergence is getting slower during the iteration, but the variable convergence speed is a quite general problem for the estimation of the remaining residual error. A more accurate estimation for the error relation in case of a variable λ_i consists in

$$S_{NT} \approx \lambda_N \cdot \Delta W_N / (1-\lambda_N), \qquad S_{OT} = \sum_{i=1}^{N} \Delta W_i + S_{NT} . \tag{7.6}$$

In case of slow convergence ($\lambda > 0,8$) convergence speed should be accelerated. The knowledge about λ can be used to optimize the over-relaxation factor. If this is not sufficient, additive block relaxation can be applied. For automated grid generation the selection of the block boundaries must also be automated because the grids are not known when the input data are prepared. It is a certain advantage of the automated grid generation that it tends to decrease bad convergence outcoming from the grid definition.

(7.4) and (7.5) are based on stable relations between the different energy errors in the whole process. These assumption are sometimes not fulfilled, particularly at the beginning or if only a part of the whole

process is performed. It is obvious that when the refinement passes from selective to uniform the residual errors pass very quickly to the stable relations mentioned above. For the cases in which these relations are not reached one could add special convergence criteria for the final grid.

8. Calculation Effort

In general most effort is used in blocks 2 and 4 of the flow diagram in fig. 1. Experience has shown that the partial efforts for the algorithms performed there are with a good approximation proportional to the number of gridpoints if a fixed number of iteration cycles is assumed. Therefore the effort for a refinement step and the following iterations (a refinement loop) is

$$t_L \approx N \cdot (t_R + t_{It}) , \qquad (8.1)$$

where N is the number of points in the finer grid and t_R, t_{It} the effort per point for refinement and iterations. For a computer IBM 370/158 the following CPU times have been measured:

$$t_R \approx 0.015 \text{ sec.}$$
$$t_{It} \approx 0.010 \ldots 0.200 \text{ sec.} \qquad (8.2)$$

While the time needed for refinement is fairly constant, the time for the iteration depends strongly on the type of the equations, the number of iteration cycles and the application of block relaxation.

In case of uniform refinement the efforts for the different refinement loops form a geometrical progression. If the ratio q_r between the point number of two successive grids is $\frac{1}{2}$ and the starting grid has a negligible number of points the total time is

$$t_{total} \approx 2 \cdot N_F \cdot (t_R + t_{It}), \qquad (8.3)$$

where N_F is the number of points in the final grid. For selective refinement the sum factor is greater than 2. The total effort for reasonable final grids of 300 - 1000 points lies between the extreme values of 15 and 400 sec. For uniform refinement a simple relation between the total effort and the overall accuracy can be established by (6.3) and (8.3):

$$t_{total} \sim \Delta W_N^{-1} . \qquad (8.4)$$

A comparison between the efforts of iterative grid generation and the input of the final grid can be done. It shows that for the same calculation time in the final grid 60 - 100 iteration cycles could be performed, where the higher value holds for good convergence. In this case the input of an optimal final grid would need less calculation time, but the absolute values are relatively small. If medium or bad convergence is present, there is in general no advantage to perform all iterations in the final grid. However, if a very good starting potential distribution is known, the use of a given final optimal grid needs less time, which can be used for the determination of nonlinear charateristics.

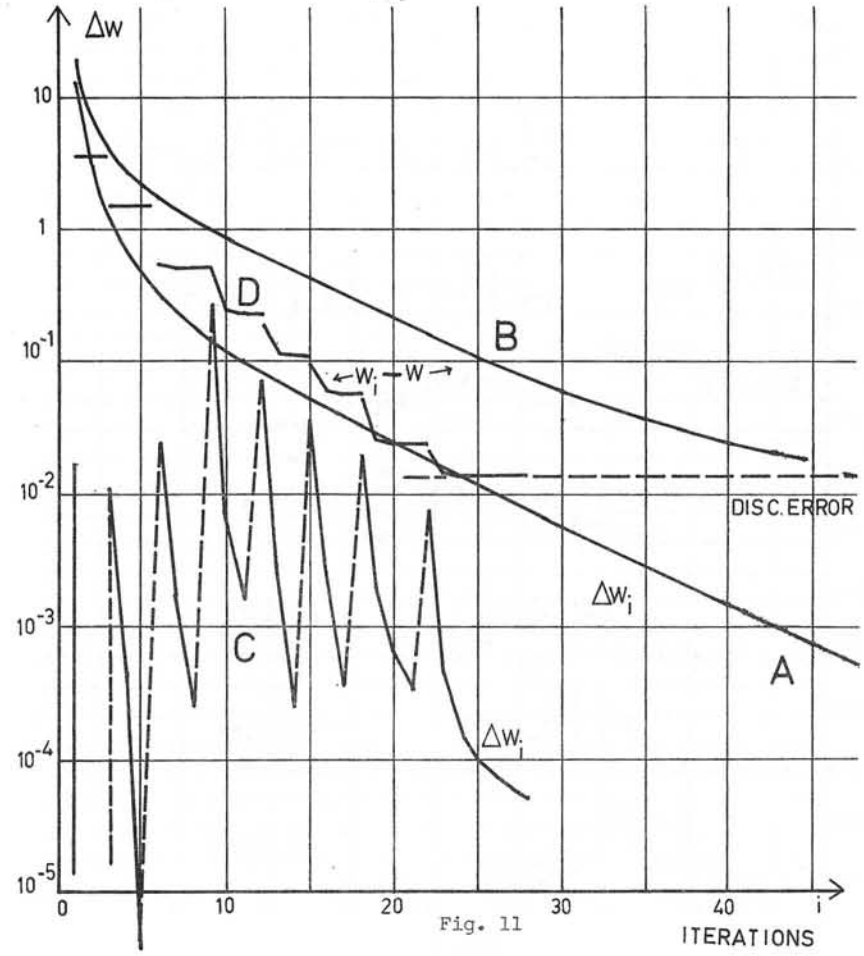

Fig. 11

9. Practical Examples

Static Field of a Magnet

The main parts of the Magnet shown in fig. 12. have a rotational symmetry. For the calculation the yoke has been modified to rotational symmetry with unchanged cross section. The r-axis represents a symmetry plane. The m.m.f. is 32'000 ampere-turns per coil, the magnetic characteristic of the iron is given by the following ν-values in A/m for equidistant B^2-values with $\Delta B^2 = 0.25$; the first value is at $B^2 = 0$, the last at $B^2 = 4.75\ T^2$:
150, 150, 150, 155, 170, 205, 285, 440, 750, 1250, 2100, 3300, 4900, 6700, 8800, 11600, 15000, 20900, 35500, 55000.

For $B^2 \geq 4.75$, $\partial H / \partial B = 1/\mu_0$ is assumed.

Fig. 13 contains the final grid with 925 points. There is a considerable grid density at the criterial points on the pole. In general the grid in regions with $\nu = \nu_0$ is much finer than in the iron due to the influence of ν on the discretisation error. In the coil a varying grid anisotropy can be observed which is principally independent on the field strength direction. At some regions in the iron, particularly at the corners where the flux lines are nearly concentrical circles there is an anisotropy whose direction is dependent on the direction of $\vec{B}$. The following table shows the refinement steps and some characteristical results for the different grids. The program takes 200 sec for the whole process. It may be concluded that the energies in the final grid have relative discretisation errors of approximately 0.2%, whereas the accuracy of the force on the coil is about 1% and of the B-values about 2-5%. To know $\vec{B}$ very accurately near the origin a separate refinement of a partial grid in this region is appropriate.

Number of Grid Points N	Field energy $\int dv \int HdB$ [J]	Coil Energy $\int A.Jdv$ [J]	Total Energy [J]	F_z=Force on the coil [kN]	B_z at z=0, r=0 [T]	B_z at z=0, r=0.02m [T]
23	371.8	-656.4	-284.6	3.04	0.182	0.181
26	383.5	-667.1	-283.6	3.15	0.342	0.192
36	539.4	-1063.9	-524.5	2.47	1.125	1.048
44	473.9	-1009.0	-535.1	2.05	0.915	0.990
68	496.3	-1062.0	-565.7	2.45	1.187	1.527
124	484.4	-1063.6	-579.2	2.39	1.373	1.526
228	485.8	-1069.1	-583.3	2.40	1.346	1.555
454	482.7	-1068.6	-585.9	2.41	1.376	1.582
925	483.7	-1070.6	-586.9	2.42	1.442	1.577

Eddy Current Losses in a Conductor-Tank-Arrangement

Fig. 14 shows a quarter of the arrangement. On the y-axis the potential is 0 (inverse current signs for $x<0$), the x-axis is a Neumann boundary (equal current signs for $y<0$). The tank is made of ferromagnetic steel with an electrical conductivity of $7.10^6 \Omega^{-1}m^{-1}$; it is considered as a nonlinear complex boundary condition [5] which takes into account the eddy currents and the field dependent reluctivity. The conductor is of copper with conductivity $5.10^7 \Omega^{-1}m^{-1}$, its total current is $\hat{I}$ = (14.14, 0.) kA. Fig. 14 and 15 show the flux lines in the moments of maximum and zero conductor current. The entrance of the flux lines into the tank is far from perpendicular because of the considerable eddy currents. The grid shown in Fig. 16 is concentrated on the conductor where a systematic anisotropy can be seen. The smaller grid density in the conductors centre coincides with the smaller current density. Some results are given in the following table for different grids; the calculation took 60 sec. on an IBM 370/158 computer. The calculation is made for a frequency of 50Hz.

Number of Grid Points N	$\hat{U}$=conductor voltage [V/m]		Conductor power loss [kW/m]	$\hat{I}$=current in a quarter of the tank, [kA]		Power loss in a $\frac{1}{4}$ tank [kW/m]
	Real	Imaginary		Real	Imaginary	
18	0.710	1.310	1.205	-7.53	-2.13	4.51
27	0.955	2.120	1.262	-9.18	-2.97	6.11
41	1.029	2.185	1.283	-8.58	-2.63	5.78
63	1.029	2.324	1.195	-8.64	-2.73	5.96
116	1.029	2.391	1.212	-8.71	-2.75	5.95
209	1.013	2.418	1.199	-8.67	-2.76	5.94

10. References

1. G.E. Forsythe, W.R. Wasow: Finite-Difference Methods for partial Differential Equations. J. Wiley and Sons, N.Y., 1965
2. R. Courant, K. Friedrichs und H. Lewy: Ueber die partiellen Differenzengleichungen in der math. Physik. Math. Ann. 100, 1928, 32-74
3. L. Collatz: The Numerical Treatment of Differential Equations. Springer Verlag, Berlin 1960
4. S. Gerschgorin: Fehlerabschätzungen für das Differenzenverfahren zur Lösung partieller Differentialgleichungen. Zeitschr. für angew. Math. und Mech., Band 10, Heft 4 August 1930, S. 373...382.
5. R. Leyvraz: Losses in the internal Parallel Bus-Bars in Transformers and the Adjacent Tank Material. Bulletin Oerlikon, Nr. 389/390, June 1969
6. R. Leyvraz: Field Calculation by an Automatic and Iterative Grid Generation with Minimum Discretisation Error. International High Voltage Symposium 1975, Bulletin of Swiss Electrotechnical Institution.

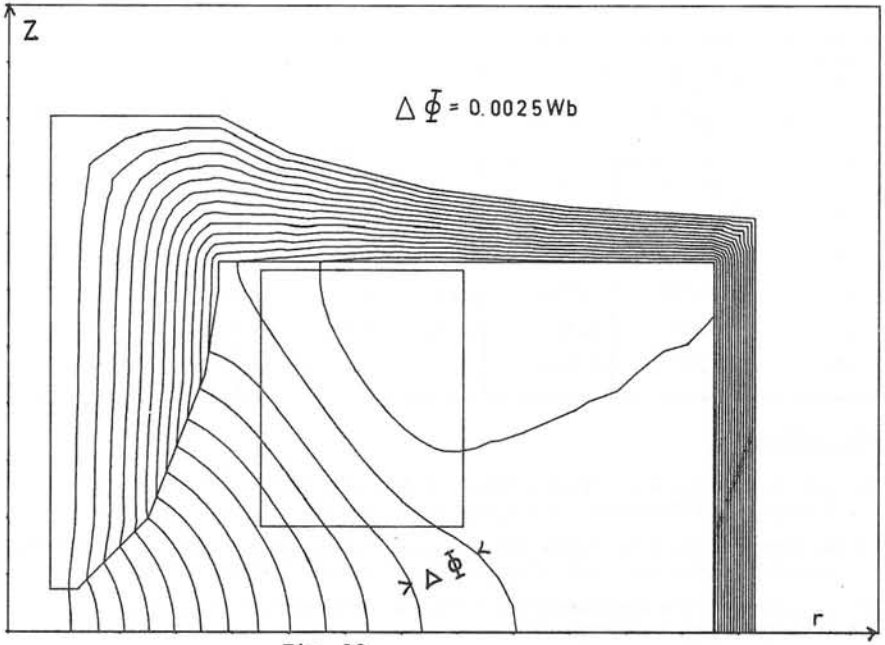

Fig. 12

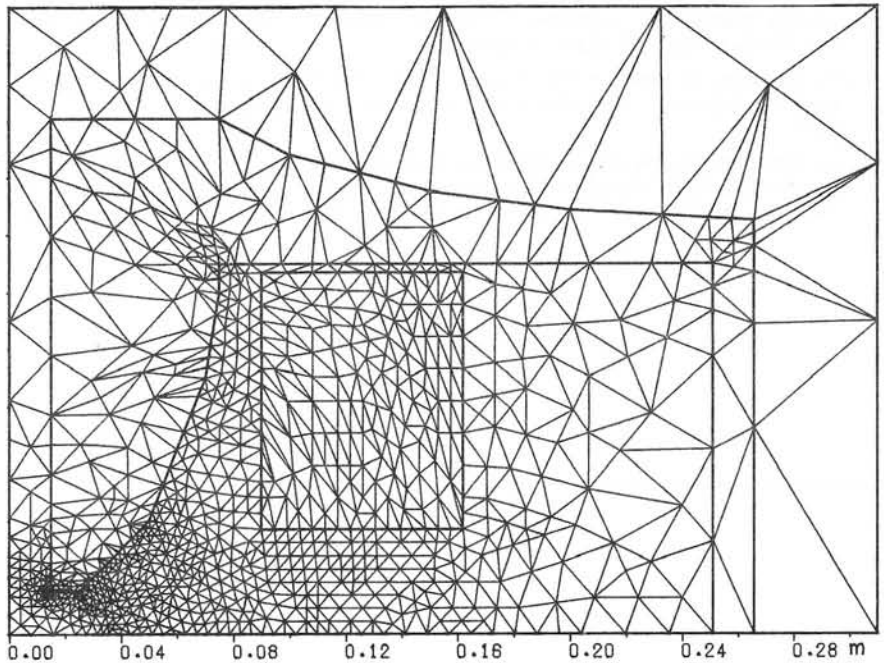

Fig. 13

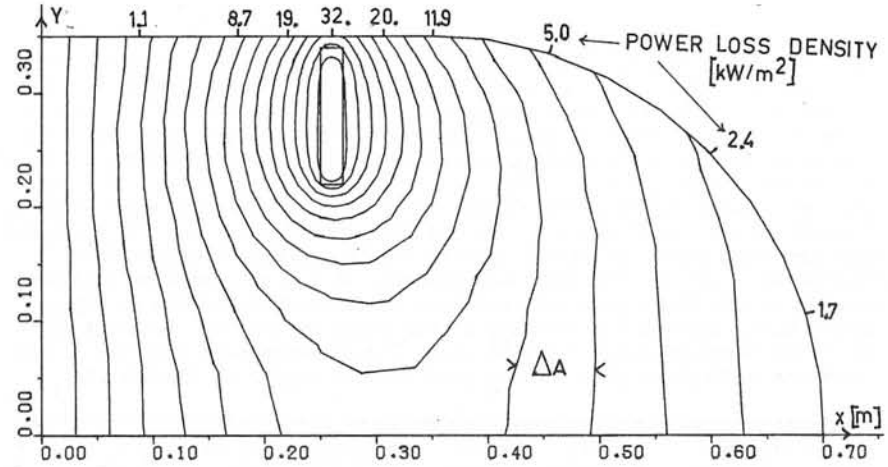

Fig. 14

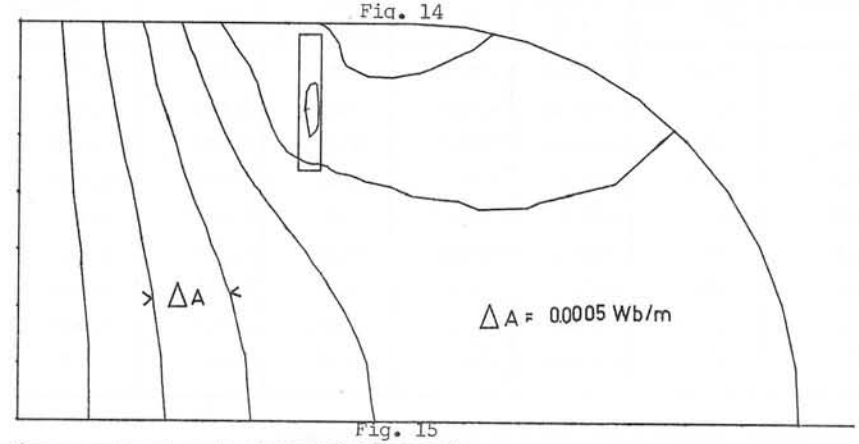

Fig. 15

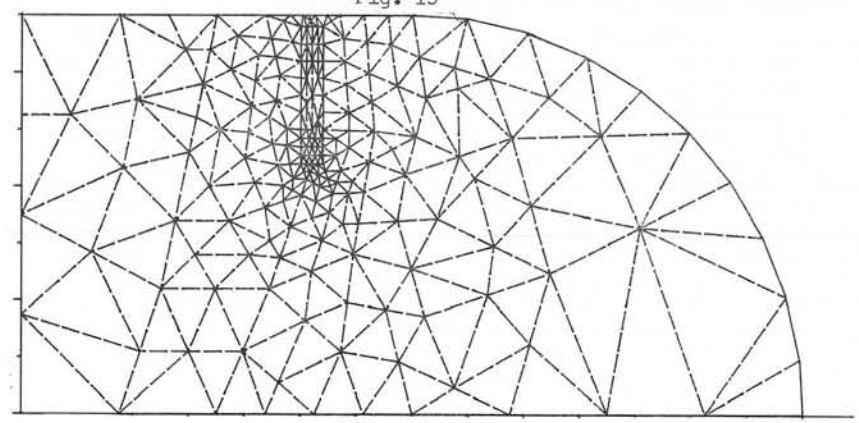

Fig. 16

Discussions following paper:

(Newman) 1) You do not include algorithms to remove mesh points. Did you not find this to be necessary

2) Could you comment on the feasibility of extending this method to three dimensions.

(Leyvraz, Zurich) 1.An algorithm to remove grid points is in general not necessary for the complete generation of a grid from the coarsest possible starting grid. However, it would be very useful in some other situations for instance if an existing grid has to be adapted to a different Potential distribution. The grid density change would then be quasi-reversible. Additional rules for the grid change sequence (selection of segments) would be needed, because the frequency distribution of the halving indices is not only compressed from the right, but also from the left.

2. The automated generation of optimal grids in 3 dimensions is even more useful tham in 2 dimensions. I can not see any principal obstacles, but there are several detail problems, as the construction of the first grid, selection of elementary operations for topology optimisation, etc. There will be also considerable problems in programming the algorithms.

(McWhirter) You mentioned solving for the eddy currents in the non-linear transformer tank wall. Could you say more about this method. Does it assume that the fields and currents resulting from the iron will not be sinusoidal.

(Leyvraz) The boundary condition used there is described in reference (5) First, the transient eddy current equation is solved in 1 dimension for the given magnetisation curve and a siniusoidal tangential H. Then the harmonies of the total flux $\underline{\Phi}$, which are fairly small, are neglected. The result can be expressed as a non linear complex boundary condition $\underline{H} = \underline{f}(|\underline{\Phi}|^2) \cdot \underline{\Phi}$. The assumption is that everywhere in the tank there is a practically fluxless zone outside, where $\underline{A}$ can be normalised to 0 which leads to $\underline{A}$ (inside) = $\underline{\Phi}$ and $\underline{H}$ (tangential, inside) = $\underline{f}(|A|^2) \cdot \underline{A}$ (inside). By this function the equations for the inside boudary nodes can be completed, for instance by choosing the way in which Stokes' theorem is applied. In some other cases the $\underline{A}_o$ - value of the fluxless zone is not known, but there is a condition of zero total current in the iron. In this case the function must be taken at $|\underline{A}-\underline{A}_o|^2$ and $\underline{A}_o$ must be adapted such that $\oint \underline{H}\, dl = 0$ over the iron conductor.

The use of a boundary condition is based on the fact that the flux lines inside the solid iron are practically parallel to the boundary.

STRESSES COMPUTATION PRODUCED BY A SUPERCONDUCTING NORMAL SINGLE COIL TRANSITION, IN A TOROIDAL MAGNET FOR FUSION RESEARCH TOKAMAK

by M. Caciotta and G. Sacerdoti

Summary

One discuss a procedure to evaluate the bending moments that might arise for the collapse of a s.c. coil, without the neighborough transition in the toroidal magnet.

All the computing programs are not reported but are available if request.

1. - INTRODUCTION

As known the large dimension Tokamak, if realized with cheap criteria need to utilize s.c. toroidal magnet.

The magnet is realized with narrow radial coils. In the exemple the number is of 36. If one of the coils collapse from s.c. to normal state, for some fault, in the neighborough winding over currents are induced.

The calculation is conceptually easy, if the coils are short-circuited. The magnetic field on the coils is changed with regard to the normal excitation of the magnet. The extra stresses are due both to the change of magnetic field shape and to the overcurrent. The normal excitated D-shaped coils should be stressed only by traction. Bending stresses arise with the fault condictions currents distribution. To protect the coils form mechanical overstresses, we might try to discharge the magnetic energy on external loads or, otherwise to locked copper rings all around the coils shape able to "absorbe" the overcurrents during the transition time.

Both the sistems present some limits and difficulties.

The toroidal magnet energy for Tokamak is between 10^{10} and 10^{11} joule. The magnet protection with fast discharge in external loads needs a high voltage electrical insulation of the windings of the magnet.

If conductors current is 10^4A, the insulation voltage about $2\text{-}10^3$V with N the number of coils, we may get, the magnitude order of discharge time by the formula:

$$N(2.10^3) \cdot (10^4) = 6.10^{10}$$

with: 6.10^{10} magnetic energy in joule

2.10^3 insulating voltage in volt

1.10^4 current in Ampere

If N = 36, we obtain τ = 66 sec. There are researches, in some laboratories, to realize few tens KV electrical insulation. The copper rings protection needs of a mechanical structure able to resist to the bending moments of the magnitude order of that should be requested in the s.c. coils without protection.

The relation between ring thickness s and the time τ in wich the rings might to screen the coils, in approximally given by relation

$$s = \left(\frac{\rho\tau}{\mu_o 4\pi}\right)^{\frac{1}{2}}$$

ρ is the electrical resistivity of copper.

The rings presence produces approximally a delay τ in the perturbation passing from one coil to the next. With a N coils magnet, the propagation time of collapse effect shall be:

$$T = \frac{N}{2} = \frac{N s^2 \mu_o 4\pi}{2\rho}$$

If

$$\rho = \frac{1}{65} \cdot 10^{-6}\ \Omega \times m; \quad s = 0{,}20\,m$$

$$N = 36 \; ; \quad T = 40 \div 45 \text{ sec}$$

This time should be increased because of the ring self-inductance.

In the present work the stresses evaluation in the worst conditions is done; this is the case in wich there are no protection at all and the magnetic flux in each coil will remain constant (naturally escluded the collapsed one).

For more realistic evaluation, we should have done hypothesises on the reasons and on the causes that give arise to the coils collape and from these to evaluate the fenomenon intrinsic constant time.

We have done some hypothesises that make a more pessimistic evaluation; they are:

a) the very fast collapse of the coil

b) the neighborough coils should be enough strong to succeded to support the raised overcurrent, without other transictions;

c) no external protection limits the currents values.

For a best explanation we apply the proposed procedure to a Tokamak fusion reactor studied at Frascati Laboratories in the 1974 (FINTOR) |1|. The different steps are:

1) the mutual inductance measurements between the magnet coils on the little size model

2) the coils overcurrents calculation when one of the coils quenches; this calculation is done with the mutual inductances measured values. If the coils are many, the mutual inductances measurements must be very precise to avoid some overcurrents oscillations with the azimut. So it is necessary to correct some little, the mutual inductances value to get a not oscillating behaviour.

3) By the measurement on the model, one obtains the magnetic field component perpendicular to the coil plane value, versus linear development of the coil, in all the azimutal possible positions.
The field has been measured along the four corner-edges of the winding. From the measurements data that are abaut two thousends and five hundreds relieved by an Hall probe gaussmeter, we carry out a magnetic field analytical expression function of the azimut and the linear development of the coil.

4) By using the just obtained formula and the overcurrents values, one calculate by a computer, the bending moments and the mechanical overstresses in the more excited coil with the following hypothesises:
   a) the magnet with the coils supported by a central cylinder;
   b) the magnet coils supported in a point of an ideal central circumference.

5) One discuss the possibility to compute both the mutual inductances and the magnetic field instead to measure its.

2. - MUTUAL INDUCTANCES MEASUREMENTS OF TOROIDAL MAGNET COILS

The calculation of the mutual inductance of the D-shaped coils, probably needs the magnetic field computation. Very good programs for the magnetic field calculation in every geometry of windings are available (see bibliography |2| for an example). We for this work have considered easier and quicker to measure on the model the mutual inductances. Its will be:

$$L = 1\$ \frac{(N_t)^2}{(N_m)^2}$$

where:

L: mutual or self-inductance of the magnet coils of Tokamak

1: mutual or self-inductance measured on the model

S: scale factor

N_t: number of coils of winding

N_m: number of coils of model

We have $N_t = 700$ $N_m = 554$ $s = 50$

The model is realized by two copper wires on plexiglass support fixed on the compass arms.

The machine inner diameter (in scale) is equal to the compass arm lenght to reproduce easily the all possible reciprocal coils positions. In fig.1 is reproduced the apparatus photos.

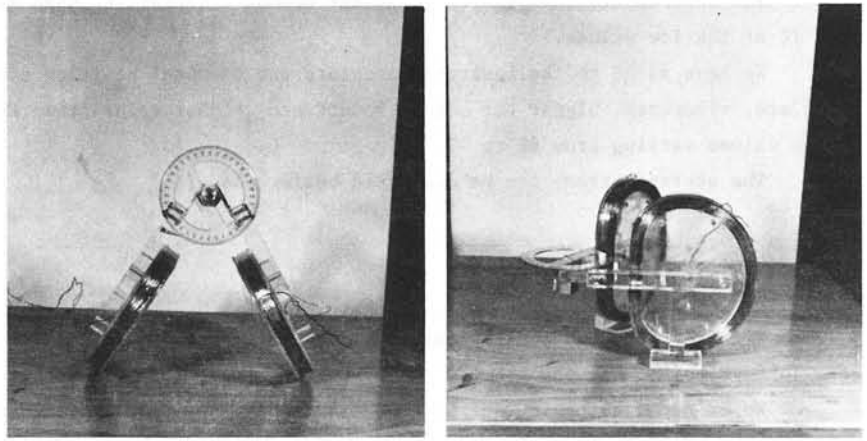

- FIG.1 -

To measure the different angles mutual inductances a volt-amperometric method has been used.

To be sure that the model metallic parts do not have influence we have accomplished the measurements at 50 Hz and at 1 KMz.

In fig.2 there are reported the experimental relieves and the two different frequencies curves are sufficiently overlapped.

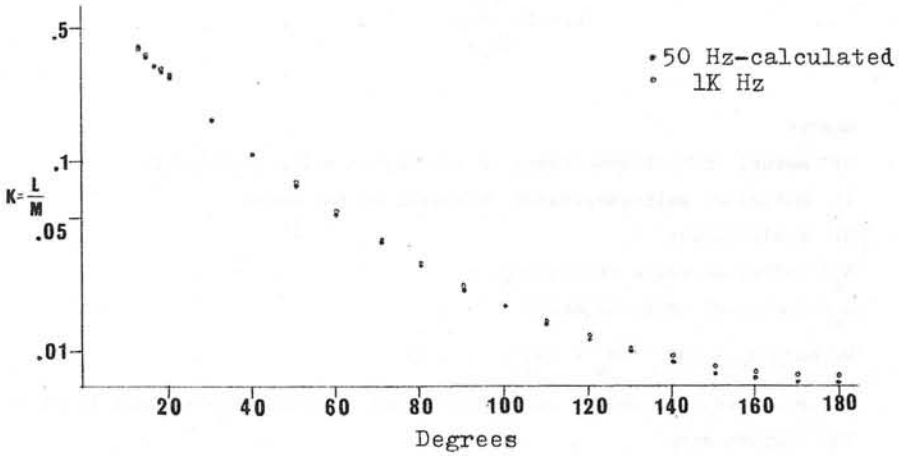

- FIG.2 -

The instruments errors are: 2% at the mutual inductances high values and 7% at the low values.

We have added to the instruments errors the azimutal position errors that are, viceversa, bigger for mutual inductance higher values than the lower values varying from 6% to 1%.

The average errors can be evaluated better than 7%

3. - OVERCURRENTS CALCULATION

With the measured coefficients the overcurrents that are induced in the Tokamak coils when one or more collapse it is possible to compute.

We do the hypothesis (see introduction) that the magnetic flux in all the s.c. coils shall remain constant.

So we can get the 35 equations in the 35 unknown currents.

The coefficients matrix is carried out by the mutual inductances measured values, and it results

$$K_{1,1} = \sum_{2j}^{36} K_{1,j}\,\Delta I_j; \qquad K_{1,j} = \frac{M_{1,j}}{M_{1,1}}$$

$$M_{1,j} = M(\varphi_{1,j}); \qquad \varphi_{1,j} = 10^\circ|1 - j| \qquad (3.1)$$

$$1 = 1,2,\ldots 35$$

Similarly when two coils collapse we may write the 34 equations in the 34 unknown currents

$$K_{1,1} + K_{1,2} = \sum_{3j}^{36} K_{1,j}\,\Delta I'_j$$

The over currents obtained resolving the sistem (3.1) are effected by oscillations (see fig.3) increasing the azimut that, we believe, are due to the mutual inductances measurements errors on the model

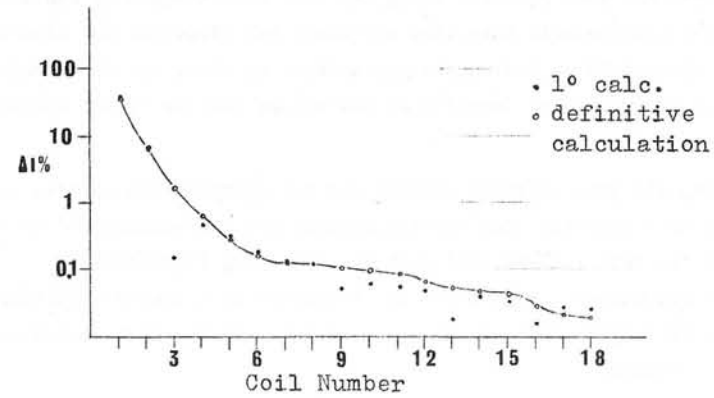

- FIG.3 -

The experimental values have been modified to eliminate oscillations by the following on the computer procedure.

From the overcurrents versus the azimut graphic, we connect the minimum with the firsts neighborough, with two segments then connecting with

a straigh-line the average points of the segments. At the minimum ascissa, we evaluate the corrected overcurrent. Easy geometrical considerations allow us to write:

$$\Delta I'_B = \frac{1}{4} (\Delta I_A + 2\Delta I_B + \Delta I_C)$$

By this method (see fig.4) we take off all the minimum points.

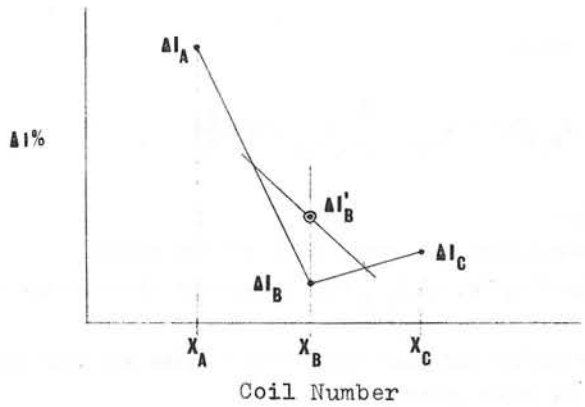

- FIG.4 -

We recalculate the mutual inductances new values to get the modified overcurrent distribution.

We may write

$$K_{1,1} = \sum_{2j}^{36} K_{1,j}\Delta I_j$$

$$K_{1,1} + \Delta K_{1,1} = \sum_{2j}^{36} (K_{1,j} + \Delta K_{1,j})(\Delta I_j + \delta\Delta I_j)$$

$$\Delta K_{1,1} = \sum_{2j}^{36} K_{1,j}\,\delta\Delta I_j$$

These relations constitue a system to evaluate the mutual inductances corrections. With the new values set we recalculate the over currents not having oscillations; otherwise we repeat the procedure.

We have controlled that always the mutual inductances values should be in the experimental errors field; otherwise, one reduces all the values by an equal coefficient to arrange the values into the experimental errors range. The coefficients set that eliminates the oscillations in surely precise better than 7%.

The mutual inductances graphic so evaluated is coincident with the fig.2 (50Hz).

	$K=\frac{L}{M}$			$K=\frac{L}{M}$	
Degrees	50 Hz	Calculated	Degrees	50 Hz	Calculated
0	1.00	1.00	100	.018	.019
10	.46	.45	110	.014	.015
20	.28	.24	120	.012	.012
30	.17	.18	130	.010	.010
40	.11	.12	140	.0088	.0090
50	.075	.081	150	.0080	.0081
60	.052	.056	160	.0074	.0074
70	.039	.042	170	.0070	.0071
80	.029	.031	180	.0069	.0069
90	.022	.024			

- TABLE I -

The Table I shows the initial and final mutual inductances.
In fig.3 is reported the overcurrents evaluations.|3|

4.1 - MAGNETIC FIELD CALCULATION |4|

On the above described model the azimutal magnetic field has been relieved. One of the two model coils has been excited by a 1A, D.C. current and the azimutal magnetic field has been relieved along the four corner-edges of the other coil by an Hall gaussmeter (model Booton ind. 3265).

Because of the magnetic field low value the measurement has been replaced changing the current from 1 A to - 1 A to eliminate the earth magnetic field influence.

The bigger errors was principally done in the self-field measurements and in the more far coils the errors were due:

a) to the strumental causes

b) to the Hall probe positioning

c) to the Hall probe physical dimensions

The strumental errors are of the 2% order.

The Hall probe physical dimensions were of abaut 6 mm x 6 mm.

The field measurements consists in about 2500 relieves (15 for each corner-edge; 4 corner-edges, 18 coils, 2 relieves for the earth magnetic field eliminations).

To utilize the data for the mechanical stresses computation we have to get an analitical magnetic field expression by a best-fit method. We have the aim to get the formula of the botton tipe.

$$B_{r,j} = f_j(s,\vartheta)$$

where j is the coil corner-edge; $B_{r,j}$ is the perpendicular to the coils plane magnetic field component; s is the corner-edge linear development, ϑ is the azimut.

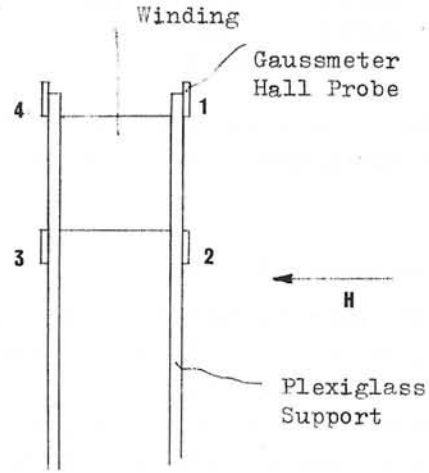

- FIG.5 -

4.2 - THE MAGNETIC FIELD EXPERIMENTAL DATA ELABORATIONS AND THE MAGNETIC INDUCTION ANALYTICAL EXPRESSION

We describe the followed procedure. For simmetry considerations the $B_{r,j}$ for s = o and s = s_m (the half perimeter of the coil j corner-edge) may have the first derivation equal to zero.

$$\left.\frac{dB_{r,j}}{ds}\right|_{s=o} = \left.\frac{dB_{r,j}}{ds}\right|_{s=s_m} = 0$$

Varying ϑ we can write:

$$B_{r,j}(s) = A_{o,j} + \sum_{1}^{N} {}_i\, A_{i,j} \cos i \frac{\pi s}{s_m}$$

for every ϑ value.

In our computation N is equal 5 for all the angles.

The computed values of $A_{i,j}$ give a magnetic field in the range of experimental errors.

The coefficients get lower when index i arise and your behaviour is strongly sharp for lower angles.

We have rapresented with an high degree of accurancy the coefficients behaviour versus angles by two functions the first taking the sharp behaviour into account and the second the great angles behaviour.

The functions are reported below:

$$A_{i,j} = \exp(b_o + b_1\vartheta^2 + b_2\vartheta^3 + b_3\vartheta^4) - 20 \qquad \text{for } \vartheta \leq \Theta_o$$

$$A_{ij} = \frac{A}{\vartheta} + \frac{B}{\vartheta^2} \qquad \text{for } \vartheta \geq \Theta_o$$

Where A and B are completely determinated by the junctions conditions and where Θ_o is the junction angle.

We obtain, for each coil corner-edge, a 6 x 5 matrix, which raws are constituted by the four $A_{i,j}$ coefficients with $\vartheta \leq \Theta_o$ and the fifth element is the junction angle.

Corner-edge 1(°)

	b_0	b_1	b_2	b_3	Θ_0
A_0	1.1660	33.747	-72.032	41.631	40
A_1	2.8599	4.6023	-9.7299	5.5434	40
A_2	2.9102	1.2804	-2.0755	.91609	50
A_3	2.8826	.79753	-1.0725	.39813	60
A_4	2.9843	-1.0357	2.9100	-2.0023	30
A_5	2.9842	-.42325	.11695	-.77607	30

Corner-edge 2

	b_0	b_1	b_2	b_3	Θ_0
A_0	4.2507	.0	-64.882	142.21	16
A_1	3.0370	19.477	-38.811	-20.644	18
A_2	2.9026	14.781	-60.810	68.545	18
A_3	2.9162	.97724	-1.5672	.68109	50
A_4	2.9512	2.1311	-23.651	49.857	18
A_5	2.9555	-.76093	1.9121	-.70984	20

Corner-edge 3

	b_0	b_1	b_2	b_3	Θ_0
A_0	4.2514	.0	-126.16	310.47	16
A_1	3.0497	6.9380	-22.315	15.449	18
A_2	2.9056	5.9675	-21.255	20.511	20
A_3	2.9333	.0	8.2799	-20.499	16
A_4	2.9559	.0	4.8434	-11.271	16
A_5	2.9596	2.0302	-7.1288	6.7337	20

Corner-edge 4

	b_0	b_1	b_2	b_3	Θ_0
A_0	1.1613	92.706	-330.74	319.94	20
A_1	2.8581	1.9272	-3.1459	1.4026	50
A_2	2.9087	1.0035	-1.6593	.75309	50
A_3	2.8810	1.1608	-1.9262	.87844	50
A_4	2.9831	.87159	-3.0789	2.9249	20
A_5	2.9831	.46941	-1.4200	1.1247	30

(°) See fig. 5

- TABLE II -

The four matrixes are reported in tab.II

In tab.III is reported the magnetic field versus the linear development of winding both for the normal and collapsed conditions.

Sector Number	Sector Co-ordinates X	Sector Co-ordinates Y	Linear Development	Normal Field	Collap. Field
0	6.16	.0	.0	3.96	4.20
1	6.16	1.11	1.11	4.01	4.28
2	6.16	2.22	2.22	4.15	4.42
3	6.21	3.29	3.30	4.13	4.44
4	6.52	4.20	4.27	3.94	4.25
5	7.55	5.42	5.86	3.45	3.77
6	9.05	6.14	7.54	3.04	3.31
7	9.19	6.18	7.69	3.03	3.29
8	10.51	6.26	9.02	2.89	3.15
9	12.73	5.45	11.37	2.81	3.04
10	14.20	4.16	13.36	2.66	2.89
11	15.10	2.73	15.07	2.61	2.84
12	15.63	.92	16.95	2.70	2.95
—	Meters	Meters	Meters	Teslas	Teslas

- TABLE III -

5.1 - BENDING MOMENTS CALCULATION WHEN A COIL COLLAPSED |5|

We consider an half coil determined by the single simmetry axis, fig.6.

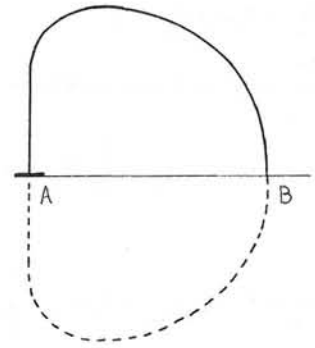

- FIG.6 -

Through the section A a force F_a and a bending moment M_a is transmi_ted. For simmetry reasons we think the half coil fitted in A and we can say that:

1) the section B cannot rotate
2) the section B displacement can be only along the simmetry axis.

With the above conditions we can compute F_a and M_a. We divide the half coil in segments fig.7

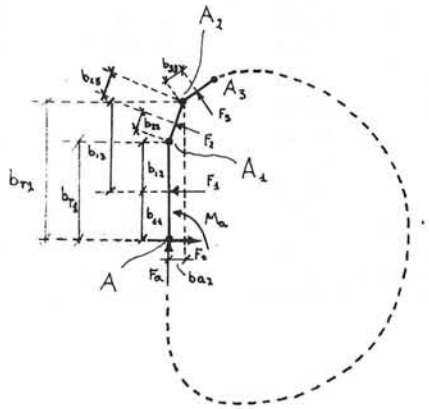

- FIG.7 -

We can write:

$$\vartheta_j = E_j J_j l_j M_j$$

If E_j and J_j are constant varying j the condition 1) can be write as:

$$\vartheta_{tot} = \sum_{1j}^{N} l_j M_j = \sum_{1j}^{N} \vartheta_j = 0 \qquad (5.1)$$

where

$$M_j = M_a + F_a b_{a,j} + F_T b_{T,j} + \sum_{1i}^{j} F_i b_{i,j} \qquad (5.2)$$

$b_{i,j}$ is the force F_i-beam referred to the segment center.

$b_{T,j}$ and $b_{a,j}$ are the F_T and F_a beams referred to the point in wich the moment is calculated.

The force F_T in fig.6 is the half-strengh reaction that opposes the displacement toward the inside. The F_T is computed adding the components along the simmetry axis of all, the F_i acting on the non constrained part of the half coil.

The (5.1) condition using the (5.2) becomes

$$M_a \sum_{1j}^{N} l_j + F_a \sum_{1j}^{N} b_{a,j} l_j + F_T \sum_{1j}^{N} b_{T,j} l_j + \sum_{1j}^{N} \sum_{1i}^{j} F_i b_{i,j} l_i = 0 \qquad (5.3)$$

In the fig.8 it is possible to observe that the generical displacement is computed from the segment $(A_j B)$ rotation.

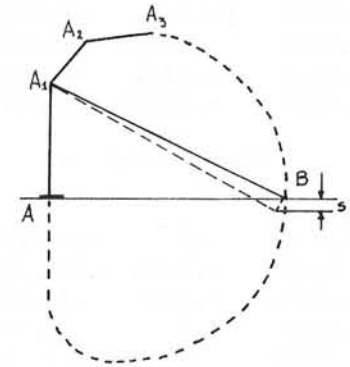

- FIG.8 -

We can write:

$$\sum_j s_j = 0$$

from above we have

$$s_j = (\overline{A_j B})_x \vartheta_j$$

Where $(\overline{A_j B})_x$ is the geometrical projection on the simmetry axis of the segment $(\overline{A_j B})$ we can so obtain the second equation:

$$M_a \sum_{1_j}^{N} l_j (\overline{A_j B})_x + F_a \sum_{1_j}^{N} l_j b_{a,j} (\overline{A_j B})_x + F_T \sum_{1_j}^{N} l_j b_{Tj} (\overline{A_j B})_x +$$

$$+ \sum_{1_j}^{N} \sum_{1_i}^{j} F_i b_{i,j} l_j (\overline{A_j B})_x = 0 \qquad (5.4)$$

Where $F_i = B_i I_i l_i$, and B_i is the magnetic induction in the segment i; l_i is the length of segment i; I_i is the current on the segment i.

A variation to the above calculation to evaluate the bending moments behaviour when the coils have the straight rib supported.

In this case the moments on the supported rib are zero, because the constrain reaction balance the electromagnetic forces.

The support can give only oriented reactions, and we might evaluate as far from A the constrain supports the rib.

For this evaluation we make a constrain displacement along the support surface with F_T equal to the projection on the simmetry axis of electromagnetic forces and from section A to section B.

F_a and M_a can be calculated from(5.3). In the table V are reported the results for thecase with central rib support and in table VI the case with supported rib both in the collapse and in the normal conditions.

Sector Number	Normal Bending Moment	Collapsed Bending Moment
0	-43.7	-59.8
1	-35.6	-48.8
2	-23.8	-32.6
3	-9.3	-12.6
4	3.3	4.7
5	20.2	27.8
6	30.5	41.9
7	31.1	42.6
8	32.2	44.1
9	20.9	28.6
10	4.6	6.3
11	-12.8	-17.4
12	-33.8	-46.1
—	KTons x Meter	KTons x Meter

Note: positive moments are clockwise (fig. 7)

- TABLE V -

Sector Number	Normal Bending Moment	Collapsed Bending Moment
0	.0	.0
1	.0	.0
2	.7	1.0
3	4.5	6.0
4	7.4	9.9
5	10.3	13.7
6	10.7	14.2
7	10.6	14.1
8	8.7	11.5
9	1.6	2.2
10	-4.3	-5.5
11	-8.8	-11.3
12	-12.6	-16.0
—	KTons x Meter	KTons x Meter

Note: positive moments are clockwise (fig. 7)

- TABLE VI -

From table VI the support both in the collapse and in the normalcase, is equally far from section A.

If we interpolate the results by the displaces support ones we obtain a difference of about 3 cm.

We foresee a better calculation with a shorter segments structure subdivision.

One can see that the bending moments in the normal conditions are not zero as it should be for a D-shaped coil.

This result is given to the causes below reported:

1) the zero bending moment shape is in the continuous toroidal solenoid hypothesis: in the radiate coils realization the bending moment arise;
2) the internal-external ratio influences the residual bending moment: in creases with the ratio;
3) in our realization the D-shaped is the internal coils perimeter;
4) in the calculation we have placed the currents in the windings center, displaced of .5 m from the D-shape;
5) our calculation consider the coil divided in linear segments instead of a continuous curve;

6) we consider that magnetic field should be evaluate in the winding center by a linear interpolation of the four corner-edges values.

The bending moment that arise in the normal action one think to be of the acceptable magnitude for the above reasons.

We think correct the problem resolution. In these conditions because of the stresses increase in the case of one coil collapse, is mainly due to the overcurrent than to a change of the magnetic field shape as it should be if the bending moment should be zero in normal excitation.

We intend to develop a computer program to evalutate the bending moments considering the current distribution in the space.

6. - CONCLUSIONS

To evaluate the bending strains in a s.c. Tokamak with the D-shaped coil we have resolved some problems.

We have evaluate the mutual inductances to compute the overcurrents in the collapse case.

We have preferred a measurements serie on the model because of the complex coils shape, instead of the resolution by a computer calculation.

The computer evaluation needs a program optimization that requires more time than the model realization and the measurements execution.

With the overcurrent we have evaluated the collapsed magnetic field.

Even in this case the experimental relieves have been preferred with a great loss of time.

In the future this procedure is not advisable because of the availability of very good programs for the magnetic field calculation . Our attention have been pointed to the bending moments evaluation.

We have carried out a computer program for the bending moments evaluation in the complex structure proposed.

The program input is the magnetic field and the currents distribution. We have carried out in a reasonable time the unknown moments distribution, but the procedure cannot easily iterate because a new model needs for the mutual inductances evaluation. We are working to replace the measurements on the model with a computer program.

Aknowledgments

We want to thank the candidate for degree Mr.F.Nesci for your accurate measurements and Mr.M.Tidei for your assistance in the drawing up the paper.

BIBLIOGRAPHY

|1| E.BERTOLINI et al: Design of a minimum size toroidal D. experimental reactor (FINTOR) - International Atomic Energy Agency - Plasma Physics and Controlled Nuclear Fusion Research - Wien 1975

|2| YANG.: A Magnetic Field Code for Handling General Current Carrying Conductors in Three Dimensions (MAFCO-W) - 4/'75 MT5 pp 203 - 208

|3| J.FILE: The Princetone Fusion Power Plant s.c. Magnet System and Cost 4/'75 MT5 pp 281 - 289

|4| BROSER et al: The Toroidal Magnetic Field Coils for the ASDEX Tokamak 4/'75 MT5 pp 332 - 336

|5| POHLCHEN-HUGUET: Shape Field and Mechanical Analysis of the JET Toroidal Field coils - 4/'75 MT5 pp 325 - 331

MECHANICAL AND THERMAL STRESSES IN DOUBLER DIPOLE MAGNETS

S.C. Snowdon
October 1975

Summary

An analytical solution for stresses has been found for a structural composite that models the Doubler dipole. Structural cylinders represent the material inside and outside of the excitation current which is represented by two cosine theta sheet current distributions. A pretensioned structural cylinder surrounds the aforementioned materials. Thermal stresses are represented only in so far as a uniform temperature differing from room temperature alters the stress-strain relation. Temperature gradients are not considered. The mechanical energy stored in the elastic field is calculated. Numerical results are given.

Thermo Elasticity

The effect of a temperature change in elasticity is obtained by considering the elastic energy density to have the form:[1]

$$W = C_{ij}\varepsilon_{ij} + \frac{1}{2}C_{ijk\ell}\varepsilon_{ij}\varepsilon_{k\ell} \ , \tag{1}$$

where the summation convention for repeated indices is used. The stress tensor is related to the strain tensor using

$$\sigma_{ij} = \frac{\partial W}{\partial \varepsilon_{ij}} = C_{ij} + C_{ijk\ell}\varepsilon_{k\ell} \ . \tag{2}$$

For homogeneous isotropic materials

$$C_{ij} = -\, k(3\lambda+2\mu)\cdot\delta_{ij} \tag{3}$$

and

$$C_{ijk\ell} = \lambda\delta_{ij}\delta_{k\ell} + \mu(\delta_{ik}\delta_{j\ell}+\delta_{i\ell}\delta_{jk}) \ , \tag{4}$$

where k is the thermal expansion coefficient integrated from 4.2°K to room temperature, λ and μ are the Lamé constants which are related to the more familiar constants Y (Young's modulus) and ν(Poisson's ratio) as follows.

$$\lambda = \frac{\nu}{(1+\nu)(1-2\nu)}\,Y \ , \qquad \mu = \frac{1}{2(1+\nu)}\,Y \ . \tag{5}$$

Under these restrictions Hooke's Law becomes

$$\sigma_{ij} = \frac{\nu}{(1+\nu)(1-2\nu)}\,Y\,\delta_{ij}\varepsilon_{kk} + \frac{1}{1+\nu}\,Y\,\varepsilon_{ij} - \frac{kY}{1-2\nu}\,\delta_{ij} \ . \tag{6}$$

The condition of equilibrium is then

$$\frac{\partial \sigma_{ij}}{\partial x_i} + f_j = 0 \ , \tag{7}$$

where f_j is the body force which in our case will be the Lorentz force $\vec{J}x\vec{B}$. Finally, since some of the boundary conditions relate to the material displacement $\vec{u}$, one needs the connection between strain and displacement

$$\varepsilon_{ij} = \frac{1}{2}\left(\frac{\partial u_i}{\partial x_j} + \frac{\partial u_j}{\partial x_i}\right) \ . \tag{8}$$

For the problem at hand the body force is handled by a surface traction and, therefore, the equilibrium condition Eq. (7) may be satisfied identically through the use of the Airy stress function ϕ:

$$\sigma_{ij} = \delta_{ij}\,\nabla^2\phi - \frac{\partial^2\phi}{\partial x_i \partial x_j} \ . \tag{9}$$

The equation satisfied by the Airy stress function is determined from the equations of compatibility which are imposed on strains since the six strains in Eq. (8) must be interrelated in order to be derivable from three displacements. If Hooke's Law, Eq. (6), is used the equations of compatibility for stresses may be found

$$\nabla^2\sigma_{ij} + \frac{1}{1+\nu}\frac{\partial^2\sigma_{kk}}{\partial x_i \partial x_j} = 0 \ . \tag{10}$$

By introducing the approximation known as generalized plane strain[2] one reduces the problem to manageable proportions. In this approximation one neglects the shear strains connected with the longitudinal or axial direction but permits a free expansion characterized by a uniform strain. For the normal stresses Eq. (4) gives

$$\sigma_{11} = \lambda(\varepsilon_{11}+\varepsilon_{22}+\varepsilon_{33}) + 2\mu\varepsilon_{11} - k(3\lambda+2\mu) \tag{11}$$

$$\sigma_{22} = \lambda(\varepsilon_{11}+\varepsilon_{22}+\varepsilon_{33}) + 2\mu\varepsilon_{22} - k(3\lambda+2\mu) \tag{12}$$

$$\sigma_{33} = \lambda(\varepsilon_{11}+\varepsilon_{22}+\varepsilon_{33}) + 2\mu\varepsilon_{33} - k(3\lambda+2\mu) \ . \tag{13}$$

Suppose that the index 3 represents the longitudinal direction. Then, from Eqs. (5, 11, 12, 13) one has

$$\sigma_{33} = \nu(\sigma_{11}+\sigma_{22}) + Y\varepsilon_{33} - kY. \tag{14}$$

Since ε_{33} is considered constant in this approximation, Eq. (10) becomes

$$\nabla^2\sigma_{ij} + \frac{\partial^2}{\partial x_i \partial x_j}(\sigma_{11}+\sigma_{22}) = 0 \ , \tag{15}$$

or, using Eq. (9) this becomes

$$\delta_{ij}\nabla^4\phi - \frac{\partial^2}{\partial x_i \partial x_j}\nabla^2\phi + \frac{\partial^2}{\partial x_i \partial x_j}(2\nabla^2\phi - \nabla^2\phi) = 0 \ . \tag{16}$$

Hence the Airy stress function satisfies the biharmonic equation

$$\nabla^4\phi = 0. \tag{17}$$

Virial Theorem

One might expect that the boundary conditions which provide for continuity of displacement and discontinuity of normal and shear stresses according to known surface tractions would be sufficient to specify all the unknowns in solving Eq. (17). However, in this plane strain approximation, information relative to the longitudinal ends is lost and must be supplied by some integral condition. For this problem it is sufficient to invoke the virial theorem which may be found as follows[3]. Let τ_{ij} be the Maxwell stress tensor for the magnetic field introduced by the current sheet. The body force f_j in Eq. (7) is then given by

$$f_j = \frac{\partial \tau_{ij}}{\partial x_i} \ . \tag{18}$$

To form the virial multiply Eq. (7) by x_j and utilize Eq. (18). Thus, after integrating over a volume

$$\int x_j \frac{\partial}{\partial x_i}(\sigma_{ij}+\tau_{ij})d^3x = 0 \ . \tag{19}$$

Integrate by parts using

$$\frac{\partial}{\partial x_i}(x_j\beta_{ij}) = \delta_{ij}\beta_{ij} + x_j\frac{\partial \beta_{ij}}{\partial x_i} \tag{20}$$

to give

$$\int_S x_j(\sigma_{ij}+\tau_{ij})dS_i - \int\delta_{ij}(\sigma_{ij}+\tau_{ij})d^3x = 0 \ . \tag{21}$$

Notice that the integrand in the volume integral is just the trace of the tensor. But the trace of the Maxwell stress tensor is the

negative of the energy density[4]. Hence

$$\int \delta_{ij}\tau_{ij}\, d^3x = - W_B \ , \tag{22}$$

the magnetic energy. Since, in the problem considered σ_{ij} is zero on the boundary but τ_{ij} exists on the iron shield, one has

$$\int \delta_{ij}\sigma_{ij}\, d^3x = \int_S x_j \tau_{ij} dS_i + W_B \ . \tag{23}$$

It should be noted that τ_{ij} is taken to be zero on the end walls. Hence one visualizes that the magnet structure has terminating ends. Equation (23) indicates that, since the right hand side is positive, a net tensile structure is required to contain magnetic forces in static equilibrium.

Pretensioned Band

A method of characterizing a pretensioned member may be found by utilizing the concept of rotational dislocation[5] whereby discontinuity in rotational displacement is permitted. Thus $u_\theta(2\pi) - u_\theta(0)$ is given a preassigned value. This condition will be used in the outer band rather than the customary continuity of displacement.

Magnetic Field

Since a continuously distributed body force as given by the Lorentz force JxB is more difficult to handle in the equations of elasticity, the region of conduction current in the dipole will be approximated by two current sheets, one at the inner edge of the region and one at the outer edge of the region. Thus the model to be considered consists of two cylindrical current sheets each carrying an axial current density of

$$i = \begin{Bmatrix} i_o \\ i_1 \end{Bmatrix} \cos\theta \quad \text{at} \quad \begin{Bmatrix} r=b \\ r=c \end{Bmatrix} \ . \tag{24}$$

See Fig. 1 for geometrical details. From the current density as given and an iron shield located at $r = r_s$, one finds the following magnetic field components.

$$H_r = - 2\pi \begin{Bmatrix} i_o(1+b^2r_s^{-2}) + i_1(1+c^2r_s^{-2}) \\ i_o(b^2r^{-2}+b^2r_s^{-2}) + i_1(1+c^2r_s^{-2}) \\ i_o(b^2r^{-2}+b^2r_s^{-2}) + i_1(c^2r^{-2}+c^2r_s^{-2}) \end{Bmatrix} \sin\theta \ , \tag{25}$$

$$H_\theta = - 2\pi \begin{Bmatrix} i_o(1+b^2r_s^{-2}) + i_1(1+c^2r_s^{-2}) \\ i_o(-b^2r^{-2}+b^2r_s^{-2}) + i_1(1+c^2r_s^{-2}) \\ i_o(-b^2r^{-2}+b^2r_s^{-2}) + i_1(-c^2r^{-2}+c^2r_s^{-2}) \end{Bmatrix} \cos\theta \ , \tag{26}$$

where the top entry refers to $o<r<b$, the middle entry to $b<r<c$ and the bottom entry to $c<r<r_s$. In order to calculate the forces one needs the average field at the current sheets.

$$\langle H_r \rangle_{Av} = - 2\pi \begin{Bmatrix} i_o(1+b^2r_s^{-2}) + i_1(1+c^2r_s^{-2}) \\ i_o(b^2c^{-2}+b^2r_s^{-2}) + i_1(1+c^2r_s^{-2}) \end{Bmatrix} \sin\theta \ , \tag{27}$$

$$\langle H_\theta \rangle_{Av} = - 2\pi \begin{Bmatrix} i_o b^2 r_s^{-2} + i_1(1+c^2r_s^{-2}) \\ i_o(-b^2c^{-2}+b^2r_s^{-2}) + i_1 c^2 r_s^{-2} \end{Bmatrix} \cos\theta \ . \tag{28}$$

Lorentz Force on Current Sheets

The force on a current sheet is given by

$$d\vec{F} = ids\ \vec{k}x(\vec{i}_r\langle H_r\rangle_{Av} + \vec{i}_\theta\langle H_\theta\rangle_{Av}) \ , \tag{29}$$

where i is given by Eq. (24) and

$$ds = \left\{ \begin{matrix} b \\ c \end{matrix} \right\} d\theta \ . \tag{30}$$

If $\vec{f}$ denotes the force per unit area on the current sheet, then

$$f_r = \pi \left\{ \begin{matrix} i_o^2 b^2 r_s^{-2} + i_o i_1 (1+c^2 r_s^{-2}) \\ i_o i_1 (-b^2 c^{-2} + b^2 r_s^{-2}) + i_1^2 c^2 r_s^{-2} \end{matrix} \right\} (1+\cos 2\theta) \ , \tag{31}$$

$$f_\theta = -\pi \left\{ \begin{matrix} i_o^2 (1+b^2 r_s^{-2}) + i_o i_1 (1+c^2 r_s^{-2}) \\ i_o i_1 (b^2 c^{-2} + b^2 r_s^{-2}) + i_1^2 (1+c^2 r_s^{-2}) \end{matrix} \right\} \sin 2\theta \tag{32}$$

Maxwell Stress Tensor

The Maxwell stress tensor is found by noting that the Lorentz force may be written as the divergence of a tensor. Thus

$$\vec{J} \times \vec{B} = \nabla \cdot \vec{\vec{\tau}} \ , \tag{33}$$

where, in cartesian components[4]

$$\vec{\vec{\tau}} = \frac{1}{4\pi} \begin{pmatrix} B_x^2 - \frac{1}{2}B^2 & B_x B_y & B_x B_z \\ B_x B_y & B_y^2 - \frac{1}{2}B^2 & B_y B_z \\ B_x B_z & B_y B_z & B_z^2 - \frac{1}{2}B^2 \end{pmatrix} \ . \tag{34}$$

From this it may be seen that the trace of the Maxwell stress tensor is

$$\mathrm{tr}\, \vec{\vec{\tau}} = -\frac{1}{8\pi} B^2 \ , \tag{35}$$

the negative of the energy density.

Application to Doubler Dipole Magnet

Since generalized plane strain is characterized by

$$\varepsilon_{rz} = \varepsilon_{\theta z} = 0 \ , \quad \varepsilon_{zz} = \text{constant} \ , \tag{36}$$

the corresponding stress in Eq. (6) becomes

$$\sigma_{rr} = (\lambda+2\mu)\varepsilon_{rr} + \lambda\varepsilon_{\theta\theta} + \lambda\varepsilon_{zz} - k(3\lambda+2\mu) \tag{37}$$

$$\sigma_{\theta\theta} = \lambda\varepsilon_{rr} + (\lambda+2\mu)\varepsilon_{\theta\theta} + \lambda\varepsilon_{zz} - k(3\lambda+2\mu) \tag{38}$$

$$\sigma_{zz} = \lambda\varepsilon_{rr} + \lambda\varepsilon_{\theta\theta} + (\lambda+2\mu)\varepsilon_{zz} - k(3\lambda+2\mu) \ . \tag{39}$$

$$\sigma_{r\theta} = 2\mu\varepsilon_{r\theta} \ . \tag{40}$$

Inversion gives

$$\varepsilon_{rr} = \frac{1}{2\mu(3\lambda+2\mu)} \cdot [2(\lambda+\mu)\sigma_{rr} - \lambda(\sigma_{\theta\theta}+\sigma_{zz})] + k \tag{41}$$

$$\varepsilon_{\theta\theta} = \frac{1}{2\mu(3\lambda+2\mu)} \cdot [2(\lambda+\mu)\sigma_{\theta\theta} - \lambda(\sigma_{rr}+\sigma_{zz})] + k \tag{42}$$

$$\varepsilon_{zz} = \frac{1}{2\mu(3\lambda+2\mu)} \cdot [2(\lambda+\mu)\sigma_{zz} - \lambda(\sigma_{rr}+\sigma_{\theta\theta})] + k \tag{43}$$

$$\varepsilon_{r\theta} = \frac{1}{2\mu}\sigma_{r\theta} \ . \tag{44}$$

Utilizing Eq. (5) one has

$$\varepsilon_{rr} = \frac{1}{Y}[\sigma_{rr} - \nu\sigma_{\theta\theta} - \nu\sigma_{zz}] + k \tag{45}$$

$$\varepsilon_{\theta\theta} = \frac{1}{Y}[-\nu\sigma_{rr} + \sigma_{\theta\theta} - \nu\sigma_{zz}] + k \tag{46}$$

$$\varepsilon_{zz} = \frac{1}{Y}[-\nu\sigma_{rr} - \nu\sigma_{\theta\theta} + \sigma_{zz}] + k \tag{47}$$

$$\varepsilon_{r\theta} = \frac{1+\nu}{Y}\sigma_{r\theta} \ . \tag{48}$$

Since ε_{zz} is taken to be constant in this approximation, Eq. (47) may be used to eliminate σ_{zz}. Thus

$$\varepsilon_{rr} = \frac{1+\nu}{Y} \cdot [(1-\nu)\sigma_{rr} - \nu\sigma_{\theta\theta}] - \nu\varepsilon_{zz} + (1+\nu)k \tag{49}$$

$$\varepsilon_{\theta\theta} = \frac{1+\nu}{Y}[-\nu\sigma_{rr} + (1-\nu)\sigma_{\theta\theta}] - \nu\varepsilon_{zz} + (1+\nu)k \ . \tag{50}$$

The relation between the stresses and the Airy stress function, Eq. (9), becomes in cylindrical coordinates

$$\sigma_{rr} = \frac{1}{r}\frac{\partial\phi}{\partial r} + \frac{1}{r^2}\frac{\partial^2\phi}{\partial\theta^2} \tag{51}$$

$$\sigma_{\theta\theta} = \frac{\partial^2\phi}{\partial r^2} \tag{52}$$

$$\sigma_{r\theta} = -\frac{\partial}{\partial r}\left(\frac{1}{r}\frac{\partial\phi}{\partial\theta}\right) . \tag{53}$$

For the problem under consideration one may take in each annular region functions of the form

$$\phi = A\ell nr + Gr^2\ell nr + Br^2 + (Cr^2+Dr^4+Er^{-2}+F)\cos 2\theta . \tag{54}$$

The constant G is related to a multivalued azimuthal displacement and is set equal to zero except in the outer band where it is used to characterize pretension.

Stresses, Strains and Displacements

One finds that Eqs. (52-55) gives

$$\sigma_{rr} = \begin{Bmatrix} A_1r^{-2} & +2B_1-(2C_1+6E_1r^{-4}+4F_1r^{-2})\cos 2\theta \\ A_2r^{-2} & +2B_2-(2C_2+6E_2r^{-4}+4F_2r^{-2})\cos 2\theta \\ A_3r^{-2}+2G_3\ell nr+G_3 & +2B_3-(2C_3+6E_3r^{-4}+4F_3r^{-2})\cos 2\theta \end{Bmatrix} \tag{55}$$

$$\sigma_{\theta\theta} = \begin{Bmatrix} -A_1r^{-2} & +2B_1+(2C_1+12D_1r^2+6E_1r^{-4})\cos 2\theta \\ -A_2r^{-2} & +2B_2+(2C_2+12D_2r^2+6E_2r^{-4})\cos 2\theta \\ -A_3r^{-2}+2G_3\ell nr+3G_3 & +2B_3+(2C_3+12D_3r^2+6E_3r^{-4})\cos 2\theta \end{Bmatrix} \tag{56}$$

$$\sigma_{r\theta} = \begin{Bmatrix} (2C_1+6D_1r^2-6E_1r^{-4}-2F_1r^{-2})\sin 2\theta \\ (2C_2+6D_2r^2-6E_2r^{-4}-2F_2r^{-2})\sin 2\theta \\ (2C_3+6D_3r^2-6E_3r^{-4}-2F_3r^{-2})\sin 2\theta \end{Bmatrix} , \tag{57}$$

where the top entry is the bore tube region a<r<b; the middle entry is the region of conductors b<r<c; and the last entry represents the pretensioned band c<r<d.

Substituting Eqs. (55-57) into Eqs. (48-50) gives for the strains

$$\frac{Y}{1+\nu}\cdot[\varepsilon_{rr}+\nu\varepsilon_{zz}-(1+\nu)k] =$$

$$\begin{Bmatrix} A_1r^{-2} & +2(1-2\nu_1)B_1 \\ & -[2C_1+12\nu_1D_1r^2+6E_1r^{-4}+4(1-\nu_1)F_1r^{-2}]\cos 2\theta \\ A_2r^{-2} & +2(1-2\nu_2)B_2 \\ & -[2C_2+12\nu_2D_2r^2+6E_2r^{-4}+4(1-\nu_2)F_2r^{-2}]\cos 2\theta \\ A_3r^{-2}+2(1-2\nu_3)G_3\ell nr+(1-4\nu_3)G_3 & +2(1-2\nu_3)B_3 \\ & -[2C_3+12\nu_3D_3r^2+6E_3r^{-4}+4(1-\nu_3)F_3r^{-2}]\cos 2\theta \end{Bmatrix} \tag{58}$$

$$\frac{Y}{1+\nu}\cdot[\varepsilon_{\theta\theta}+\nu\varepsilon_{zz}-(1+\nu)k] =$$

$$\begin{Bmatrix} -A_1r^{-2} & +2(1-2\nu_1)B_1 \\ & +[2C_1+12(1-\nu_1)D_1r^2+6E_1r^{-4}+4\nu_1F_1r^{-2}]\cos 2\theta \\ -A_2r^{-2} & +2(1-2\nu_2)B_2 \\ & +[2C_2+12(1-\nu_2)D_2r^2+6E_2r^{-4}+4\nu_2F_2r^{-2}]\cos 2\theta \\ -A_3r^{-2}+2(1-2\nu_3)G_3\ell nr+(3-4\nu_3)G_3 & +2(1-2\nu_3)B_3 \\ & +[2C_3+12(1-\nu_3)D_3r^2+6E_3r^{-4}+4\nu_3F_3r^{-2}]\cos 2\theta \end{Bmatrix} \tag{59}$$

$$\frac{Y}{1+\nu}\varepsilon_{r\theta} = \begin{Bmatrix} (2C_1+6D_1r^2-6E_1r^{-4}-2F_1r^{-2})\sin 2\theta \\ (2C_2+6D_2r^2-6E_2r^{-4}-2F_2r^{-2})\sin 2\theta \\ (2C_3+6D_3r^2-6E_3r^{-4}-2F_3r^{-2})\sin 2\theta \end{Bmatrix} . \tag{60}$$

The relation between strain and displacement given in Eq. (8) expressed in cylindrical coordinates becomes

$$\varepsilon_{rr} = \frac{\partial u_r}{\partial r} \tag{61}$$

$$\varepsilon_{\theta\theta} = \frac{u_r}{r} + \frac{1}{r}\frac{\partial u_\theta}{\partial \theta} \tag{62}$$

$$\varepsilon_{r\theta} = \frac{1}{2}\left(\frac{\partial u_\theta}{\partial r} - \frac{u_\theta}{r} + \frac{1}{r}\frac{\partial u_r}{\partial \theta}\right) . \tag{63}$$

Utilizing Eqs. (58-60) one finds by partial integration

$$\frac{Y}{1+\nu}[u_r+\nu\varepsilon_{zz}r-(1+\nu)kr] =$$

$$\begin{Bmatrix} -A_1 r^{-1} & +2(1-2\nu_1)B_1 r \\ -[2C_1 r+4\nu_1 D_1 r^3-2E_1 r^{-3}-4(1-\nu_1)F_1 r^{-1}]\cos 2\theta & \\ -A_2 r^{-1} & +2(1-2\nu_2)B_2 r \\ -[2C_2 r+4\nu_2 D_2 r^3-2E_2 r^{-3}-4(1-\nu_2)F_2 r^{-1}]\cos 2\theta & \\ -A_3 r^{-1}+2(1-2\nu_3)G_3 r(\ln r-1)+(1-4\nu_3)G_3 r+2(1-2\nu_3)B_3 r & \\ -[2C_3 r+4\nu_3 D_3 r^3-2E_3 r^{-3}-4(1-\nu_3)F_3 r^{-1}]\cos 2\theta & \end{Bmatrix} \tag{64}$$

$$\frac{Y}{1+\nu}\cdot u_\theta = \begin{Bmatrix} 2[C_1 r+(3-2\nu_1)D_1 r^3+E_1 r^{-3}-(1-2\nu_1)F_1 r^{-1}]\sin 2\theta \\ 2[C_2 r+(3-2\nu_1)D_2 r^3+E_2 r^{-3}-(1-2\nu_2)F_2 r^{-1}]\sin 2\theta \\ 4(1-\nu_3)G_3 r\theta+2[C_3 r+(3-2\nu_3)D_3 r^3+E_3 r^{-3}-(1-2\nu_3)F_3 r^{-1}]\sin 2\theta \end{Bmatrix} \tag{65}$$

$$u_z = \varepsilon_{zz} z . \tag{66}$$

The unknown functions in the partial integration are set to zero in order not to introduce rigid body rotations.

Boundary Conditions

At r=a no traction is transmitted. Hence

$$\sigma_{rr} = \sigma_{r\theta} = 0 , \tag{67}$$

or

$$A_1 a^{-2} + 2B_1 = 0 \tag{68}$$

$$2C_1 + 6E_1 a^{-4} + 4F_1 a^{-2} = 0 \tag{69}$$

$$2C_1 + 6D_1 a^2 - 6E_1 a^{-4} - 2F_1 a^{-2} = 0 . \tag{70}$$

At r=b the equilibrium condition is

$$\sigma_{rr}^{(+)} - \sigma_{rr}^{(-)} + f_r = 0 , \tag{71}$$

and

$$\sigma_{r\theta}^{(+)} - \sigma_{r\theta}^{(-)} + f_\theta = 0 , \tag{72}$$

where f_r and f_θ are given by Eqs. (31-32). Thus

$$(A_2-A_1)b^{-2} + 2(B_2-B_1) = -\pi i_o[i_o b^2 r_s^{-2}+i_1(1+c^2 r_s^{-2})] \tag{73}$$

$$-2(C_2-C_1)-6(E_2-E_1)b^{-4}-4(F_2-F_1)b^{-2} = -\pi i_o[i_o b^2 r_s^{-2}+i_1(1+c^2 r_s^{-2})] \tag{74}$$

$$2(C_2-C_1)+6(D_2-D_1)b^2-6(E_2-E_1)b^{-4}-2(F_2-F_1)b^{-2} = \pi i_o[i_o(1+b^2 r_s^{-2})+i_1(1+c^3 r_s^{-2})] \tag{75}$$

Also at r=b the displacements are continuous.

$$u_r^{(+)} - u_r^{(-)} = u_\theta^{(+)} - u_\theta^{(-)} = 0 . \tag{76}$$

From Eqs. (64-65) one obtains

$$\frac{1+\nu_2}{Y_2}[-A_2 b^{-1}+2(1-2\nu_2)B_2 b] - \frac{1+\nu_1}{Y_1}[-A_1 b^{-1}+2(1-2\nu_1)B_1 b]$$

$$-(\nu_2-\nu_1)\varepsilon_{zz}b = -(1+\nu_2)k_2b+(1+\nu_1)k_1b \tag{77}$$

$$\frac{1+\nu_2}{Y_2}[-2C_2b-4\nu_2D_2b^3+2E_2b^{-3}+4(1-\nu_2)F_2b^{-1}]$$

$$-\frac{1-\nu_1}{Y_1}[-2C_1b-4\nu_1D_1b^3+2E_1b^{-3}+4(1-\nu_1)F_1b^{-1}] = 0 \tag{78}$$

$$\frac{1+\nu_2}{Y_2}[2C_2b+2(3-2\nu_2)D_2b^3+2E_2b^{-3}-2(1-2\nu_2)F_2b^{-1}]$$

$$-\frac{1+\nu_1}{Y_1}[2C_1b+2(3-2\nu_1)D_1b^3+2E_1b^{-3}-2(1-2\nu_1)F_1b^{-1}] = 0 . \tag{79}$$

At r=c the equilibrium condition is

$$\sigma_{rr}^{(+)}-\sigma_{rr}^{(-)}+f_r = 0, \quad \sigma_{r\theta}^{(+)}-\sigma_{r\theta}^{(+)}+f_\theta = 0 . \tag{80}$$

Hence, using Eqs. (55) and (57)

$$(A_3-A_2)c^{-2}+(2\ell nc+1)G_3+2(B_3-B_2) = -\pi i_1[i_o(-b^2c^{-2}+b^2r_s^{-2})+i_1c^2r_s^{-2}] \tag{81}$$

$$-2(C_3-C_2)-6(E_3-E_2)c^{-4}-4(F_3-F_2)c^{-2} = -\pi i_1[i_o(-b^2c^{-2}+b^2r_s^{-2})+i_1c^2r_s^{-2}] \tag{82}$$

$$2(C_3-C_2)+6(D_3-D_2)c^2-6(E_3-E_2)c^{-4}-2(F_3-F_2)c^{-2} = \pi i_1[i_o(b^2c^{-2}+b^2r_s^{-2})+i_1(1+c^2r_s^{-2})] . \tag{83}$$

At r=c u_r is continuous or

$$u_r^{(+)}-u_r^{(-)} = 0 . \tag{84}$$

The pretension condition in the band is formulated by utilizing the notion of rotational dislocation[5] whereby a small angle α is removed from the band. Subsequently this angle is closed up and held by welding, slippage between the band and region 2 being permitted. Thus, for region 3 and r=c

$$u_\theta(2\pi)-u_\theta(0) = c\alpha . \tag{85}$$

After removal of the term responsible for pretensioning, subsequent slippage is not allowed and then for r=c

$$u_\theta^{(+)} \text{ minus term prop. to } \theta = u_\theta^{(-)}. \tag{86}$$

The conditions of Eqs. (84-86) yield

$$\frac{1+\nu_3}{Y_3}[-A_3c^{-1}+2(1-2\nu_3)G_3c(\ell nc-1)+(1-4\nu_3)G_3c+2(1-2\nu_3)B_3c]$$

$$-\frac{1+\nu_2}{Y_2}[-A_2c^{-1}+2(1-2\nu_2)B_2c]-(\nu_3-\nu_2)\varepsilon_{zz}c = -(1+\nu_3)k_3c+(1+\nu_2)k_2c \tag{87}$$

$$\frac{1+\nu_3}{Y_3}[-2C_3c-4\nu_3D_3c^3+2E_3c^{-3}+4(1-\nu_3)F_3c^{-1}]$$

$$-\frac{1+\nu_2}{Y_2}[-2C_2c-4\nu_2D_2c^3+2E_2c^{-3}+4(1-\nu_2)F_2c^{-1}] = 0 \tag{88}$$

$$4\frac{(1-\nu_3^2)}{Y_3}G_3c2\pi = c\alpha \tag{89}$$

$$\frac{1+\nu_3}{Y_3}[C_3c+(3-2\nu_3)D_3c^3+E_3c^{-3}-(1-2\nu_3)F_3c^{-1}]$$

$$-\frac{1+\nu_2}{Y_2}[C_2c+(3-2\nu_2)D_2c^3+E_2c^{-3}-(1-2\nu_2)F_2c^{-1}] = 0 . \tag{90}$$

At r=d no traction is transmitted. Hence

$$\sigma_{rr} = \sigma_{r\theta} = 0 \tag{91}$$

or

$$A_3 d^{-2} + (2\ell nd+1)G_3 = 0 \tag{92}$$

$$-2C_3 - 6E_3 d^{-4} - 4F_3 d^{-2} = 0 \tag{93}$$

$$2C_3 + 6D_3 d^2 - 6E_3 d^{-4} - 2F_3 d^{-2} = 0 \ . \tag{94}$$

Note that Eqs. (68-70, 73-75, 77-79, 81-83, 87-90, 92-94) provide 19 conditions among the 20 variables A_1 B_1 C_1 D_1 E_1 F_1 A_2 B_2 C_2 D_2 E_2 F_2 A_3 G_3 B_3 C_3 D_3 E_3 F_3 ϵ_{zz}.

Use of Virial Theorem

The virial theorem in Eq. (23) may be expressed as

$$\int_V \mathrm{tr}\vec{\vec{\sigma}}dV = \int_S \vec{r}\cdot\vec{\vec{\tau}}\cdot\vec{n}dS + W_B \ . \tag{95}$$

But the traction on the surface is[6]

$$\vec{\vec{\tau}}\cdot\vec{n} = \frac{1}{4\pi}[\vec{H}(\vec{H}\cdot\vec{n}) - \frac{1}{2}H^2\vec{n}] \ . \tag{96}$$

It is assumed that the magnet is of finite length and that the end surfaces used to specify S are sufficiently far removed so that no fields are present. On the cylindrical iron surface $r=r_s$

$$\vec{r}\cdot\vec{\vec{\tau}}\cdot\vec{n} = \frac{1}{8\pi}(H_r^2 - H_\theta^2)r_s \ . \tag{97}$$

Using Eq. (25-26) for the fields

$$\int_S \vec{r}\cdot\vec{\vec{\tau}}\cdot\vec{n}ds = \frac{2\ell\pi^2}{r_s^2}(i_o b^2 + i_1 c^2)^2 \ . \tag{98}$$

The magnetic energy is given by Eqs. (25-26) and (35)

$$W_B = \ell\pi^2[i_o^2 b^2 + 2i_o i_1 b^2 + i_1^2 c^2 + (i_o b^2 + i_1 c^2)^2 r_s^{-2}] \ , \tag{99}$$

which, together with Eq. (98), gives

$$\int_V \mathrm{tr}\vec{\vec{\sigma}}dV = \ell\pi^2[i_o^2 b^2 + 2i_o i_1 b^2 + i_1^2 c^2 + 3(i_o b^2 + i_1 c^2)^2 r_s^{-2}] \ . \tag{100}$$

Then, using Eq. (14) to eliminate σ_{zz} one has after cancelling the effective length ℓ

$$\int\int[(1+\nu)(\sigma_{rr}+\sigma_{\theta\theta}) + Y(\epsilon_{zz}-k)]rdrd\theta =$$

$$\pi^2[i_o^2 b^2 + 2i_o i_1 b^2 + i_1^2 c^2 + 3(i_o b^2 + i_1 c^2)^2 r_s^{-2}] \ . \tag{101}$$

Using Eqs. (55-56) this gives the condition

$$4\pi(1+\nu_1)(b^2-a^2)B_1 + 4\pi(1+\nu_2)(c^2-b^2)B_2$$

$$+2\pi(1+\nu_3)[d^2(2\ell nd+1)+c^2(2\ell nc+1)]G_3 + 4\pi(1+\nu_3)(d^2-c^2)B_3$$

$$+\pi[Y_1(b^2-a^2)+Y_2(c^2-b^2)+Y_3(d^2-c^2)]\epsilon_{zz}$$

$$= \pi[k_1 Y_1(b^2-a^2)+k_2 Y_2(c^2-b^2)+k_3 Y_3(d^2-c^2)]$$

$$+\pi^2[i_o^2 b^2 + 2i_o i_1 b^2 + i_1^2 c^2 + 3(i_o b^2 + i_1 c^2)^2 r_s^{-2}] \ , \tag{102}$$

which provides the last condition necessary for determining all of the unknowns. The current densities i_o and i_1 can be chosen in many ways. The following choice comes from equating respectively the current and radial moment of the current in the two sheet dipoles to the same quantities in the thick cosine theta dipole and expressing the result in terms of the central magnetic field H_o. Thus Eq. (24) becomes

$$i = \begin{Bmatrix} cb^{-1}+2 \\ bc^{-1}+2 \end{Bmatrix} \cdot \frac{H_o \cos\theta}{12\pi[1+\frac{1}{3}(b^2+bc+c^2)r_s^{-2}]} \ . \tag{103}$$

Internal Energy

The expression for the internal energy in Eq. (1) may be obtained using the strains in cylindrical coordinates by partially integrating Eq. (2) using Eqs. (37 - 40). Thus

$$W = \tfrac{1}{2}(\lambda+2\mu)(\varepsilon_{rr}^2+\varepsilon_{\theta\theta}^2+\varepsilon_{zz}^2) + \lambda(\varepsilon_{rr}\varepsilon_{\theta\theta}+\varepsilon_{\theta\theta}\varepsilon_{zz}+\varepsilon_{zz}\varepsilon_{rr}) + \mu\varepsilon_{r\theta}^2 - k(3\lambda+2\mu)(\varepsilon_{rr}+\varepsilon_{\theta\theta}+\varepsilon_{zz}) \quad (104)$$

After rearrangement and use of Eqs. (37-40), the strain energy may be written in terms of stresses and strains:

$$W = \tfrac{1}{2}\left\{[\sigma_{rr}-k(3\lambda+2\mu)]\varepsilon_{rr} + [\sigma_{\theta\theta}-k(3\lambda+2\mu)]\varepsilon_{\theta\theta} + [\sigma_{zz}-k(3\lambda+2\mu)]\varepsilon_{zz} + \sigma_{r\theta}\,\varepsilon_{r\theta}\right\}. \quad (105)$$

Stress Distribution in Iron Shield

In the region of the iron shield between $r=r_s$ and $r=R_s$ the Airy stress function may be taken as

$$\phi = A\ell nr + Br^2 + (Cr^2+Dr^4+Er^{-2}+F)\cos 2\theta . \quad (106)$$

Equations (51-54) then give

$$\sigma_{rr} = Ar^{-2} + 2B - (2C+6Er^{-4}+4Fr^{-2})\cos 2\theta \quad (107)$$

$$\sigma_{\theta\theta} = -Ar^{-2} + 2B + (2C+12Dr^2+6Er^{-4})\cos 2\theta \quad (108)$$

$$\sigma_{r\theta} = (2C+6Dr^2-6Er^{-4}-2Fr^{-2})\sin 2\theta \quad (109)$$

The boundary conditions at $r=r_s$ are ($\sigma_{rr}^{(-)} = \tau_{rr}^{(+)} = 0$)

$$\sigma_{rr}^{(+)} - \tau_{rr}^{(-)} = 0 \quad (110)$$

$$\sigma_{r\theta}^{(+)} = 0 , \quad (111)$$

where, from Eqs. (96) and (25)

$$\tau_{rr}^{(-)} = \frac{1}{8\pi} H_r^2 = \pi(i_o b^2+i_1 c^2)^2 r_s^{-4}(1-\cos 2\theta) . \quad (112)$$

Hence

$$Ar_s^{-2} + 2B = -\pi(i_o b^2+i_1 c^2)^2 r_s^{-4} , \quad (113)$$

$$-2C - 6Er_s^{-4} - 4Fr_s^{-2} = \pi(i_o b^2+i_1 c^2)^2 r_s^{-4} \quad (114)$$

$$2C + 6Dr_s^2 - 6Er_s^{-4} - 2Fr_s^{-2} = 0 . \quad (115)$$

At $r=R_s$ the boundary conditions are

$$\sigma_{rr} = \sigma_{r\theta} = 0 . \quad (116)$$

Hence

$$AR_s^{-2} + 2B = 0 \quad (117)$$

$$2C + 6ER_s^{-4} + 4FR_s^{-2} = 0 \quad (118)$$

$$2C + 6DR_s^2 - 6ER_s^{-4} - 2FR_s^{-2} = 0 . \quad (119)$$

Note that Eqs. (113-115, 117-119) provide six equations for determining the six unknowns (A-F).

As in the previous problem the generalized plane strain approximation will be used. Since this introduces one more unknown, the longitudinal strain, the virial theorem will be used to provide the last condition. Thus using Eq. (95) and (97) with an inwardly directed normal gives

$$\iint(\sigma_{rr}+\sigma_{\theta\theta}+\sigma_{zz})r\,dr\,d\theta = -2\pi^2(i_o b^2+i_1 c^2)^2 r_s^{-2} . \quad (120)$$

Equation (47) may be used to eliminate σ_{zz}. In this case since the iron shield remains at room temperature k=0. Thus

$$\iint[(1+\nu)(\sigma_{rr}+\sigma_{\theta\theta})+Y\varepsilon_{zz}]rdrd\theta = -2\pi^2(i_o b^2+i_1 c^2)^2\, r_s^{-2} . \quad (121)$$

Integrating after using Eqs. (107-108) for the stresses gives

$$\pi(R_s^2-r_s^2)[4(1+\nu)B+Y\varepsilon_{zz}] = -2\pi^2(i_o b^2+i_1 c^2)^2\, r_s^{-2} . \quad (122)$$

Thus the longitudinal strain is determined.

Numerical Calculations

The stresses and strains that exist in the three nested hollow cylinders have been calculated as a function of the central magnetic field. Twenty algebraic relations in Eqs. (68, 69, 70, 73, 74, 75, 77, 78, 79, 81, 82, 83, 87, 88, 89, 90, 92, 93, 94, 102) among the nineteen coefficients in the Airy stress functions (A_1 B_1 C_1 D_1 E_1 F_1 A_2 B_2 C_2 D_2 E_2 F_2 A_3 G_3 B_3 C_3 D_3 E_3 F_3) and the longitudinal strain ε_{zz} have been solved. Thus the stress and strain of any point in the dipole model structure may be found. For simplicity in the presentation of numerical results, however, only the values on the median plane are given. It is usually clear whether a quantity is stress or strain. Otherwise, R is radial, T is theta or azimuthal, Z is axial or longitudinal. With regard to position A, B, C, D are the points on the median plane at the cylindrical boundaries between the various media. To indicate the side of the point, P is used for positive and M for negative. Thus, for example, RTBP indicates the (r, θ) component at the positive side of point B.

The boundary between elastic and plastic isotropic media is a function of the invariants of the tensor representing the deviation of stress from the mean stress. A generally accepted simplification of this condition regards the onset of plastic flow as being determined only by the second invariant of this tensor[6]

$$J_2 = \tfrac{1}{6}[(\sigma_{rr}-\sigma_{\theta\theta})^2+(\sigma_{\theta\theta}-\sigma_{zz})^2+(\sigma_{zz}-\sigma_{rr})^2] + \sigma_{r\theta}^2 . \quad (123)$$

Since the condition may be stated as

$$3J_2 = Y_t^2 , \quad (124)$$

where Y_t is the yield stress in tension, the $\sqrt{3J_2}$ has been tabulated for ready comparison of the state of stress with the yield point. Note that for 45 kG the band stress slightly exceeds the elastic limit.

A comment relative to the appearance of negative elastic energies is in order. Equation (1) is actually an expression for the density of free energy (u-Tη) where u is the internal energy and η is the entropy density[7]. However, the term in Tη that depends only on the temperature has been dropped since it does not affect the state of stress. Hence, negative values of the free energy are caused by positive values of the entropy density.

For completeness the effect of the distortions caused by banding, cooldown, and magnetic excitation are indicated by their multipole contribution[8] to an otherwise pure dipole field. At the reference radius let

$$\Delta B = \Delta B_1 + \Delta B_3 \quad (125)$$

where ΔB_1 is the change in the dipole component and ΔB_3 is the change in the sextupole component of the resulting field. Further,

let

$$\Delta B_1 = \Delta B_{1c} + \Delta B_{1s} \qquad \Delta B_3 = \Delta B_{3c} + \Delta B_{3s} \ , \tag{126}$$

where the subscript c refers to the contribution due to the conductor alone and the subscript s refers to the contribution from the shield. Also let

$$R_1 = \frac{\Delta B_1}{B} \qquad R_3 = \frac{\Delta B_3}{B} \ , \tag{127}$$

where B is the original magnetic field for zero mechanical displacement field. Thus, the output lists ΔB_{1c}, ΔB_{1s}, R_1 and ΔB_{3c}, ΔB_{3s}, R_3 for the displacement field that results from each state of strain.

No calculations have been made for the stresses in the iron since the inner iron surface field is modest.

References

1. R.W. Little, Elasticity, Prentice Hall, Inc., Englewood Cliffs, New Jersey, 1964, p. 78.
2. Chi-Teh Wang, Applied Elasticity, McGraw Hill Book Co., New York, 1953, p. 44. Note that the auxiliary condition does not apply in the presence of body forces.
3. G. Schmidt, Physics of Fluids 3, 481 (1960); see also C.L. Longmire, Elementary Plasma Physics, Interscience Publishers, New York, 1963, p. 68. Note that his sign convention regarding both the Maxwell stress tensor and the mechanical stress tensor is different from that normally used; see also C. Truesdell and R. Toupin, Classical Field Theories, Handb. der Physik III, Springer-Verlag, Berlin, 1960, pp. 586-577, who discuss the history of the virial theorem.
4. J.A. Stratton, Electromagnetic Theory, McGraw Hill Book Co., Inc., New York, 1940, p. 97.
5. R.W. Little, Elasticity, Prentice Hall Inc., New Jersey, 1944, p. 162. See also A.E.H. Love, A Treatise on the Mathematical Theory of Elasticity, Dover Publications Inc., New York., 1944, p. 221.
6. R. Hill, The Mathematical Theory of Plasticity, Clarendon Press, Oxford, p. 20 (1950).
7. B.A. Boley and J.H. Weiner, Theory of Thermal Stress, John Wiley and Sons, Inc., p. 27 and p. 269 (1960); See also, A.M. Freudenthal and H. Geiringer, The Inelastic Continuum, Handb. der Physik 6, p. 263 (1958).
8. S.C. Snowdon, Magnetic Multipoles Induced by Mechanical and Thermal Stresses in Doubler Dipole, TM-621.

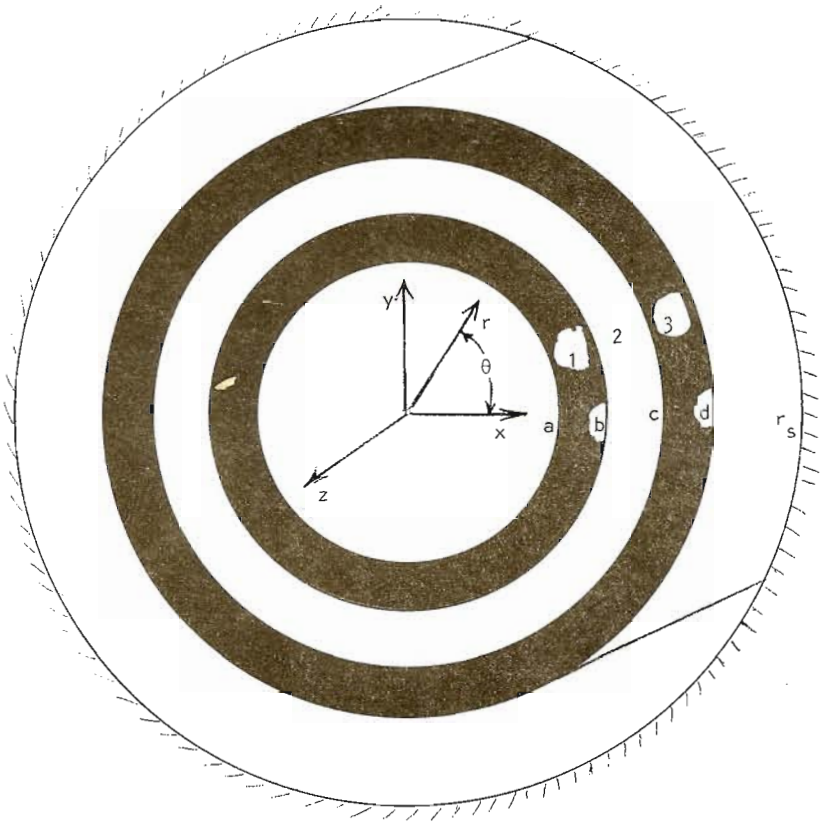

Fig. 1. Geometric Details of Doubler Dipole Model